Universiteit Twente

Bachelor thesis

Monolayer MoS_2 on a substrate of hexagonal boron nitride

Author:
Ruben Jaarsma
Period:
2-3-2014 - 4-24-2014

Supervisor:
Nirmal Ganguli
Chair:
Computational Materials Science

April 17, 2014

Abstract

In this research we want to see if hexagonal boron nitride is a suitable candidate as a substrate for a monolayer of molybdenum disulfide. For a monolayer of molybdenum disulfide on top of a monolayer of hexagonal boron nitride we calculate two possible optimized structures with a distance between the planes of 4.89 Å with a binding energy per molybdenum disulfide unit cell of -2.778 eV and 8.10 Å with a binding energy per molybdenum disulfide unit cell of -2.634 eV. We plot the total energy versus the seperation distance en find that the structure with a seperation of 4.89 Å is a stable structure and the structure with the seperation of 8.10 Å is a metastable structure.

We plot the band structure for the metastable structure and find a direct band gap of 1.83 eV at K point. For the band structure of the stable structure we find that the band gap is indirect between H and K. We find that this is because of the bands with nitrogen p_z character that have moved down due to hybridization to create an indirect band gap. We plot the projected density of states for the boron nitride atoms and the molybdenum disulfide atoms for the stable structure and find a band gap of 1.83 eV.

We conclude that hexagonal boron nitride is a suitable candidate as a substrate for a monolayer of molybdenum disulfide. We note that the band gap is indirect for a stable structure of a monolayer of molybdenum disulfide on top of a monolayer of hexagonal boron nitride. We also note that there is a direct band gap for the metastable structure. Further research may be done to find a stable structure with a direct band gap.

Contents

Introduction **3**
Background . . . 3
Problem . . . 3
Plan of action . . . 4

Theoretical aspects **5**
Tight binding method . . . 5
Density functional theory . . . 6
Structure . . . 7
Binding . . . 8

Computational aspects **9**
VASP . . . 9
Density of states . . . 10
Band structure . . . 10

Results **11**

Discussion **16**

Conclusion **17**
Possibilities for future research . . . 17

Appendix 1 - Assignments **21**
Assignment 1 - Radial Schrödinger Equation . . . 21
Assignment 2 - Tight binding . . . 24
Assignment 3 - Densities of States . . . 36
Assignment 4 . . . 41
Assignment 5 - Tight Binding Method . . . 44
Assignment 6 . . . 55

Appendix 2 - VASP-calculations **57**
Carbon . . . 57
Silicon . . . 61
Germanium . . . 61
Boron nitride . . . 62
Aluminium phosphide . . . 67
Gallium arsenide . . . 69
Zinc selenide . . . 69
Further analysis . . . 72

Report

Introduction

Background

Technology is getting smaller and more compact. Therefore, scientists are always looking for stable materials of very small size with interesting properties. In recent history there has been a lot of talk and research about graphene, a monolayer of graphite. This two-dimensional material has very interesting properties, namely a high carrier mobility and mechanical strength [1]. But it's not a semiconductor.

After scientists were able to create graphene in the laboratory one knew that is was possible to extract a monolayer of a material. The search for more of these materials continued. A semiconductor material would be especially interesting.

Molybdenum disulfide might be a good candidate for this. A monolayer of molybdenum disulfide has a direct band gap of 1.8 eV [2], which makes it suitable for opto-electronic applications. If one is to create a monolayer of this material however, a substrate is needed to support this monolayer. Hexagonal boron nitride is used as a substrate for graphene. They have the same honeycomb structure and their in-plane lattice parameters are very similar.

Molybdenum disulfide also has the same honeycomb structure as graphene [3], however it's in-plane lattice parameter is significantly larger than that of boron nitride. Therefore one may wonder if boron nitride is a good candidate for a substrate. If it is questions arise about how this would effect the direct band gap in monolayer molybdenum disulfide, since bulk molybdenum disulfide has an indirect band gap [2].

Problem

In this thesis we investigate if hexagonal boron nitride is a suitable candidate as a substrate for a monolayer of molybdenum disulfide. This will be done by answering the following three more specific questions:

- Are there one or more stable heterostructures of molybdenum disulfide on boron nitride?
- Does the direct band gap of monolayer molybdenum disulfide remain direct upon formation of the heterostructure and what is the size of it?
- How does the electronic structure qualitatively change upon formation of the heterostructure?

Plan of action

To be able to do this research as a third year bachelor student a lot of preperation had to be done. First an understanding of the electronic structure of solids via tight binding approximation had to be achieved. Several assignments related to tight binding were done of which the results can be found in appendix 1. The chapter Theory has a section dedicated to this subject explaining tight binding and the conclusions that were made from those exercises. These conclusions will be used in analyzing and discussing the results in the chapters Results and Discussion.

Besides the above the program VASP [4] [5] had to be learned. VASP is software used to calculate the electronic properties of materials. To get a good understanding of the software and learn how to extract useful information a lot of calculations were done with group IV, III-V and II-VI semiconductors as well as with carbon. Information about the software VASP is given in the chapter Computational aspects.

The results and an analysis of these VASP calculations can be found in appendix 2. The results were used to discuss the trends found in this region of the periodic table. For example, the band gap size of carbon, silicon and germanium was compared to their lattice constant, as well for germanium, gallium arsenide and zinc selenide. Furthermore, of materials that exist in different structures the most stable structure was calculated based on the total energy per atom.

Besides the key theoretical and computational aspects mentioned above, some aspects needed to understand this work can be found in the chapters Theoretical aspects and Computational aspects. Following these chapters is the chapter Results containing an overview of the important results needed to answer the questions mentioned under Problem. In the chapters Discussion and Conclusion the results will be discussed and the questions will be answered. This is followed by the references and the appendices, the latter containing the solutions to the assignments and VASP calculations done in preparation of this research.

Theoretical aspects

Tight binding method

The tight binding method is a way of describing solid materials and from there calculate the electronic properties of this material. In tight binding, the solid is seen as "a collection of weakly interacting neutral atoms" where "the overlap of the wave functions is enough to require corrections to the picture of isolated atoms, but not so much as to render the atomic description completely irrelevant." [6]

For this thesis, the focus will be on the results and interpretation of the tight binding method. Using this model, the Schrödinger equation can be rewritten to become

$$\begin{aligned}(\varepsilon(\boldsymbol{k}) - E_m)b_m = -(\varepsilon(\boldsymbol{k}) - E_m)\sum_n (\sum_{\boldsymbol{R}\neq 0}\int \psi_m^*(\boldsymbol{r})\psi_n(\boldsymbol{r}-\boldsymbol{R})e^{i\boldsymbol{k}\cdot\boldsymbol{R}}d\boldsymbol{r})b_n \\ +\sum_n (\int \psi_m^*(\boldsymbol{r})\Delta U(\boldsymbol{r})\psi_n(\boldsymbol{r})d\boldsymbol{r})b_n + \sum_n (\sum_{\boldsymbol{R}\neq 0}\int \psi_m^*(\boldsymbol{r})\Delta U(\boldsymbol{r})\psi_n(\boldsymbol{r}-\boldsymbol{R})e^{i\boldsymbol{k}\cdot\boldsymbol{R}}d\boldsymbol{r})b_n\end{aligned} \tag{1}$$

[6]

In this equation $\varepsilon(\boldsymbol{k})$ is the energy dispersion with $\boldsymbol{k}$ the position in k-space in m^{-1}. E_m is the atomic energy. Both the energy dispersion and atomic energy have SI units of joule but it's in some situations convenient to work with the unit of eV. The indices m and n indicate the atomic orbitals and b is a unit vector. $\boldsymbol{R}$ and $\boldsymbol{r}$ describe the positions of the atoms and are given in meters. The wave function is represented by ψ in units of $\mathrm{m}^{-3N/2}$ in three dimensions with N the total number of atoms and the potential by U, which should be given in the same units as the energy dispersion and atomic energy.

Equation (1) can be used to calculate the energies of different atomic orbitals. For a (non-degenerate) s-level equation (1) will become one single equation. For (triply degenerate) p-levels it will become a 3×3 secular problem and so on.

The tight binding method is of course an approximation, but it's a good method for simple systems. In appendix 1, several assignments were done using the tight binding method, that is assignments 2, 4, 5 & 6. An insight about the electronic structure of solids was gained from these assignments that can be used in analyzing the results of this research.

First of all, in assignment 3, figure 17 shows the dispersion for an infinite chain of hydrogen atoms with one atom in the unit cell. When a bigger unit cell is used, a phenomena called folding enters the picture, of which the effects can be seen in figure 18 and is briefly explained in the assignment. Also, two energy levels can be seen, one bonding and one anti-bonding. Then, the energy of the second atom in the unit cell is changed so that the infinite hydrogen chain becomes an inifinte dimer chain. Now a band gap arises, with a bonding and anti bonding state on each side of the Fermi level, as can be seen in figure 20.

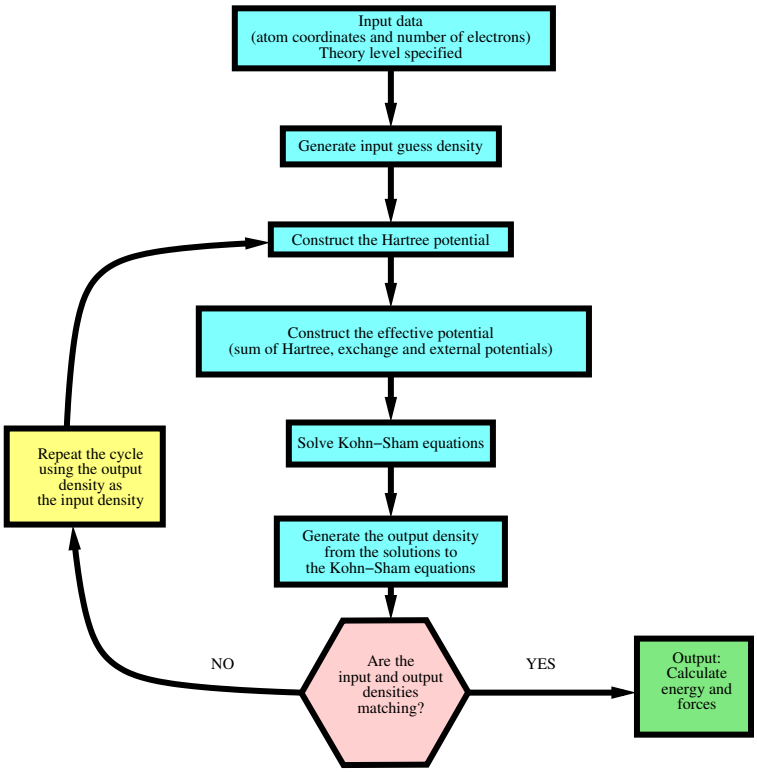

Figure 1: Flow chart visualizing density functional theory.

In assignments 4 & 5 the tight binding method is used to calculate the p-bands. Calculating these requires exploiting all the symmetries in the system and can only be done analytically for special k-points. In assignment 6, the π (p_z) bands of graphene were calculated using thight binding. A comparison between figure 33 and figures 38 and 39 shows how accurate the tight binding method can be.

Density functional theory

Density functional theory (DFT) can be best explained in the words of Walter Kohn, developer of DFT:

> DFT is an alternative approach to the theory of electronic structure, in which the electron density distribution n(r), rather than the many electron wave function plays a central role. [7]

DFT works in the following steps: guess an electron density, construct the different potentials, solve the Kohn-Sham equations, generate the output density and see if it matches the input density. This is visualized in the flow chart in figure 1.

There are some known limitations of DFT. Two of them are expected to be relevant for this research. The first is the band gap problem: band gaps in semiconductors and insulators are almost always underestimated. Another one is the neglect of van der Waals interactions. [8] Examples of these limitations can be found in appendix 2. All the calculated band gaps are underestimated. The effect of the neglect of the van der Waals forces can be seen in graphene and the monolayer of hexagonal boron nitride. There are possible solutions to these problems, but it's is probably not necessary to implement those if one keeps these limitations in mind when analyzing the results.

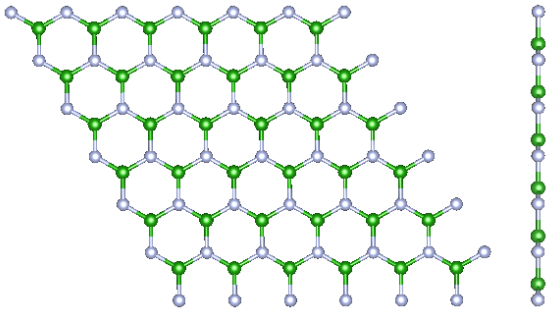

(a) Top down and side view of a monolayer of hexagonal boron nitride. The boron atoms are shown in green and the nitrogen atoms are shown in grey.

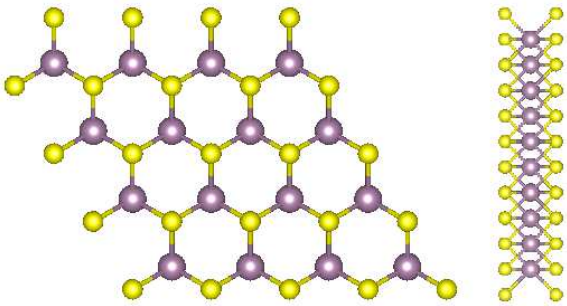

(b) Top down and side view of a monolayer of molybdenum disulfide. The molybdenum atoms are shown in purple and the sulfur atoms are shown in yellow.

Figure 2: Structures of boron nitride and molybdenum disulfide. Images were made using VESTA [11].

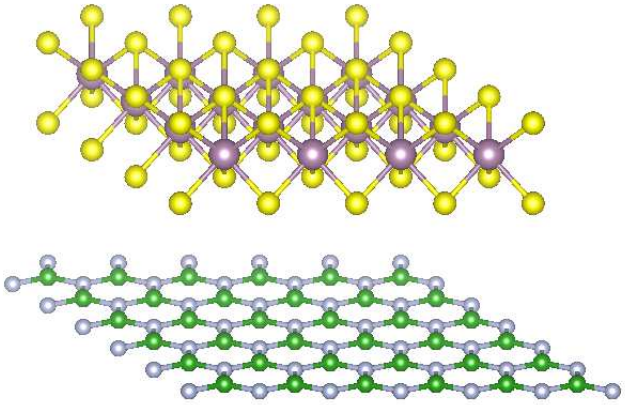

Figure 3: Supercell of a 4×4 monolayer of molybdenum disulfide on top of a 5×5 monolayer of boron nitride. The image was made using VESTA [11].

Structure

A monolayer of hexagonal boron nitride has a well known structure, which is shown in figure 2a. It has a honeycomb lattice where for each atom the three nearest neighbors are of the different atomic species. [9] The in-plane lattice constant a_{BN} is 2.50 Å[10].

Molybdenum disulfide also has a hexagonal honeycomb structure. However a monolayer of molybdenum disulfide actually exists of two layers of sulfur atoms with one layer of molybdenum atoms in between. In figure 2b a top down and side view of molybdenum disulfide can be seen. The distance between the sulfur atoms is 3.1 Å. The in-plane lattice parameter a_{MoS_2} is 3.12 Å. [3]

To create a heterostructure of these two materials a supercell, that is a multiple of one unit cell, has to be found where the lattice parameters match. The smallest supercell with $< 1.0\%$ strain is a four by four molybdenum disulfide lattice on top of a five by five boron nitride lattice. This structure is sketched in figure 3. The out-of-plane lattice constant c has to be determined. The distance between the molybdenum and the boron nitride is $\frac{c}{2}$.

Binding

If binding between the layer of boron nitride and molybdenum disulfide will be achieved can be determined in a few ways. First of all one can calculate if the total energy is at a minimum. A second way is to calculate the binding energy. This binding energy is the total energy of the heterostructure minus the total energy of isolated molybdenum disulfide, that is the supercell of the heterostructure without the boron nitride layer, and minus the total energy of isolated boron nitride, the supercell without the layer of molybdenum disulfide. This can therefore be calculated using the following equation:

$$E_b = E_{tot_{het}} - E_{tot_{MoS_2}} - E_{tot_{BN}} \tag{2}$$

where E_b is the binding energy, $E_{tot_{het}}$ the total energy of the heterostructure, $E_{tot_{MoS_2}}$ the total energy of the isolated molybdenum disulfide and $E_{tot_{BN}}$ the total energy of the isolated boron nitride. All energies should be inputted in the same unit, which can be joule, electronvolt or a different unit of energy. If the binding energy is smaller than zero there is binding between the layers.

Computational aspects

VASP

VASP, short for Vienna ab-initio simulation package, is software used for density functional calculations. In this thesis it is used for three things: calculating the optimal structure, the electronic ground state and the band structure of a material. For all of the calculations it needs at least the input files containing the structure of the material, the potential, the k-points that need to be sampled and a file containing different parameters specifying the details of the calculation.

Self consistent calculation This calculation is used to calculate the electronic ground state. The structure of a material should be used as input along with the other mandatory input files. VASP then calculates the electronic ground state properties of the material sampling the whole first Brillouin zone. The output contains but is not limited to the charge densities, the density of states and the energy eigenvalues.

Relaxation This technique is used to calculate the optimal structure. An educated guess of the structure is used as input. Then a self consistent calculation is done. VASP then varies the positions of the atoms and does another self consistent calculation, trying to minimize the force. Once a predefined threshold is reached the output contains the optimal structure.

Band structure calculation To calculate the band structure along a predefined path, the file containing the k-points has to list all of these k-points explicitly. Contrary to the self consistent calculation VASP then calculates the energy eigenvalues only at these k-points instead of the whole first Brillouin zone. To speed up the calculation the charge densities from the self consistent calculation should be used as input so that VASP can use these in it's calculations. The output contains the energy eigenvalues that can be used to plot the band structure.

The VASP calculations that were done to learn working with VASP had several results. First of all it was found in figure 53 that the size of the band gap decreases linearly with the lattice constant for diamond, silicon and germanium, all group IV elements. It was also found that for group IV, III-V and II-VI materials of the same period the lattice constant is almost the same while the band gap is biggest for group II-VI materials and smallest for group IV materials. More properties were calculated, like the most stable structure of an element, and the band structures and densities of states were plotted and analyzed.

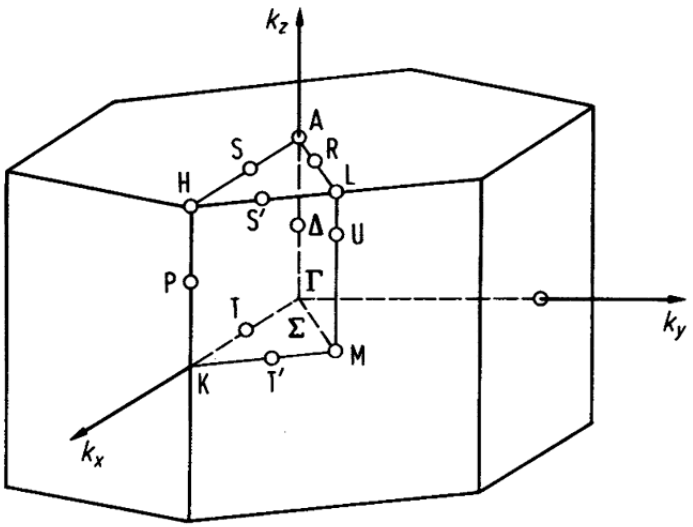

Figure 4: First Brillouin zone of a hexagonal lattice, showing the high symmetry points. [12]

Density of states

From the VASP output files the density of states can be determined. It can be used to easily see the band gap and show band widths. From the VASP output files also the projected density of states can be determined. The projected density of states shows the density of states for certain atoms, for example for one species of atoms. This is used in this research to see which bands are boron nitride bands, which are molybdenum disulfide bands and which are hybridized bands.

Band structure

The band structure can be calculated along certain high symmetry lines connecting high symmetry points using the output from VASP. The high symmetry points of a hexagonal lattice are shown in figure 4.

Results

The heterostructure described in the section Structure of the chapter Theoretical aspects has first been relaxed. Two guesses were made for the distance between the planes, namely 5.0 Å and 8.0 Å, so for the supercell we have $c = 10.0$ Å and $c = 16.0$ Å respectively. From there the relaxations were started and two different optimized structures were found of which the distance between the planes is shown in table 1.

A check was done to see if both structures are stable. For different values of c a self consistent calculation was done, from which the total energy was plotted. In figure 5 the total energy versus the distance between the planes is plotted. The highest total energy was set to zero, with the rest of the values in reference to this. In this figure one can see that there is actually just one stable structure, the one with a distance between the planes of 4.89 Å.

The other structure might be metastable. To check that the binding energies were calculated using equation (2). In table 1 the binding energies for the two solutions are shown. One can see that there is binding for both of the structures, although the structure with a distance of 4.89 Å between the planes has stronger binding. Therefore we conclude that the structure with a distance between the planes of 8.10 Å is a metastable structure.

Band structure calculations were done for the metastable structure. The results of these calculations are plotted in figure 6. In this figure also the character of the bands was plotted. All graphs have a different character of the bands plotted. The first one shows the molybdenum disulfide d_{xy} bands in red. The second one shows the molybdenum disulfide $d_{x^2-y^2}$ bands in magenta. The third one shows the nitrogen p_z bands in green. The Fermi level was set to zero in this figure, and is marked by the dotted line.

In this figure, one can see there is an direct band gap at K point where the top of the valence band is a band with nitrogen p_z character. The size of the band gap, extracted from this figure, is 1.83 eV.

Band structure calculations were also done for the stable structure, shown in figure 7. This figure also shows the character of the bands in three different graphs, again with the first one showing the molybdenum disulfide d_{xy} bands in red, the second one showing the molybdenum disulfide $d_{x^2-y^2}$ bands in magenta and the third one showing the nitrogen p_z bands in green. In this figure the Fermi level was again set to zero and marked by the dotted line.

Table 1: Distance between the planes and binding energy per molybdenum disulfide unit cell for two optimal structures found with the relaxation. There is stronger binding for the structure with a distance of 4.89 Å between the planes.

Distance between the planes [Å]	Binding energy per MoS_2 unit cell [eV]
4.89	-2.778
8.10	-2.634

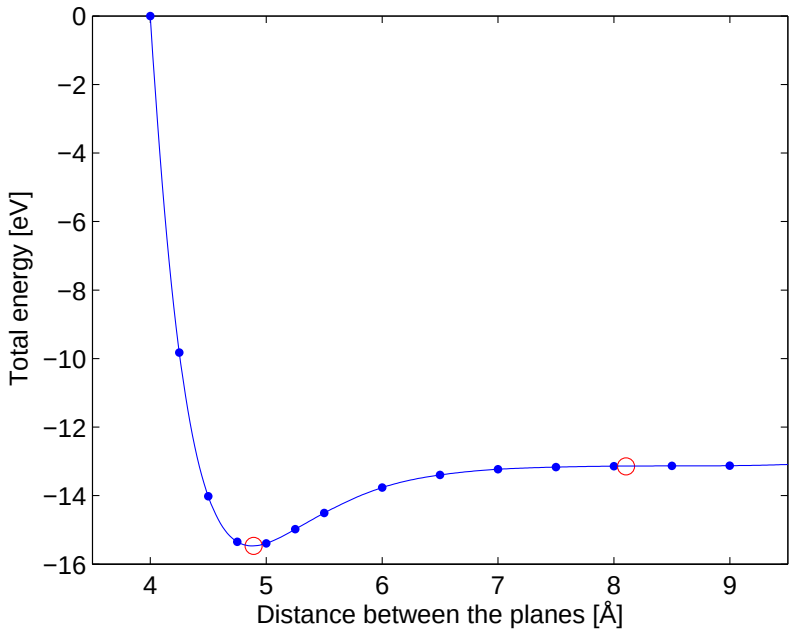

Figure 5: Total energy versus the distance between the planes. The highest total energy was set to zero and the rest of the values are in reference to this zero. The two structures that were found with the relaxation are marked by red circles. One can see that there is actually just one stable structure. The other structure might be metastable.

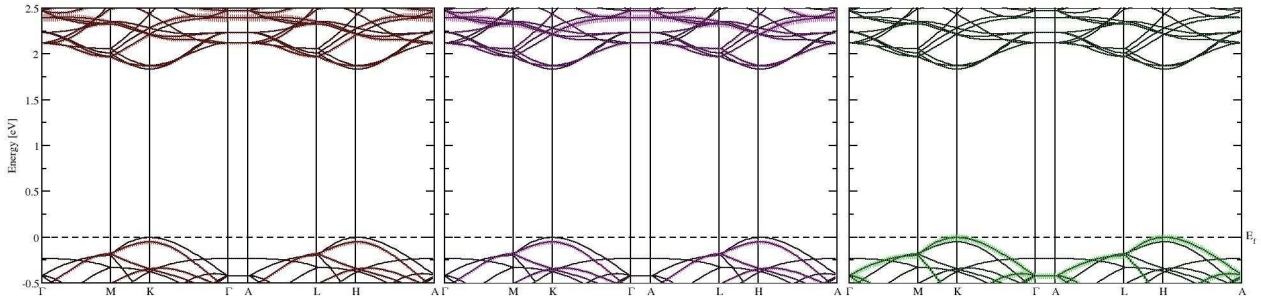

Figure 6: Region around the band gap for the heterostructure with a distance between the planes of 8.10 Å. The character of the bands is shown in the different graphs. The first one contains the molybdenum disulfide d_{xy} bands in red. The second one contains the molybdenum disulfide $d_{x^2-y^2}$ bands in magenta. The third one contains the nitrogen p_z bands in green.

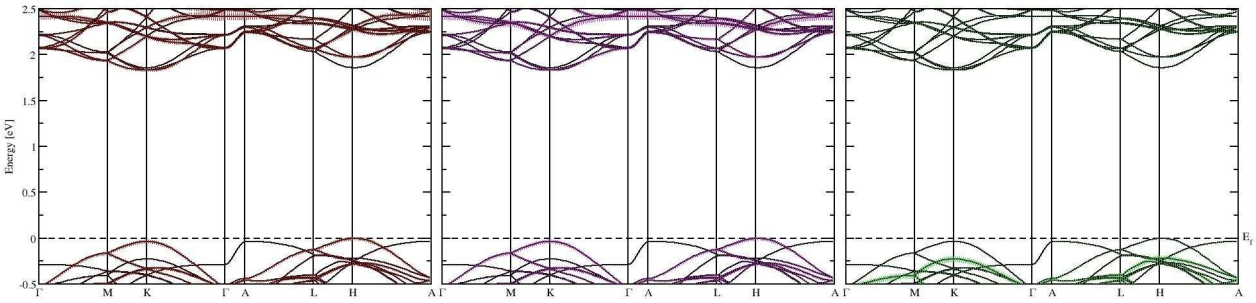

Figure 7: Region around the band gap for the heterostructure with a distance between the planes of 4.89 Å. The character of the bands is shown in the different graphs. The first one contains the molybdenum disulfide d_{xy} bands in red. The second one contains the molybdenum disulfide $d_{x^2-y^2}$ bands in magenta. The third one contains the nitrogen p_z bands in green.

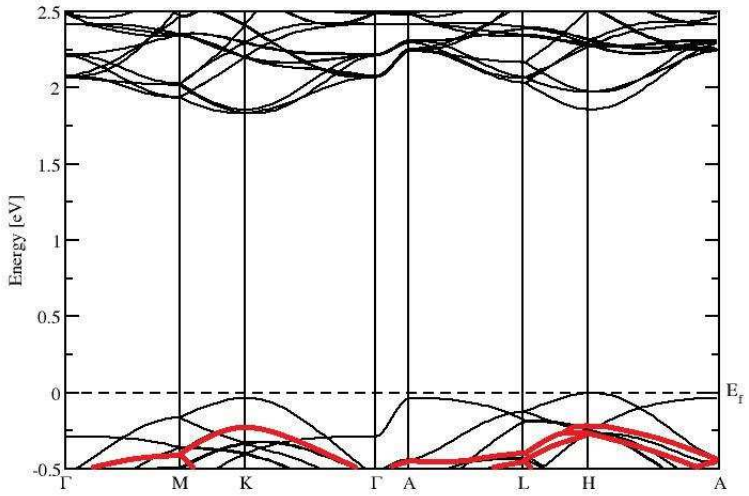

Figure 8: Band structure in the energy range around the band gap for the stable heterostructure. The Fermi level is set to zero and marked by a dotted line. The bands marked in red are the bands that are not visible in the band structure of isolated molybdenum disulfide.

One can see in figure 7 that the direct band gap has become an indirect gap between H and K. The band with p_z character that was at the top of the valence band for the metastable structure has actually shifted down a lot. The top of the valence band now consists of bands with a lot of molybdenum disulfide d character.

To get a better understanding as to why the band with nitrogen p_z character has shifted down, the band structure for the stable structure was plotted in figure 8. Also, the bands structure for isolated molybdenum disulfide of the stable structure has been plotted in figure 9. In both figures again the Fermi energy was set to zero and marked by a dotted line. The bands that are not visible in the bands structure for isolated molybdenum disulfide have been marked red in figure 8. Since they aren't visible in the band structure for isolated molybdenum disulfide, and they have a lot of nitrogen p_z character, these bands are predominantly boron nitride bands, which suggests that the change from a direct to an indirect band gap for the metastable structure to the stable structure is due to hybridization. Also, the top of the valence band has moved up a little, so the direct band gap at K is of the same size as the direct band gap at H.

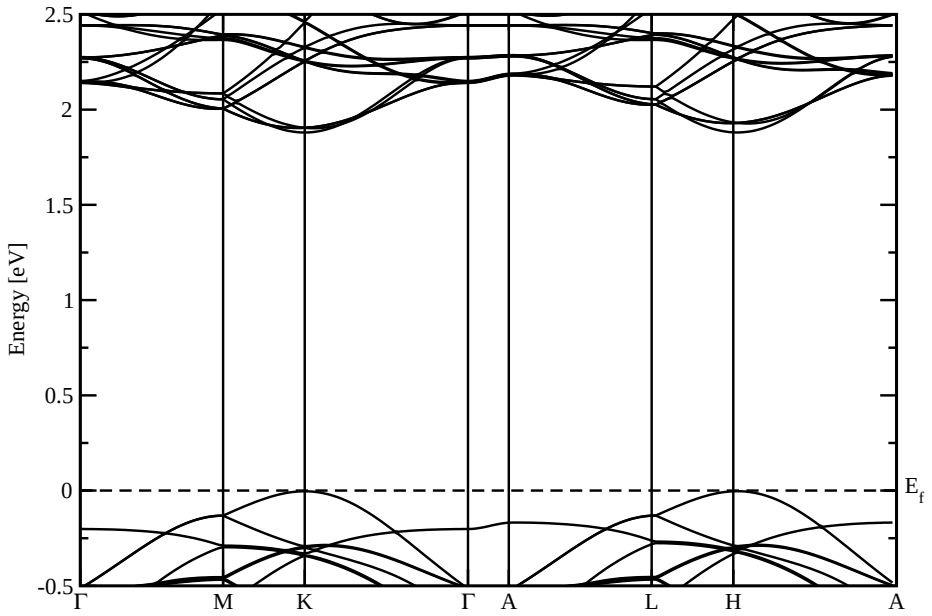

Figure 9: Band structure in the energy range around the band gap for isolated molybdenum disulfide from the stable structure. The Fermi level is set to zero and marked by a dotted line.

To visualize the hybridization the projected density of states for the boron nitride bands and the molybdenum disulfide bands was calculated for the stable structure. The projected density of states is plotted in figure 10. This figure shows that the top of the valence band consists of hybridized boron nitride - molybdenum disulfide bands.

Also from figure 10 the band gap can be determined. The size of the band gap is 1.83 eV, the same as for the metastable structure. The bottom of the conduction band consists of solely molybdenum disulfide bands. The boron nitride bands start from 3.9 eV above the Fermi level.

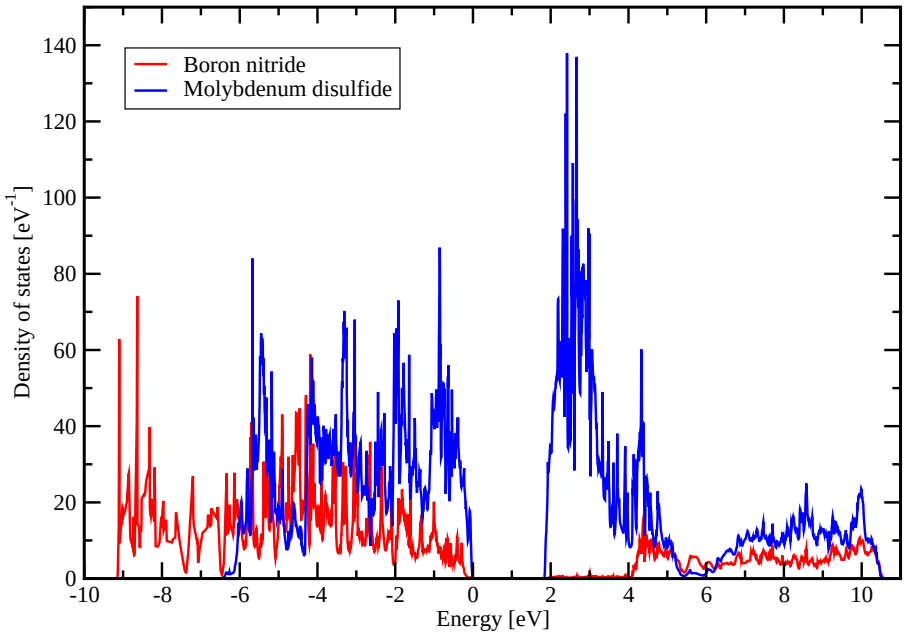

Figure 10: Density of states of the heterostructure projected onto the boron nitride part and the molybdenum disulfide part are shown using red and blue lines respectively.

Discussion

A stable structure with a distance between the planes of 4.89 Å was found. A stable structure was expected, since there was nothing suggesting there wouldn't be one. The strain is 0.16%, and both materials have a hexagonal structure. Also a metastable structure with a distance between the planes of 8.10 Å was found.

Comparing figures 6 and 7 one can notice that the band gap changes from an indirect to a direct band gap if the distance between the layers is increased. This is probably because when the distances between two layers is increased, there is less overlap between the wave functions of these layers. Therefore, there is less hybridization and the band with nitrogen p_z character makes up the top of the valence band.

This can also be seen in figures 8 and 9. The top valence band at K-point in isolated molybdenum disulfide is still the top valence band at K-point in the heterostructure, however it's not the general top of the valence band anymore. It has probably shifted a little because of hybridization due to the layer of boron nitride in between.

In figure 10 one can also see that the top of the valence band consists of hybridized molybdenum disulfide and boron nitride bands, although the number of molybdenum disulfide states is higher. Since the band gap of boron nitride is bigger then that of molybdenum disulfide [13] [2] one would expect the bottom of the conduction band to be just molybdenum disulfide bands, as is the case in figure 10.

Also, the change in the band gap from direct to indirect for the metastable structure to the stable structure cannot be due to the molybdenum disulfide layers interacting as in the bulk matrial. Bulk molybdenum disulfide has the top of the valence band at gamma which is clearly not the case in figure 8. [14]

Along the path Γ-A the bands move up in energy as can be seen in figure 8. The difference in energy between Γ and A gets smaller for bands that are higher in energy. This can be explained by looking at the extent of the wave functions. Wave functions for bands with a higher energy have a smaller barrier to the vacuum level. Therefore these wave functions have a larger extent and the slope of the energy band is smaller.

The size of the band gap is found to be 1.83 eV, for the stable as well as the metastable structure. For a monolayer of molybdenum disulfide the band gap is 1.8 eV [2]. Similar values have been found with DFT calculations. It seems that the band gap is therefore not underestimated by DFT.

Conclusion

The main question posed in the introduction was if hexagonal boron nitride is a suitable candidate as a substrate for a monolayer of molybdenum disulfide. We found first of all that there is one stable structure consisting of a monolayer of hexagonal boron nitride and a monolayer of molybdenum disulfide, with a distance between the planes of 4.89 Å. We also found a metastable structure with a distance between the planes of 8.10 Å.

We found that the direct band gap of a monolayer of molybdenum disulfide does not stay direct for the stable structure. The top of the valence band in isolated molybdenum disulfide moves down a little so an indirect band gap is created between the high symmetry points H and K. This was explained as an effect of hybridization.

From the projected density of states we know that the size of the band gap is 1.83 eV, which matches the size of the band gap for a monolayer of molybdenum disulfide. We know the band gap for the metastable structure, which is also 1.83 eV, from the band structure calculation.

In the heterostructure we saw bands with nitrogen p_z character which weren't visible in the band structure of isolated molybdenum disulfide. We found that for the structure with a distance between the planes of 8.10 eV this band moves up to create a direct band gap at the high symmetry K point.

We can conclude that hexagonal boron nitride in fact is a suitable candidate as a substrate for a monolayer of molybdenum disulfide. However, for a monolayer of molybdenum disulfide on top of a monolayer of hexagonal boron nitride the band gap becomes indirect for the stable structure. It does stay direct for the metastable structure.

Possibilities for future research

In the future tight binding calculations can be done for the hybridization of p and d orbitals from K to H to get more insight as to why the bands shift and the band gap becomes indirect between H and K.

One of the possibilities may be to see what happens if there are more layers of boron nitride. This might lead to the formation of a stable structure with a direct band gap, which is interesting for opto-electronic applications.

A final improvement could be to increase the accuracy of the calculations. Different potentials could be used as well as hybrid-functionals.

Bibliography

[1] A. K. Geim, *Graphene: Status and Prospects*, Science **324**, 1530 (2009).

[2] K. F. Mak, C. Lee, J. Hone, J. Shan, and T. F. Heinz, *Atomically Thin MoS_2: A New Direct-Gap Semiconductor*, Physical Review Letters **105**, 136805 (2010).

[3] T. Cao, G. Wang, W. Han, H. Ye, C. Zhu, J. Shi, Q. Niu, P. Tan, E. Wang, B. Liu, and J. Feng, *Valley-selective circular dichroism of monolayer molybdenum disulphide*, Nature communications **3**, 887 (2012).

[4] G. Kresse and J. Hafner, *Ab initio molecular dynamics for liquid metals*, Physical Review B **47**, 558 (1993).

[5] G. Kresse and J. Furthmüller, *Efficient iterative schemes for ab initio total-energy calculations using a plane-wave basis set*, Physical Review B **54**, 11169 (1996).

[6] N. W. Ashcroft and N. D. Mermin, *Solid State Physics*, college ed. (Thomson Learning, Inc., Berkshire House, 168-173 High Holborn, London WC1 V7AA, United Kingdom, 1976).

[7] W. Kohn, "Electronic structure of matter - wave functions and density functionals," http://www.nobelprize.org/nobel_prizes/chemistry/laureates/1998/kohn-lecture.pdf (1999), Nobel Lecture.

[8] J. Hafner, "Foundations of density functional theory," https://www.vasp.at/vasp-workshop/slides/dft_introd.pdf.

[9] N. D. Drummond, V. Zólyomi, and V. I. Fal'ko, "Electronic structure of two-dimensional crystals of hexagonal boron nitride," http://www.tcm.phy.cam.ac.uk/~mdt26/tti_talks/qmcitaa_13/drummond_tti2013.pdf (2013).

[10] S. Majety, J. Li, X. K. Cao, R. Dahal, J. Y. Lin, and H. X. Jiang, *Metal-semiconductor-metal neutron detectors based on hexagonal boron nitride epitaxial layers*, Proc. SPIE **8507**, 85070R (2012).

[11] K. Momma and F. Izumi, *VESTA 3 for three-dimensional visualization of crystal, volumetric and morphology data*, Journal of Applied Crystallography **44**, 1272 (2011).

[12] "Brillouin zone of the hexagonal lattice," http://www.ioffe.ru/SVA/NSM/Semicond/Append/figs/fmd21_5.gif.

[13] M. Bernardi, M. Palummo, and J. C. Grossman, *Optoelectronic Properties in Monolayers of Hybridized Graphene and Hexagonal Boron Nitride*, Physical Review Letters **108**, 226805 (2012).

[14] E. Cappelluti, R. Roldán, J. A. Silva-Guillén, P. Ordejón, and F. Guinea, *Tight-binding model and direct-gap/indirect-gap transistion in single-layer and multilayer MoS_2*, Physical Review B **88**, 075409 (2013).

[15] D. J. Griffiths, *Introduction to Quantum Mechanics*, second international ed. (Pearson Education, Inc., Upper Saddle River, NJ 07458, USA, 2005).

[16] "P-orbitals," http://www.sparknotes.com/chemistry/fundamentals/atomicstructure/section1.rhtml.

[17] D. Glötzel, B. Segall, and O. Andersen, *Self-consistent electronic structure of Si, Ge and diamond by the LMTO-ASA method*, Solid State Communications **36**, 403 (1980).

[18] *Wide Bandgap Semiconductors: Pursuing the Promise*, Tech. Rep. (U.S. Department of Energy, 2013).

[19] K. Kobayashi, "Graphite band structure," http://www.bandstructure.jp/Table/BAND/Graph.html ().

[20] D. D. L. Chung, *Review Graphite*, Journal of Materials Science **37**, 1475 (2002).

[21] C. Kittel, *Introduction to Solid State Physics*, eighth ed. (John Wiley & Sons, Inc, 111 River Street, Hoboken, NJ 07030-5774, 2005).

[22] N. A. Abdulkareem and B. H. Elias, *First Principle Band Structure Calculations of Zinc-Blende BN and GaN Compounds*, International Journal of Scientific & Engineering Research **4** (2013).

[23] R. M. Chrenko, *Ultraviolet and infrared spectra of cubic boron nitride*, Solid State Communications **14**, 511 (1974).

[24] K. Kobayashi, "wBN band structure," http://www.bandstructure.jp/Table/BAND/band_png/wBN.png ().

[25] Y.-N. Xu and W. Y. Ching, *Calculation of ground-state and optical properties of boron nitrides in the hexagonal, cubic, and wurtzite structures*, Physical Review B **44**, 7787 (1991).

[26] K. Kobayashi, "hBN band structure," http://www.bandstructure.jp/Table/BAND/band_png/hBN_bh_P_0G.png ().

[27] X. Blase, A. Rubio, S. G. Louie, and M. L. Cohen, *Quasiparticle band structure of bulk hexagonal boron nitride and related systems*, Physical Review B **51**, 6868 (1995).

[28] A. Saliev, "Electronic properties of aluminium phosphide," http://www.institute.loni.org/lasigma/reu/documents/presentations2013/IsaacSaliev_FinalPresentation.pdf (2013).

[29] R. Ahmed, Fazal-e-Aleem, S. J. Hashemifar, and H. Akbarzadeh, *First-principles study of the structural and electronic properties of III-phosphides*, Physica B: Condensed Matter **403**, 1876 (2008).

[30] A. J. Danner, "An introduction to the empirical pseudopotential mehtod," http://www.ece.nus.edu.sg/stfpage/eleadj/pseudopotential.htm (2011).

[31] J. E. Bernard and A. Zunger, *Electronic structure of ZnS, ZnSe, ZnTe, and their pseudobinary alloys*, Physical Review B **36**, 3199 (1987).

[32] O. Zakharov, A. Rubio, X. Blase, M. L. Cohen, and S. G. Louie, *Quasiparticle band structures of six II-VI compounds: ZnS, ZnSe, ZnTe, CdS, CdSe, and CdTe*, Physical Review B **50**, 10780 (1994).

Appendices

Appendix 1 - Assignments

Assignment 1 - Radial Schrödinger Equation

For this assignment, the radial Schrödinger Equation will be solved numerically for a Coulomb potential. The energies of the bound states (1s, 2s, 3s; 2p, 3p) of hydrogen will be found, as well as the corresponding eigenfunctions.

The differential equation for the radial wave function is:

$$\frac{d^2u}{d\rho^2} = [1 - \frac{\rho_0}{\rho} + \frac{l(l+1)}{\rho^2}]u = f(\rho)u \tag{3}$$

[15]

with $\rho \equiv \kappa r$, $\rho_0 \equiv \frac{me^2}{2\pi\epsilon_0\hbar^2\kappa}$ and $\kappa \equiv \frac{\sqrt{-2mE}}{\hbar}$.

Because the equation is solved numerically, the following formula was used:

$$u_{i+1} = 2u_i - u_{i-1} + f(\rho)u_i(\Delta\rho)^2 \tag{4}$$

The strategy is to integrate the radial equation outwards from the origin and inwards from ∞. For the outwards integration the asymptotic form for $\rho \to 0$ was used:

$$u(\rho) \sim C\rho^{l+1} \tag{5}$$

[15]

Then equation (4) was used to calcualate the rest of the terms.

For the inwards integration the asymptotic form for $\rho \to \infty$ was used:

$$u(\rho) \sim Ae^{-\rho} \tag{6}$$

[15]

The two wavefunctions were matched at a turning point. In this case the point where the energy is equal to the potential energy was chosen, so that is:

$$E = -\frac{e^2}{4\pi\epsilon_0}\frac{1}{r} = -\frac{e^2}{4\pi\epsilon_0}\frac{\kappa}{\rho_{tp}} \to \rho_{tp} = -\frac{e^2\kappa}{4\pi\epsilon_0 E} \tag{7}$$

The matching was done by multiplying the inward integrated function with a constant so that the value of the wavefunction would be equal at the turning point ρ_{tp}. Then, the resulting wavefunction was normalized.

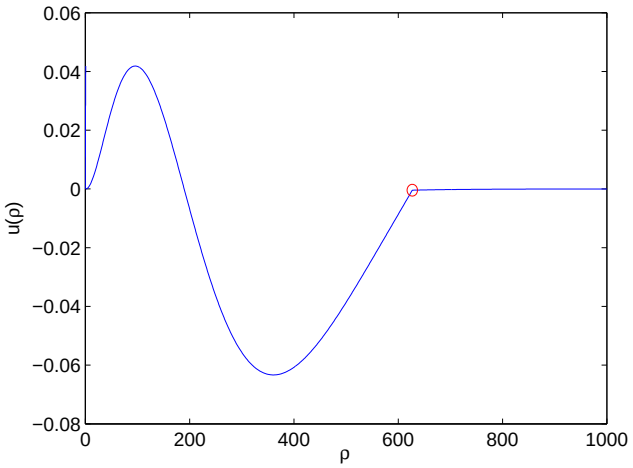

Figure 11: Example of a kink at the point where the wavefunctions were matched. The kink is marked in red. The solution was found for $l = 0$ and $n = 3$.

The principal quantum number n was determined by counting the number of nodes, that is the number of crossings of the x-axis, using $\#_{nodes} = n - l - 1 \Rightarrow n = \#_{nodes} + l + 1$.

One starts with choosing an energy E, an angular momentum l and a principal quantum number. Then, after calculating what the principal quantum number of the found solution is, change the energy until the correct solution is found.

The found solution still contains a kink, that is a point wich isn't differentiable, at the turning point where the wavefunctions were matched. An example of such a kink can be seen in figure 11. At the point marked in figure 11 the wavefunction is continuous but not differentiable. The solution for the eigenenergy won't contain a kink. Therefore, the kink should be reduced by making small changes in the eigenenergies. This way the eigenenergy can be found. The found solution still contains a kink, that is a point wich isn't differentiable, at the turning point where the wavefunctions were matched. An example of such a kink can be seen in figure 11. At the point marked in figure 11 the wavefunction is continuous but not differentiable. The solution for the eigenenergy won't contain a kink. Therefore, the kink should be reduced by making small changes in the eigenenergies. This way the eigenenergy can be found. The found solution still contains a kink, that is a point wich isn't differentiable, at the turning point where the wavefunctions were matched. An example of such a kink can be seen in figure 11. At the point marked in figure 11 the wavefunction is continuous but not differentiable. The solution for the eigenenergy won't contain a kink. Therefore, the kink should be reduced by making small changes in the eigenenergies. This way the eigenenergy can be found.

However, this program is not the best at finding the exact energies for the bound states. The program will scan a whole energy range looking for only one solution. Then it repeats itself with a smaller energy step value until the desired accuracy of the solution is reached. Finding the eigenenergies with high accuracy takes too long.

To solve the problems mentioned above a different program was made wich calculates the energies where the kink is zero. It determines the size of the kink for different energies and then interpolates to find the energy where there is no kink. This can be seen in figure 12, where plots of the energy vs. the size of the kink are shown. In these plots, every x-axis crossing is an eigenenergy.

This program also calculates the wavefunction for $n = 1, 2, 3$. The program does this for $l = 0$

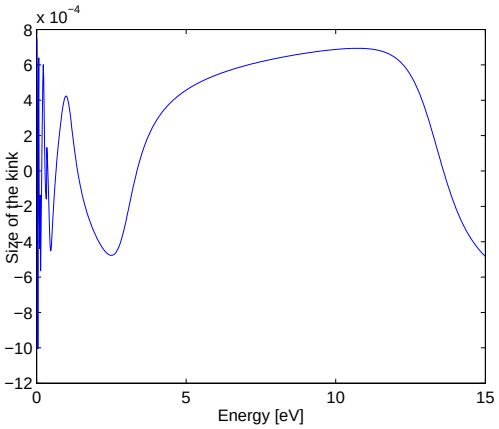

(a) Energy vs. kink size plot for l = 0

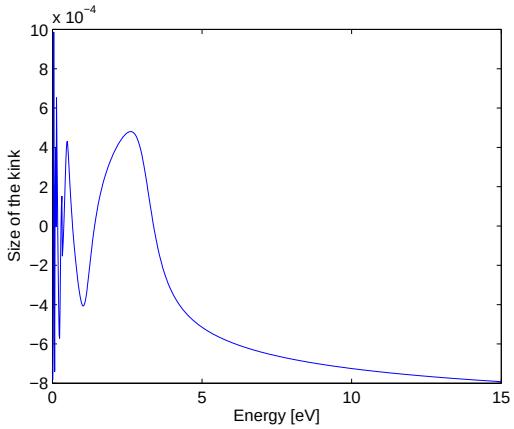

(b) Energy vs. kink size plot for l = 1

Figure 12: Energy vs. kink size plots.

(figure 13a) and for $l = 1$ (figure 13b). These plots contain the eigenfunctions of the bound states 1s, 2s, 3s, 2p & 3p of hydrogen.

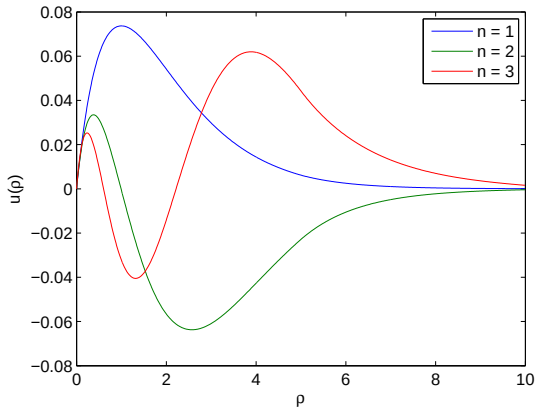

(a) Radial wave functions for l = 0, n = 1..3

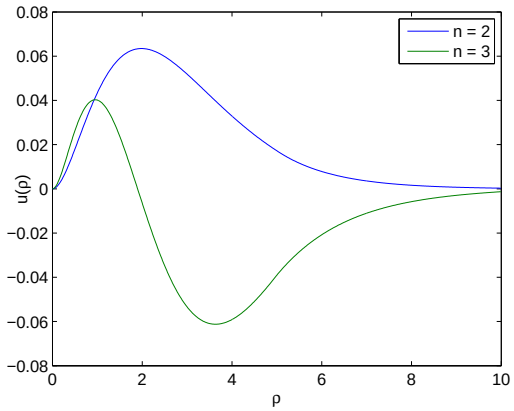

(b) Radial wave function for l = 1, n = 2, 3

Figure 13: Radial wave functions.

The energies of these bound states were determined by finding the x-axis crossings in the plots in figure 12. They are $E_{1s} = -12.5625$ eV, $E_{2s} = -3.2025$ eV, $E_{3s} = -1.4475$ eV, $E_{2p} = -3.3075$ eV and $E_{3p} = -1.4625$ eV.

Solving the problem analytically gives us:

$$E_n = -[\frac{m}{2\hbar^2}(\frac{e^2}{4\pi\epsilon_0})^2]\frac{1}{n^2} \tag{8}$$

[15]

So the analytical solved values for the energies are $E_1 = -13.6058$ eV, $E_2 = -3.4015$ eV and $E_3 = -1.5118$ eV.

The numerical solutions above are not exact, although they are better then the results found with the first program, wich gave, for example, $E_1 = -12.2800$ eV. To get better results, some of the parameters had to be adjusted. Options were the value of $\Delta\rho$, the total number of points N and the number of steps of the energy, E_{steps}.

Increasing E_{steps} and thus decreasing the step size of the energy did not yield better results. Therefore, $\Delta\rho$ and N had to be adjusted. N should be chosen large enough get the necessary range of ρ. However, a smaller $\Delta\rho$ did also not yield better results.

A different option was changing the turning point. The definition of the turning point was changed to be $N/2$. With this turning point, the energies $E_{1s} = -13.5975$ eV, $E_{2s} = -3.3525$ eV, $E_{3s} = -1.3725$ eV, $E_{2p} = -3.3825$ eV, $E_{3p} = -1.4025$ eV were found. These were the best results acquired.

Assignment 2 - Tight binding

This section contains the solutions to the tight binding assignments from the Theoretical Solid State Physics course.

1. Linear H_3

(a) The value of β is not the same for all three atoms, since the atom in the middle has two atoms around it.

(b) Considering that the atom in the middle has two atoms around it we have:

$$\begin{aligned}\langle\psi\,|\,H\,|\,\psi\rangle &= |a_1|^2(\varepsilon-\beta) - a_1^* a_2 t - a_2^* a_1 t + |a_2|^2(\varepsilon-2\beta) - a_2^* a_3 t - a_3^* a_2 t + |a_3|^2(\varepsilon-\beta)\\ \langle\psi\,|\,H\,|\,\psi\rangle &= |a_1|^2\varepsilon' - a_1^* a_2 t - a_2^* a_1 t + |a_2|^2\varepsilon'' - a_2^* a_3 t - a_3^* a_2 t + |a_3|^2\varepsilon'\end{aligned} \tag{9}$$

with $\varepsilon' = \varepsilon - \beta$ and $\varepsilon'' = \varepsilon - 2\beta$

The equation to solve therefore becomes:

$$\begin{vmatrix}\varepsilon'-E & -t & 0\\ -t & \varepsilon''-E & -t\\ 0 & -t & \varepsilon'-E\end{vmatrix} = 0 \tag{10}$$

Finding a solutions gives us:

$$\begin{aligned}(\varepsilon'-E)[(\varepsilon''-E)(\varepsilon'-E)-t^2] - t^2(\varepsilon'-E) &= 0\\ (\varepsilon'-E)[(\varepsilon''-E)(\varepsilon'-E)-2t^2] &= 0\\ E = \varepsilon' \vee (\varepsilon''-E)(\varepsilon'-E) - 2t^2 &= 0\\ E = \varepsilon' \vee E^2 - (\varepsilon'+\varepsilon'')E + \varepsilon'\varepsilon'' - 2t^2 &= 0\\ E = \varepsilon' \vee E = \frac{1}{2}(\varepsilon'+\varepsilon'') \pm \frac{1}{2}\sqrt{(\varepsilon'-\varepsilon'')^2 - 4(\varepsilon'\varepsilon''-2t^2)}\end{aligned} \tag{11}$$

Finding a solution for the energy is a lot harder but in this case still doable. One can imagine that calculating the wave functions would be even harder. Simplifying the algebra by taking β the same for all three atoms makes this a lot easier to do.

(c) For $E = \varepsilon'$ we have

$$\begin{aligned}
\begin{bmatrix} 0 & -t & 0 \\ -t & 0 & -t \\ 0 & -t & 0 \end{bmatrix} \begin{bmatrix} a_1 \\ a_2 \\ a_3 \end{bmatrix} &= \begin{bmatrix} 0 \\ 0 \\ 0 \end{bmatrix} \\
\begin{bmatrix} -t & 0 & -t \\ 0 & -t & 0 \\ 0 & 0 & 0 \end{bmatrix} \begin{bmatrix} a_1 \\ a_2 \\ a_3 \end{bmatrix} &= \begin{bmatrix} 0 \\ 0 \\ 0 \end{bmatrix} \\
\begin{bmatrix} 1 & 0 & 1 \\ 0 & 1 & 0 \\ 0 & 0 & 0 \end{bmatrix} \begin{bmatrix} a_1 \\ a_2 \\ a_3 \end{bmatrix} &= \begin{bmatrix} 0 \\ 0 \\ 0 \end{bmatrix}
\end{aligned} \tag{12}$$

thus the eigenvector for $E = \varepsilon'$ is $\frac{1}{\sqrt{2}} \begin{bmatrix} 1 \\ 0 \\ -1 \end{bmatrix}$ and the wavefunction is

$$\psi_A(\boldsymbol{r}) = \frac{1}{\sqrt{2}}[\phi(\boldsymbol{r} - \boldsymbol{R_1}) - \phi(\boldsymbol{r} - \boldsymbol{R_3})] \tag{13}$$

For $E = \varepsilon' + \sqrt{2}t$ we have

$$\begin{aligned}
\begin{bmatrix} -\sqrt{2}t & -t & 0 \\ -t & -\sqrt{2}t & -t \\ 0 & -t & -\sqrt{2}t \end{bmatrix} \begin{bmatrix} a_1 \\ a_2 \\ a_3 \end{bmatrix} &= \begin{bmatrix} 0 \\ 0 \\ 0 \end{bmatrix} \\
\begin{bmatrix} -\sqrt{2}t & -t & 0 \\ 0 & -\frac{1}{2}\sqrt{2}t & -t \\ 0 & -t & -\sqrt{2}t \end{bmatrix} \begin{bmatrix} a_1 \\ a_2 \\ a_3 \end{bmatrix} &= \begin{bmatrix} 0 \\ 0 \\ 0 \end{bmatrix} \\
\begin{bmatrix} -\sqrt{2}t & -t & 0 \\ 0 & -\frac{1}{2}\sqrt{2}t & -t \\ 0 & 0 & 0 \end{bmatrix} \begin{bmatrix} a_1 \\ a_2 \\ a_3 \end{bmatrix} &= \begin{bmatrix} 0 \\ 0 \\ 0 \end{bmatrix} \\
\begin{bmatrix} -\sqrt{2}t & -t & 0 \\ 0 & 1 & \sqrt{2} \\ 0 & 0 & 0 \end{bmatrix} \begin{bmatrix} a_1 \\ a_2 \\ a_3 \end{bmatrix} &= \begin{bmatrix} 0 \\ 0 \\ 0 \end{bmatrix} \\
\begin{bmatrix} -\sqrt{2}t & 0 & \sqrt{2}t \\ 0 & 1 & \sqrt{2} \\ 0 & 0 & 0 \end{bmatrix} \begin{bmatrix} a_1 \\ a_2 \\ a_3 \end{bmatrix} &= \begin{bmatrix} 0 \\ 0 \\ 0 \end{bmatrix} \\
\begin{bmatrix} 1 & 0 & -1 \\ 0 & 1 & \sqrt{2} \\ 0 & 0 & 0 \end{bmatrix} \begin{bmatrix} a_1 \\ a_2 \\ a_3 \end{bmatrix} &= \begin{bmatrix} 0 \\ 0 \\ 0 \end{bmatrix}
\end{aligned} \tag{14}$$

thus the eigenvector for $E = \varepsilon' + \sqrt{2}t$ is $\frac{1}{2} \begin{bmatrix} 1 \\ -\sqrt{2} \\ 1 \end{bmatrix}$ and the wavefunction is

$$\psi_B(\boldsymbol{r}) = \frac{1}{2}[\phi(\boldsymbol{r} - \boldsymbol{R_1}) - \sqrt{2}\phi(\boldsymbol{r} - \boldsymbol{R_2}) + \phi(\boldsymbol{r} - \boldsymbol{R_3})] \tag{15}$$

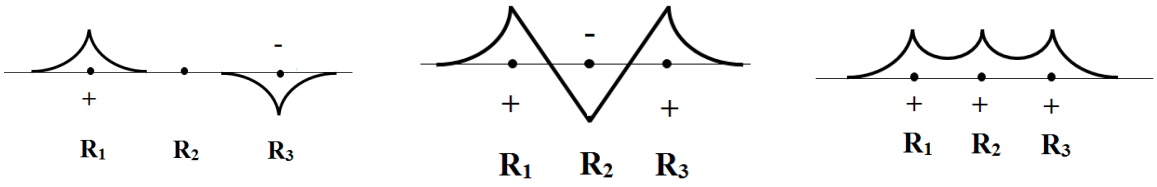

(a) Sketch of ψ_A.

(b) Sketch of ψ_B.

(c) Sketch of ψ_C.

Figure 14: Sketches of the wave functions of a linear H_3 molecule chain.

For $E = \varepsilon' - \sqrt{2}t$ we have

$$\begin{bmatrix} \sqrt{2}t & -t & 0 \\ -t & \sqrt{2}t & -t \\ 0 & -t & \sqrt{2}t \end{bmatrix} \begin{bmatrix} a_1 \\ a_2 \\ a_3 \end{bmatrix} = \begin{bmatrix} 0 \\ 0 \\ 0 \end{bmatrix}$$
$$\begin{bmatrix} \sqrt{2}t & -t & 0 \\ 0 & \frac{1}{2}\sqrt{2}t & -t \\ 0 & -t & \sqrt{2}t \end{bmatrix} \begin{bmatrix} a_1 \\ a_2 \\ a_3 \end{bmatrix} = \begin{bmatrix} 0 \\ 0 \\ 0 \end{bmatrix}$$
$$\begin{bmatrix} \sqrt{2}t & -t & 0 \\ 0 & \frac{1}{2}\sqrt{2}t & -t \\ 0 & 0 & 0 \end{bmatrix} \begin{bmatrix} a_1 \\ a_2 \\ a_3 \end{bmatrix} = \begin{bmatrix} 0 \\ 0 \\ 0 \end{bmatrix}$$
$$\begin{bmatrix} \sqrt{2}t & -t & 0 \\ 0 & 1 & -\sqrt{2} \\ 0 & 0 & 0 \end{bmatrix} \begin{bmatrix} a_1 \\ a_2 \\ a_3 \end{bmatrix} = \begin{bmatrix} 0 \\ 0 \\ 0 \end{bmatrix} \tag{16}$$
$$\begin{bmatrix} \sqrt{2}t & 0 & -\sqrt{2}t \\ 0 & 1 & -\sqrt{2} \\ 0 & 0 & 0 \end{bmatrix} \begin{bmatrix} a_1 \\ a_2 \\ a_3 \end{bmatrix} = \begin{bmatrix} 0 \\ 0 \\ 0 \end{bmatrix}$$
$$\begin{bmatrix} 1 & 0 & -1 \\ 0 & 1 & -\sqrt{2} \\ 0 & 0 & 0 \end{bmatrix} \begin{bmatrix} a_1 \\ a_2 \\ a_3 \end{bmatrix} = \begin{bmatrix} 0 \\ 0 \\ 0 \end{bmatrix}$$

thus the eigenvector for $E = \varepsilon' - \sqrt{2}t$ is $\frac{1}{2}\begin{bmatrix} 1 \\ \sqrt{2} \\ 1 \end{bmatrix}$ and the wavefunction is

$$\psi_C(\boldsymbol{r}) = \frac{1}{2}[\phi(\boldsymbol{r} - \boldsymbol{R_1}) + \sqrt{2}\phi(\boldsymbol{r} - \boldsymbol{R_2}) + \phi(\boldsymbol{r} - \boldsymbol{R_3})] \tag{17}$$

All the three wave functions ψ_A, ψ_B and ψ_C are sketched in figure 14.

2. Linear H_4 A linear chain of four hydrogen atoms is considered, as drawn in figure 15. The equation that needs to be solved is

$$\begin{vmatrix} \varepsilon' - E & -t & 0 & 0 \\ -t & \varepsilon' - E & -t & 0 \\ 0 & -t & \varepsilon' - E & -t \\ 0 & 0 & -t & \varepsilon' - E \end{vmatrix} = 0 \tag{18}$$

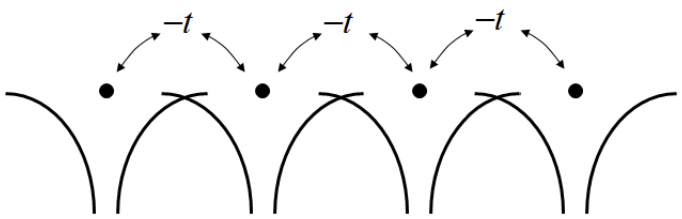

Figure 15: Linear chain of 4 hydrogen atoms spaced equally apart. The -t between the atoms represents the hopping element.

which gives

$$
\begin{aligned}
(\varepsilon' - E)\begin{vmatrix} \varepsilon' - E & -t & 0 \\ -t & \varepsilon' - E & -t \\ 0 & -t & \varepsilon' - E \end{vmatrix} + t\begin{vmatrix} -t & -t & 0 \\ 0 & \varepsilon' - E & -t \\ 0 & -t & \varepsilon' - E \end{vmatrix} &= 0 \\
(\varepsilon' - E)^2[(\varepsilon' - E)^2 - 2t^2] - t^2[(\varepsilon' - E)^2 - t^2] &= 0 \\
(\varepsilon' - E)^2[(\varepsilon' - E)^2 - 3t^2] + t^4 &= 0 \\
(\varepsilon' - E)^4 - 3t^2(\varepsilon' - E)^2 + t^4 &= 0 \\
(\varepsilon' - E)^2 &= \frac{3t^2 \pm t^2\sqrt{5}}{2} \\
(\varepsilon' - E) &= \pm t\sqrt{\frac{1}{2}(3 \pm \sqrt{5})} \\
E &= \varepsilon' \pm c^{\pm}t
\end{aligned}
\tag{19}
$$

where $c^{\pm} = \sqrt{\frac{1}{2}(3 \pm \sqrt{5})}$

To find the eigenvectors we solve:

$$
\begin{bmatrix} \varepsilon' - E & -t & 0 & 0 \\ -t & \varepsilon' - E & -t & 0 \\ 0 & -t & \varepsilon' - E & -t \\ 0 & 0 & -t & \varepsilon' - E \end{bmatrix} \begin{bmatrix} a_1 \\ a_2 \\ a_3 \\ a_4 \end{bmatrix} = \begin{bmatrix} 0 \\ 0 \\ 0 \\ 0 \end{bmatrix} \tag{20}
$$

So for $E_{++} = \varepsilon' + c^+ t$ we have:

$$
\begin{bmatrix} -c^+t & -t & 0 & 0 \\ -t & -c^+t & -t & 0 \\ 0 & -t & -c^+t & -t \\ 0 & 0 & -t & -c^+t \end{bmatrix} \begin{bmatrix} a_1 \\ a_2 \\ a_3 \\ a_4 \end{bmatrix} = \begin{bmatrix} 0 \\ 0 \\ 0 \\ 0 \end{bmatrix}
$$

$$
\begin{bmatrix} -c^+t & -t & 0 & 0 \\ 0 & -t & -t & 0 \\ 0 & -t & -c^+t & -t \\ 0 & 0 & -t & -c^+t \end{bmatrix} \begin{bmatrix} a_1 \\ a_2 \\ a_3 \\ a_4 \end{bmatrix} = \begin{bmatrix} 0 \\ 0 \\ 0 \\ 0 \end{bmatrix}
$$

$$
\begin{bmatrix} -c^+t & -t & 0 & 0 \\ 0 & -t & -t & 0 \\ 0 & 0 & -c^-t & -t \\ 0 & 0 & -t & -c^+t \end{bmatrix} \begin{bmatrix} a_1 \\ a_2 \\ a_3 \\ a_4 \end{bmatrix} = \begin{bmatrix} 0 \\ 0 \\ 0 \\ 0 \end{bmatrix}
$$

$$
\begin{bmatrix} -c^+t & -t & 0 & 0 \\ 0 & -t & -t & 0 \\ 0 & 0 & -c^-t & -t \\ 0 & 0 & 0 & 0 \end{bmatrix} \begin{bmatrix} a_1 \\ a_2 \\ a_3 \\ a_4 \end{bmatrix} = \begin{bmatrix} 0 \\ 0 \\ 0 \\ 0 \end{bmatrix}
$$

$$
\begin{bmatrix} -c^+t & -t & 0 & 0 \\ 0 & -t & 0 & c^+t \\ 0 & 0 & -c^-t & -t \\ 0 & 0 & 0 & 0 \end{bmatrix} \begin{bmatrix} a_1 \\ a_2 \\ a_3 \\ a_4 \end{bmatrix} = \begin{bmatrix} 0 \\ 0 \\ 0 \\ 0 \end{bmatrix}
$$

$$
\begin{bmatrix} -c^+t & 0 & 0 & -c^+t \\ 0 & -t & 0 & c^+t \\ 0 & 0 & -c^-t & -t \\ 0 & 0 & 0 & 0 \end{bmatrix} \begin{bmatrix} a_1 \\ a_2 \\ a_3 \\ a_4 \end{bmatrix} = \begin{bmatrix} 0 \\ 0 \\ 0 \\ 0 \end{bmatrix}
$$

$$
\begin{bmatrix} 1 & 0 & 0 & 1 \\ 0 & 1 & 0 & -c^+ \\ 0 & 0 & 1 & c^+ \\ 0 & 0 & 0 & 0 \end{bmatrix} \begin{bmatrix} a_1 \\ a_2 \\ a_3 \\ a_4 \end{bmatrix} = \begin{bmatrix} 0 \\ 0 \\ 0 \\ 0 \end{bmatrix}
$$

$$
\begin{bmatrix} a_1 \\ a_2 \\ a_3 \\ a_4 \end{bmatrix} = \frac{1}{\sqrt{5+\sqrt{5}}} \begin{bmatrix} 1 \\ -c^+ \\ c^+ \\ -1 \end{bmatrix} \tag{21}
$$

and the wave function becomes:

$$
\psi_A(\boldsymbol{r}) = \frac{1}{\sqrt{5+\sqrt{5}}} [\phi(\boldsymbol{r} - \boldsymbol{R_1}) - c^+ \phi(\boldsymbol{r} - \boldsymbol{R_2}) + c^+ \phi(\boldsymbol{r} - \boldsymbol{R_3}) - \phi(\boldsymbol{r} - \boldsymbol{R_4})] \tag{22}
$$

For $E_{-+} = \varepsilon' - c^+ t$ we have:

$$
\begin{bmatrix} c^+t & -t & 0 & 0 \\ -t & c^+t & -t & 0 \\ 0 & -t & c^+t & -t \\ 0 & 0 & -t & c^+t \end{bmatrix} \begin{bmatrix} a_1 \\ a_2 \\ a_3 \\ a_4 \end{bmatrix} = \begin{bmatrix} 0 \\ 0 \\ 0 \\ 0 \end{bmatrix}
$$

$$
\begin{bmatrix} c^+t & -t & 0 & 0 \\ 0 & t & -t & 0 \\ 0 & -t & c^+t & -t \\ 0 & 0 & -t & c^+t \end{bmatrix} \begin{bmatrix} a_1 \\ a_2 \\ a_3 \\ a_4 \end{bmatrix} = \begin{bmatrix} 0 \\ 0 \\ 0 \\ 0 \end{bmatrix}
$$

$$
\begin{bmatrix} c^+t & -t & 0 & 0 \\ 0 & t & -t & 0 \\ 0 & 0 & c^-t & -t \\ 0 & 0 & -t & c^+t \end{bmatrix} \begin{bmatrix} a_1 \\ a_2 \\ a_3 \\ a_4 \end{bmatrix} = \begin{bmatrix} 0 \\ 0 \\ 0 \\ 0 \end{bmatrix}
$$

$$
\begin{bmatrix} c^+t & -t & 0 & 0 \\ 0 & t & -t & 0 \\ 0 & 0 & c^-t & -t \\ 0 & 0 & 0 & 0 \end{bmatrix} \begin{bmatrix} a_1 \\ a_2 \\ a_3 \\ a_4 \end{bmatrix} = \begin{bmatrix} 0 \\ 0 \\ 0 \\ 0 \end{bmatrix}
$$

$$
\begin{bmatrix} c^+t & -t & 0 & 0 \\ 0 & t & 0 & -c^+t \\ 0 & 0 & c^-t & -t \\ 0 & 0 & 0 & 0 \end{bmatrix} \begin{bmatrix} a_1 \\ a_2 \\ a_3 \\ a_4 \end{bmatrix} = \begin{bmatrix} 0 \\ 0 \\ 0 \\ 0 \end{bmatrix}
$$

$$
\begin{bmatrix} c^+t & 0 & 0 & -c^+t \\ 0 & t & 0 & -c^+t \\ 0 & 0 & c^-t & -t \\ 0 & 0 & 0 & 0 \end{bmatrix} \begin{bmatrix} a_1 \\ a_2 \\ a_3 \\ a_4 \end{bmatrix} = \begin{bmatrix} 0 \\ 0 \\ 0 \\ 0 \end{bmatrix}
$$

$$
\begin{bmatrix} 1 & 0 & 0 & -1 \\ 0 & 1 & 0 & -c^+ \\ 0 & 0 & 1 & -c^+ \\ 0 & 0 & 0 & 0 \end{bmatrix} \begin{bmatrix} a_1 \\ a_2 \\ a_3 \\ a_4 \end{bmatrix} = \begin{bmatrix} 0 \\ 0 \\ 0 \\ 0 \end{bmatrix}
$$

$$
\begin{bmatrix} a_1 \\ a_2 \\ a_3 \\ a_4 \end{bmatrix} = \frac{1}{\sqrt{5+\sqrt{5}}} \begin{bmatrix} 1 \\ c^+ \\ c^+ \\ 1 \end{bmatrix} \tag{23}
$$

and the wave function becomes:

$$
\psi_B(\boldsymbol{r}) = \frac{1}{\sqrt{5+\sqrt{5}}} [\phi(\boldsymbol{r} - \boldsymbol{R_1}) + c^+ \phi(\boldsymbol{r} - \boldsymbol{R_2}) + c^+ \phi(\boldsymbol{r} - \boldsymbol{R_3}) + \phi(\boldsymbol{r} - \boldsymbol{R_4})] \tag{24}
$$

For $E_{+-} = \varepsilon' + c^- t$ we have:

$$
\begin{bmatrix} -c^-t & -t & 0 & 0 \\ -t & -c^-t & -t & 0 \\ 0 & -t & -c^-t & -t \\ 0 & 0 & -t & -c^-t \end{bmatrix} \begin{bmatrix} a_1 \\ a_2 \\ a_3 \\ a_4 \end{bmatrix} = \begin{bmatrix} 0 \\ 0 \\ 0 \\ 0 \end{bmatrix}
$$

$$
\begin{bmatrix} -c^-t & -t & 0 & 0 \\ 0 & t & -t & 0 \\ 0 & -t & -c^-t & -t \\ 0 & 0 & -t & -c^-t \end{bmatrix} \begin{bmatrix} a_1 \\ a_2 \\ a_3 \\ a_4 \end{bmatrix} = \begin{bmatrix} 0 \\ 0 \\ 0 \\ 0 \end{bmatrix}
$$

$$
\begin{bmatrix} -c^-t & -t & 0 & 0 \\ 0 & t & -t & 0 \\ 0 & 0 & -c^+t & -t \\ 0 & 0 & -t & -c^-t \end{bmatrix} \begin{bmatrix} a_1 \\ a_2 \\ a_3 \\ a_4 \end{bmatrix} = \begin{bmatrix} 0 \\ 0 \\ 0 \\ 0 \end{bmatrix}
$$

$$
\begin{bmatrix} -c^-t & -t & 0 & 0 \\ 0 & t & -t & 0 \\ 0 & 0 & -c^+t & -t \\ 0 & 0 & 0 & 0 \end{bmatrix} \begin{bmatrix} a_1 \\ a_2 \\ a_3 \\ a_4 \end{bmatrix} = \begin{bmatrix} 0 \\ 0 \\ 0 \\ 0 \end{bmatrix}
$$

$$
\begin{bmatrix} -c^-t & -t & 0 & 0 \\ 0 & t & 0 & c^-t \\ 0 & 0 & -c^+t & -t \\ 0 & 0 & 0 & 0 \end{bmatrix} \begin{bmatrix} a_1 \\ a_2 \\ a_3 \\ a_4 \end{bmatrix} = \begin{bmatrix} 0 \\ 0 \\ 0 \\ 0 \end{bmatrix}
$$

$$
\begin{bmatrix} -c^-t & 0 & 0 & c^-t \\ 0 & t & 0 & c^-t \\ 0 & 0 & -c^+t & -t \\ 0 & 0 & 0 & 0 \end{bmatrix} \begin{bmatrix} a_1 \\ a_2 \\ a_3 \\ a_4 \end{bmatrix} = \begin{bmatrix} 0 \\ 0 \\ 0 \\ 0 \end{bmatrix}
$$

$$
\begin{bmatrix} 1 & 0 & 0 & -1 \\ 0 & 1 & 0 & c^- \\ 0 & 0 & 1 & c^- \\ 0 & 0 & 0 & 0 \end{bmatrix} \begin{bmatrix} a_1 \\ a_2 \\ a_3 \\ a_4 \end{bmatrix} = \begin{bmatrix} 0 \\ 0 \\ 0 \\ 0 \end{bmatrix}
$$

$$
\begin{bmatrix} a_1 \\ a_2 \\ a_3 \\ a_4 \end{bmatrix} = \frac{1}{\sqrt{5-\sqrt{5}}} \begin{bmatrix} 1 \\ -c^- \\ -c^- \\ 1 \end{bmatrix} \tag{25}
$$

and the wave function becomes:

$$
\psi_C(\boldsymbol{r}) = \frac{1}{\sqrt{5-\sqrt{5}}} [\phi(\boldsymbol{r} - \boldsymbol{R_1}) - c^- \phi(\boldsymbol{r} - \boldsymbol{R_2}) - c^- \phi(\boldsymbol{r} - \boldsymbol{R_3}) + \phi(\boldsymbol{r} - \boldsymbol{R_4})] \tag{26}
$$

For $E_{--} = \varepsilon' - c^- t$ we have:

$$
\begin{aligned}
&\begin{bmatrix} c^-t & -t & 0 & 0 \\ -t & c^-t & -t & 0 \\ 0 & -t & c^-t & -t \\ 0 & 0 & -t & c^-t \end{bmatrix} \begin{bmatrix} a_1 \\ a_2 \\ a_3 \\ a_4 \end{bmatrix} = \begin{bmatrix} 0 \\ 0 \\ 0 \\ 0 \end{bmatrix} \\
&\begin{bmatrix} c^-t & -t & 0 & 0 \\ 0 & -t & -t & 0 \\ 0 & -t & c^-t & -t \\ 0 & 0 & -t & c^-t \end{bmatrix} \begin{bmatrix} a_1 \\ a_2 \\ a_3 \\ a_4 \end{bmatrix} = \begin{bmatrix} 0 \\ 0 \\ 0 \\ 0 \end{bmatrix} \\
&\begin{bmatrix} c^-t & -t & 0 & 0 \\ 0 & -t & -t & 0 \\ 0 & 0 & c^+t & -t \\ 0 & 0 & -t & c^-t \end{bmatrix} \begin{bmatrix} a_1 \\ a_2 \\ a_3 \\ a_4 \end{bmatrix} = \begin{bmatrix} 0 \\ 0 \\ 0 \\ 0 \end{bmatrix} \\
&\begin{bmatrix} c^-t & -t & 0 & 0 \\ 0 & -t & -t & 0 \\ 0 & 0 & c^+t & -t \\ 0 & 0 & 0 & 0 \end{bmatrix} \begin{bmatrix} a_1 \\ a_2 \\ a_3 \\ a_4 \end{bmatrix} = \begin{bmatrix} 0 \\ 0 \\ 0 \\ 0 \end{bmatrix} \\
&\begin{bmatrix} c^-t & -t & 0 & 0 \\ 0 & -t & 0 & -c^-t \\ 0 & 0 & c^+t & -t \\ 0 & 0 & 0 & 0 \end{bmatrix} \begin{bmatrix} a_1 \\ a_2 \\ a_3 \\ a_4 \end{bmatrix} = \begin{bmatrix} 0 \\ 0 \\ 0 \\ 0 \end{bmatrix} \\
&\begin{bmatrix} c^-t & 0 & 0 & c^-t \\ 0 & -t & 0 & -c^-t \\ 0 & 0 & c^+t & -t \\ 0 & 0 & 0 & 0 \end{bmatrix} \begin{bmatrix} a_1 \\ a_2 \\ a_3 \\ a_4 \end{bmatrix} = \begin{bmatrix} 0 \\ 0 \\ 0 \\ 0 \end{bmatrix} \\
&\begin{bmatrix} 1 & 0 & 0 & 1 \\ 0 & 1 & 0 & c^- \\ 0 & 0 & 1 & c^- \\ 0 & 0 & 0 & 0 \end{bmatrix} \begin{bmatrix} a_1 \\ a_2 \\ a_3 \\ a_4 \end{bmatrix} = \begin{bmatrix} 0 \\ 0 \\ 0 \\ 0 \end{bmatrix} \\
&\begin{bmatrix} a_1 \\ a_2 \\ a_3 \\ a_4 \end{bmatrix} = \frac{1}{\sqrt{5-\sqrt{5}}} \begin{bmatrix} 1 \\ c^- \\ -c^- \\ -1 \end{bmatrix}
\end{aligned}
\tag{27}
$$

and the wave function becomes:

$$\psi_D(\boldsymbol{r}) = \frac{1}{\sqrt{5-\sqrt{5}}}[\phi(\boldsymbol{r}-\boldsymbol{R_1}) + c^-\phi(\boldsymbol{r}-\boldsymbol{R_2}) - c^-\phi(\boldsymbol{r}-\boldsymbol{R_3}) - \phi(\boldsymbol{r}-\boldsymbol{R_4})] \tag{28}$$

The wave functions ψ_A, ψ_B, ψ_C and ψ_D are sketched in figure 16.

3. Infinite chain with s-orbitals

(a) The result from the lecture is

$$\varepsilon(\boldsymbol{k}) = \varepsilon_s - \frac{\beta + \sum_{R\neq 0}\gamma(\boldsymbol{R})e^{i\boldsymbol{k}\cdot\boldsymbol{R}}}{1 + \sum_{R\neq 0}\alpha(\boldsymbol{R})e^{i\boldsymbol{k}\cdot\boldsymbol{R}}} \tag{29}$$

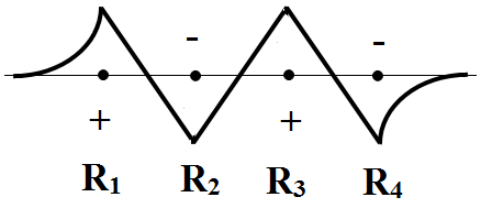

(a) Sketch of the wave function from equation (22).

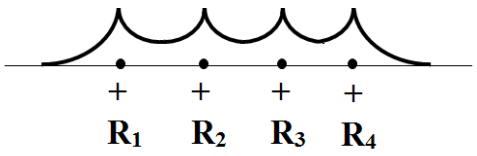

(b) Sketch of the wave function from equation (24).

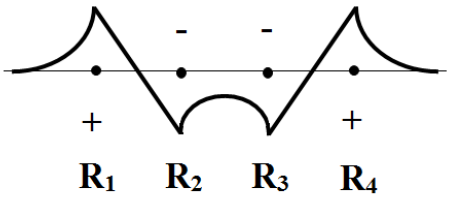

(c) Sketch of the wave function from equation (26).

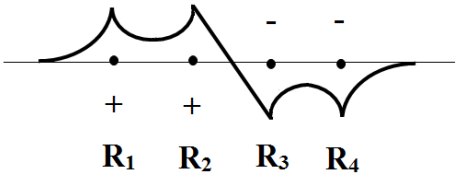

(d) Sketch of the wave function from equation (28).

Figure 16

We neglect α, we only consider nearest neighbors and we take $\beta = 0$. This means equation (29) becomes:

$$\varepsilon(\boldsymbol{k}) = \varepsilon_s - \sum_{n.n.} \gamma(\boldsymbol{R}) e^{i\boldsymbol{k}\cdot\boldsymbol{R}} \tag{30}$$

For an infinite chain of hydrogen atoms, the nearest neighbors are the atoms at positions $\pm a$, so we can calculate

$$\varepsilon(k) = \varepsilon_s - t(e^{ika} + e^{-ika}) = \varepsilon_s - 2t\cos(ka) \tag{31}$$

The result is sketched in figure 17 from $k = -\frac{\pi}{a}$ to $k = \frac{\pi}{a}$.

(b) The Fermi energy is the energy level to which the band is filled. We have a half filled band, so the Fermi energy would be the energy at k_f with $k_f = \frac{\pi}{2a}$. This means that $\varepsilon_f = \varepsilon(\frac{\pi}{2a}) = \varepsilon_s$. The level ε_s is marked in figure 17. Since the band is only half filled, the electrons are able to conduct so the chain is conducting.

(c) We start at the equation from the slides:

$$\begin{aligned}[\varepsilon(\boldsymbol{k}) - E_m]b_m = -[\varepsilon(\boldsymbol{k}) - E_m] \sum_n \sum_{R\neq 0} \left\langle \psi_m(\boldsymbol{r}) | \psi_n(\boldsymbol{r} - \boldsymbol{R}) e^{i\boldsymbol{k}\cdot\boldsymbol{R}} \right\rangle b_n \\ + \sum_n \left\langle \psi_m \,|\, \Delta U(\boldsymbol{r}) \,|\, \psi_n \right\rangle b_n + \sum_n \sum_{R\neq 0} \left\langle \psi_m(\boldsymbol{r}) \,\middle|\, \Delta U(\boldsymbol{r}) \,\middle|\, \psi_n(\boldsymbol{r} - \boldsymbol{R}) e^{i\boldsymbol{k}\cdot\boldsymbol{R}} \right\rangle b_n\end{aligned} \tag{32}$$

Again, α is neglected and $\beta = 0$. Equation (32) can now be written as:

$$[\varepsilon(\boldsymbol{k}) - E_m]b_m = \sum_n \sum_{R\neq 0} \left\langle \psi_m(\boldsymbol{r}) \,\middle|\, \Delta U(\boldsymbol{r}) \,\middle|\, \psi_n(\boldsymbol{r} - \boldsymbol{R}) e^{i\boldsymbol{k}\cdot\boldsymbol{R}} \right\rangle b_n \tag{33}$$

This equation can be written in matrix form, since we have two atoms:

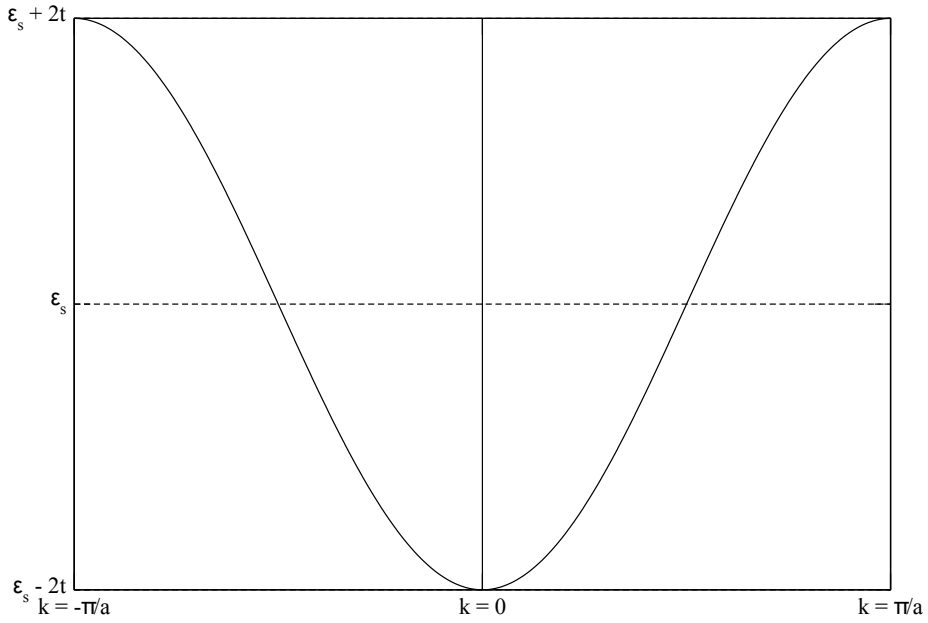

Figure 17: Dispersion of an infinite chain of hydrogen atoms.

$$\begin{bmatrix} \varepsilon(\boldsymbol{k}) - E_{s,1} & 0 \\ 0 & \varepsilon(\boldsymbol{k}) - E_{s,2} \end{bmatrix} \begin{bmatrix} b_1 \\ b_2 \end{bmatrix} = \\ \begin{bmatrix} \sum_{R\neq 0} \langle \phi_{s,1}(\boldsymbol{r}) \,|\, \Delta U(\boldsymbol{r}) \,|\, \phi_{s,1}(\boldsymbol{r}-\boldsymbol{R}) \rangle \, e^{i\boldsymbol{k}\cdot\boldsymbol{R}} & \sum_{R\neq 0} \langle \phi_{s,1}(\boldsymbol{r}) \,|\, \Delta U(\boldsymbol{r}) \,|\, \phi_{s,2}(\boldsymbol{r}-\boldsymbol{R}) \rangle \, e^{i\boldsymbol{k}\cdot\boldsymbol{R}} \\ \sum_{R\neq 0} \langle \phi_{s,2}(\boldsymbol{r}) \,|\, \Delta U(\boldsymbol{r}) \,|\, \phi_{s,1}(\boldsymbol{r}-\boldsymbol{R}) \rangle \, e^{i\boldsymbol{k}\cdot\boldsymbol{R}} & \sum_{R\neq 0} \langle \phi_{s,2}(\boldsymbol{r}) \,|\, \Delta U(\boldsymbol{r}) \,|\, \phi_{s,2}(\boldsymbol{r}-\boldsymbol{R}) \rangle \, e^{i\boldsymbol{k}\cdot\boldsymbol{R}} \end{bmatrix} \begin{bmatrix} b_1 \\ b_2 \end{bmatrix} \tag{34}$$

Because we consider s-orbitals, which are always real, one can argue that

$$\langle \phi_{s,1}(\boldsymbol{r}) \,|\, \Delta U(\boldsymbol{r}) \,|\, \phi_{s,2}(\boldsymbol{r}-\boldsymbol{R}) \rangle = \langle \phi_{s,2}(\boldsymbol{r}) \,|\, \Delta U(\boldsymbol{r}) \,|\, \phi_{s,1}(\boldsymbol{r}-\boldsymbol{R}) \rangle = -\gamma \tag{35}$$

and, since we have two atoms in the unit cell,

$$\langle \phi_{s,1}(\boldsymbol{r}) \,|\, \Delta U(\boldsymbol{r}) \,|\, \phi_{s,1}(\boldsymbol{r}-\boldsymbol{R}) \rangle = \langle \phi_{s,2}(\boldsymbol{r}) \,|\, \Delta U(\boldsymbol{r}) \,|\, \phi_{s,2}(\boldsymbol{r}-\boldsymbol{R}) \rangle = 0 \tag{36}$$

and lastly we take $E_{s,1} = E_{s,2} = E$, so equation (34) becomes:

$$\begin{bmatrix} \varepsilon(\boldsymbol{k}) - E & 0 \\ 0 & \varepsilon(\boldsymbol{k}) - E \end{bmatrix} \begin{bmatrix} b_1 \\ b_2 \end{bmatrix} = \begin{bmatrix} 0 & -\sum_{R\neq 0} \gamma e^{i\boldsymbol{k}\cdot\boldsymbol{R}} \\ -\sum_{R\neq 0} \gamma e^{i\boldsymbol{k}\cdot\boldsymbol{R}} & 0 \end{bmatrix} \begin{bmatrix} b_1 \\ b_2 \end{bmatrix} \tag{37}$$

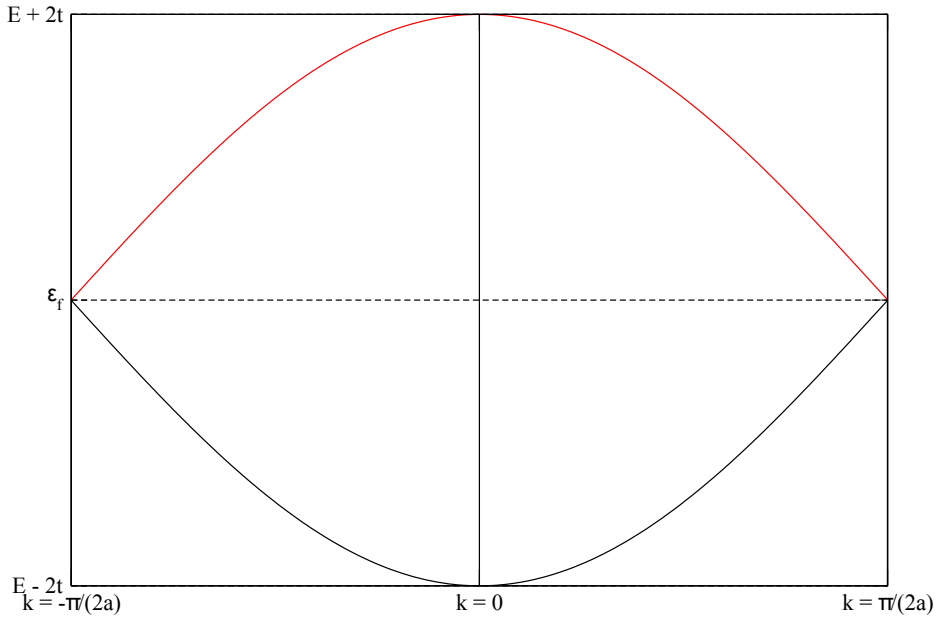

Figure 18: Dispersion of an infinite chain of hydrogen atoms with two atoms per unit cell. The values of k cover the first Brillouin zone. The Fermi energy is marked by a dotted line. The red line represents the solution $\varepsilon(k) = E + 2t\cos(ka)$ while the black line represents the solution $\varepsilon(k) = E - 2t\cos(ka)$.

The energy $\varepsilon(\boldsymbol{k})$ can be found by solving:

$$\begin{aligned}
\begin{vmatrix} \varepsilon(\boldsymbol{k}) - E & \sum_{R\neq 0} \gamma e^{i\boldsymbol{k}\cdot\boldsymbol{R}} \\ \sum_{R\neq 0} \gamma e^{i\boldsymbol{k}\cdot\boldsymbol{R}} & \varepsilon(\boldsymbol{k}) - E \end{vmatrix} &= 0 \\
\begin{vmatrix} \varepsilon(k) - E & t(e^{ika} + e^{-ika}) \\ t(e^{ika} + e^{-ika}) & \varepsilon(k) - E \end{vmatrix} &= 0 \\
\begin{vmatrix} \varepsilon(k) - E & 2t\cos(ka) \\ 2t\cos(ka) & \varepsilon(k) - E \end{vmatrix} &= 0 \\
(\varepsilon(k) - E)^2 - 4t^2\cos^2(ka) &= 0 \\
(\varepsilon(k) - E)^2 &= 4t^2\cos^2(ka) \\
\varepsilon(k) - E &= \pm 2t\cos(ka) \\
\varepsilon(k) &= E \pm 2t\cos(ka)
\end{aligned} \tag{38}$$

The dispersion found in equation (38) is plotted in figure 18. In this figure, the Fermi energy is marked by a dotted line. The whole first Brillouin zone is shown.

(d) Since the unit cell contains two atoms, the first Brillouin zone is a half smaller. Half of the bands which were in the first Brillouin zone in figure 17 but now outside of it are folded back in.

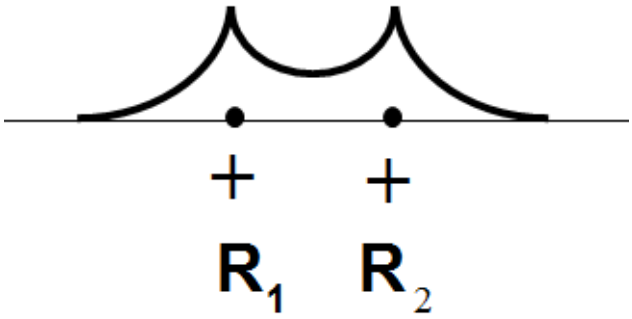

Figure 19: Wave functions of two atoms in a linear chain of hydrogen atoms.

(e) In the case of problem a we found a wavefunction for each atom of the type

$$\psi(\boldsymbol{r}) = \phi(\boldsymbol{r} - \boldsymbol{R}) \tag{39}$$

with $\boldsymbol{R}$ the location of each atom.

For problem c we found wavefunctions for each two atoms of the type

$$\psi(\boldsymbol{r}) = \frac{1}{\sqrt{2}}[\phi(\boldsymbol{r} - \boldsymbol{R_1}) + \phi(\boldsymbol{r} - \boldsymbol{R_2})] \tag{40}$$

as well as

$$\psi(\boldsymbol{r}) = \frac{1}{\sqrt{2}}[\phi(\boldsymbol{r} - \boldsymbol{R_1}) - \phi(\boldsymbol{r} - \boldsymbol{R_2})] \tag{41}$$

The wave function of equation (39) as well as the wave function of equation (40) both look like the sketch in figure 19 when they are drawn for two atoms. Essentially, both these methods have the same results. However, problem c also seems to give rise to an anti-bonding wave function in equation (41) which is not a result of problem a.

(f) We restart the calculation from problem c at the point where the we take $E_{s,1} = E_{s,2} = E$, ignore that part and continue from an equation similar to equation (37).

$$\begin{bmatrix} \varepsilon(\boldsymbol{k}) - E_{s,+} & 0 \\ 0 & \varepsilon(\boldsymbol{k}) - E_{s,-} \end{bmatrix} \begin{bmatrix} b_1 \\ b_2 \end{bmatrix} = \begin{bmatrix} 0 & -\sum_{R\neq 0} \gamma e^{i\boldsymbol{k}\cdot\boldsymbol{R}} \\ -\sum_{R\neq 0} \gamma e^{i\boldsymbol{k}\cdot\boldsymbol{R}} & 0 \end{bmatrix} \begin{bmatrix} b_1 \\ b_2 \end{bmatrix} \tag{42}$$

We can again find the energy $\varepsilon(\boldsymbol{k})$ by solving

$$\begin{aligned}
\begin{vmatrix} \varepsilon(\boldsymbol{k}) - E_{s,+} & \sum_{R\neq 0} \gamma e^{i\boldsymbol{k}\cdot\boldsymbol{R}} \\ \sum_{R\neq 0} \gamma e^{i\boldsymbol{k}\cdot\boldsymbol{R}} & \varepsilon(\boldsymbol{k}) - E_{s,-} \end{vmatrix} &= 0 \\
\begin{vmatrix} \varepsilon(k) - E_{s,+} & t(e^{ika} + e^{-ika}) \\ t(e^{ika} + e^{-ika}) & \varepsilon(k) - E_{s,-} \end{vmatrix} &= 0 \\
\begin{vmatrix} \varepsilon(k) - E_{s,+} & 2t\cos(ka) \\ 2t\cos(ka) & \varepsilon(k) - E_{s,-} \end{vmatrix} &= 0 \\
(\varepsilon(k) - E_{s,+})(\varepsilon(k) - E_{s,-}) - 4t^2\cos^2(ka) &= 0 \\
\varepsilon^2(k) - (E_{s,+} + E_{s,-})\varepsilon(k) + E_{s,+}E_{s,-} - 4t^2\cos^2(ka) &= 0 \\
\varepsilon(k) = \frac{1}{2}(E_{s,+} + E_{s,-}) \pm \frac{1}{2}\sqrt{E_{s,+}^2 + E_{s,-}^2 - 2E_{s,+}E_{s,-} + 16t^2\cos^2(ka)} & \\
\varepsilon(k) = E_0 \pm \frac{1}{2}\sqrt{\Delta^2 + 16t^2\cos^2(ka)} &
\end{aligned} \tag{43}$$

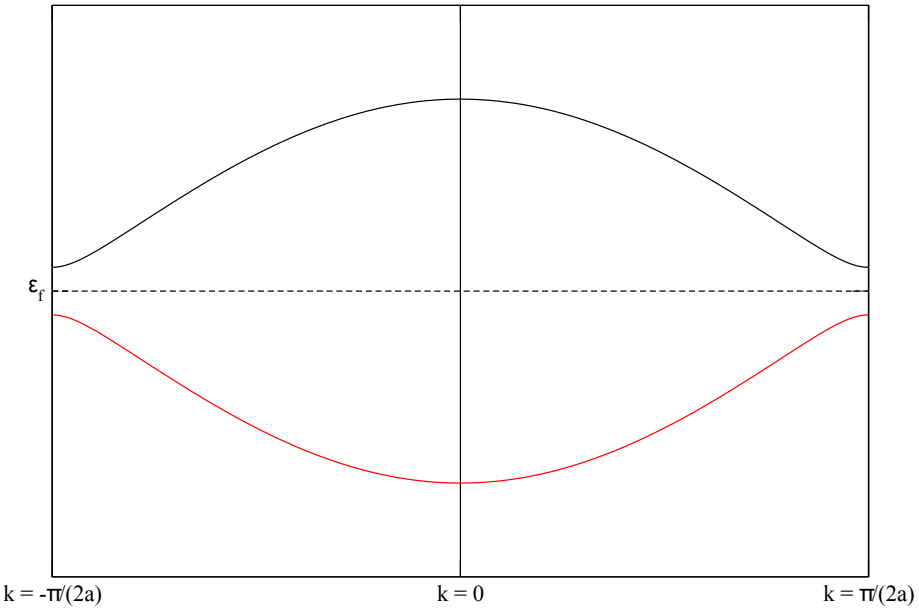

Figure 20: Dispersion of an infinite dimer chain with s-orbitals. The values of k cover the first Brillouin zone. The Fermi energy is marked by a dotted line. The red line represents the solution $\varepsilon(k) = E_0 - \frac{1}{2}\sqrt{\Delta^2 + 16t^2\cos^2(ka)}$ while the black line represents the solution $\varepsilon(k) = E_0 + \frac{1}{2}\sqrt{\Delta^2 + 16t^2\cos^2(ka)}$

making use of the fact that $E_{s,\pm} = E_0 \pm \frac{\Delta}{2}$.

The calculated dispersion is plotted in figure 20. In this figure, the Fermi energy is marked by a dotted line. The whole first Brillouin zone is shown.

(g) The most important difference between dispersion relations calculated in other problems and the one in figure 20 is the band gap. The size of the band gap determines if it's a semiconductor or an insulator and thus if conduction is possible. The size of the band gap is equal to Δ, so if the material conducts depens on Δ.

Assignment 3 - Densities of States

Three methods (one analytical, two numerical) of calculating the density of states and the number of states for a one dimensional linear chain of hydrogen atoms with one s orbital per atom will be compared and discussed. The dispersion in this case is

$$\varepsilon(k) = \varepsilon_0 - 2t\cos(ka) \tag{44}$$

(i) - Analytical method The density of states is defined as

$$D(\varepsilon) = \frac{dN}{d\varepsilon} \tag{45}$$

We know that the number of electrons at energy $\varepsilon(k)$ is equal to the length between $\varepsilon(k)$ and $\varepsilon(k+dk)$ divided by the length of one state, keeping in mind that we have two electrons per state. Therefore,

$$dN = 2\frac{dk}{\frac{2\pi}{L}} = \frac{Ldk}{\pi} \tag{46}$$

Equation (44) can be used to calculate $d\varepsilon$:

$$\frac{d\varepsilon}{dk} = 2ta\sin(ka) \Rightarrow d\varepsilon = 2ta\sin(ka)dk \tag{47}$$

Substituting equations (46) and (47) into equation (45) gives us the density of states:

$$D(\varepsilon) = \frac{\frac{Ldk}{\pi}}{2ta\sin(ka)dk} = \frac{L}{2\pi ta\sin(ka)} \tag{48}$$

However, this is dependent on k instead of ε, so we rewrite equation (44):

$$\begin{aligned} \varepsilon(k) &= \varepsilon_0 - 2t\cos(ka) \\ \cos(ka) &= \frac{\varepsilon_0 - \varepsilon}{2t} \\ ka &= \cos^{-1}(\frac{\varepsilon_0 - \varepsilon}{2t}) \end{aligned} \tag{49}$$

Substituting equation (49) into equation (48) gives:

$$D(\varepsilon) = \frac{L}{2\pi ta\sin(\cos^{-1}(\frac{\varepsilon_0-\varepsilon}{2t}))} = \frac{L}{2\pi ta\sqrt{1-(\frac{\varepsilon_0-\varepsilon}{2t})^2}} \tag{50}$$

In figure 21a the density of states is plotted in units of $\frac{L}{a}$. In this plot, $\varepsilon_0 = 0$ for convenience and $t = 1$.

To calculate the number of states $N(\varepsilon)$ we use

$$N(\varepsilon) = \int_{-\infty}^{\varepsilon} D(\varepsilon')d\varepsilon' \tag{51}$$

However, one can show that the minimum of equation (44) is $\varepsilon_0 - 2t$. Inserting this as the lower boundary of the integral allows us to calculate $N(\varepsilon)$:

$$N(\varepsilon) = \int_{\varepsilon_0-2t}^{\varepsilon} D(\varepsilon')d\varepsilon' = \frac{L}{2\pi ta}\int_{\varepsilon_0-2t}^{\varepsilon} \frac{1}{\sqrt{1-(\frac{\varepsilon_0-\varepsilon'}{2t})^2}}d\varepsilon' \tag{52}$$

The substitution $\frac{\varepsilon_0-\varepsilon'}{2t} = \sin(\theta)$ and $\varepsilon' = \varepsilon_0 - 2t\sin(\theta) \Rightarrow \frac{d\varepsilon'}{d\theta} = -2t\cos(\theta) \Rightarrow d\varepsilon' = -2t\cos(\theta)d\theta$ gives:

$$N(\varepsilon) = -\frac{L}{\pi a}\int_{\varepsilon_0-2t}^{\varepsilon} \frac{\cos(\theta)}{\sqrt{1-\sin^2(\theta)}}d\theta = -\frac{L}{\pi a}\int_{\varepsilon_0-2t}^{\varepsilon} d\theta = -\frac{L}{\pi a}\theta\Big|_{\varepsilon_0-2t}^{\varepsilon} \tag{53}$$

Substituting $\frac{\varepsilon_0-\varepsilon'}{2t} = \sin(\theta) \Rightarrow \theta = \sin^{-1}(\frac{\varepsilon_0-\varepsilon'}{2t})$ into equation (53) gives

$$\begin{aligned} N(\varepsilon) = -\frac{L}{\pi a}\sin^{-1}(\frac{\varepsilon_0-\varepsilon'}{2t})\Big|_{\varepsilon_0-2t}^{\varepsilon} = -\frac{L}{\pi a}\sin^{-1}(\frac{\varepsilon_0-\varepsilon}{2t}) + \frac{L}{\pi a}\sin^{-1}(1) = \\ -\frac{L}{\pi a}\sin^{-1}(\frac{\varepsilon_0-\varepsilon}{2t}) + \frac{L}{2a} \end{aligned} \tag{54}$$

Equation (54) is plotted in figure 21b. It's plotted in units of $\frac{L}{a}$. In this plot, again, $\varepsilon_0 = 0$ for convenience and $t = 1$.

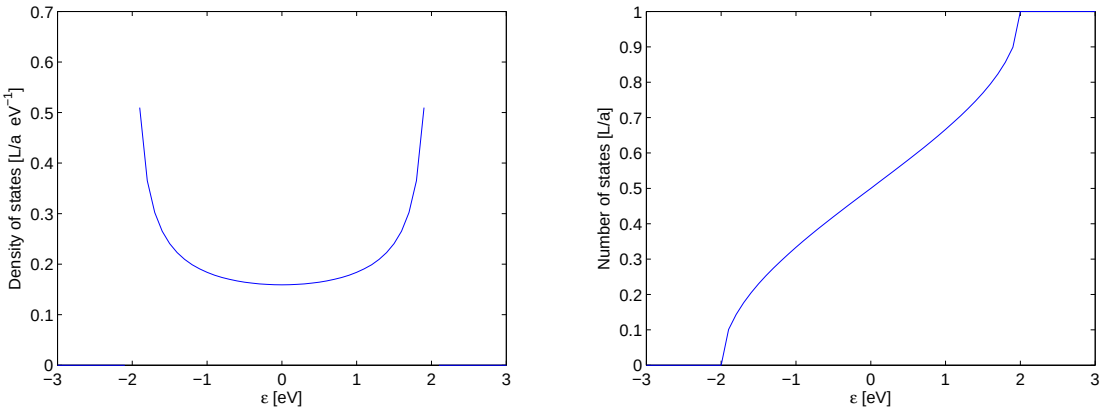

(a) Density of states (b) Number of states

Figure 21: The density of states and number of states per energy value of a one dimensional linear chain of hydrogen atoms. The density of states as well as the number of states are given in units of $\frac{L}{a}$.

(ii) - Histogram method (numerical) The next method used was a numerical one, namely the histogram method. The dispersion was calculated for different numbers of k-points using equation (44). Then the values of the energy were spread out over a different numbers of bins and a histogram was made to calculate the density of states. Then, the number of states was calculated by summing the different bins cumulatively. The results are shown in figure 22. There the density of states is shown on the left and the number of states is shown on the right. They are plotted for respectively 100 k-points and 10 energy intervals (figures 22a and 22b), 1000 k-points and 100 energy intervals (figures 22c and 22d), 10000 k-points and 1000 energy intervals (figures 22e and 22f) and 100000 k-points and 10000 energy intervals (figures 22g and 22h).

(iii) - Linear analytic method (numerical) Another numerical method was used, namely the linear analytic method. The idea behind this method is as follows. We know that the total number of states N at energy ε is:

$$N(\varepsilon) = \frac{\Delta k}{\frac{2\pi}{L}} = \frac{L\Delta k}{2\pi} \tag{55}$$

with Δk the distance between $+\varepsilon$ and $-\varepsilon$ which equals $2k$ since our dispersion is equation (44) with again $\varepsilon_0 = 0$ and $t = 1$. This means we have:

$$N(\varepsilon) = \frac{Lk}{\pi} \tag{56}$$

The density of states is the derivative of the total number of states to the energy, so:

$$D(\varepsilon) = \frac{dN}{d\varepsilon} = \frac{dN}{dk}\frac{dk}{d\varepsilon} = \frac{L}{\pi}\frac{dk}{d\varepsilon} = \frac{\frac{L}{\pi}}{\frac{d\varepsilon}{dk}} \tag{57}$$

Using equation (57) the density of states can be calculated numerically. Since the minimum of equation (44) is at $k = 0$ and the maximum is at $k = \frac{\pi}{a}$, we consider only this region. First, $\varepsilon(k)$ is calculated using equation (44). Then, we calculate

$$\frac{d\varepsilon}{dk} = \frac{\varepsilon(k + dk) - \varepsilon(k)}{dk} \tag{58}$$

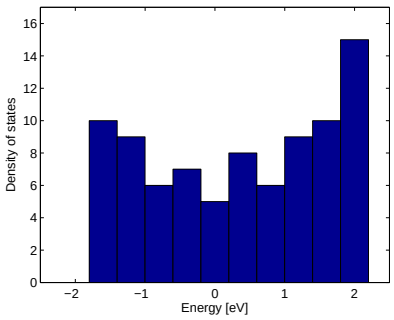

(a) Density of states for 100 k-points and 10 energy intervals.

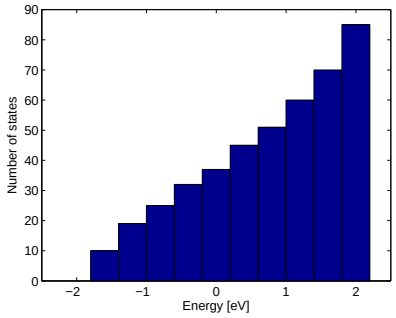

(b) Number of states for 100 k-points and 10 energy intervals.

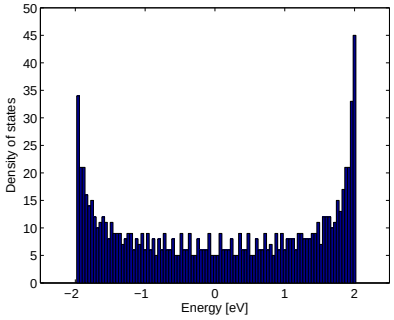

(c) Density of states for 1000 k-points and 100 energy intervals.

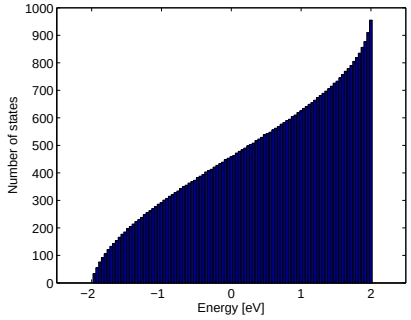

(d) Number of states for 1000 k-points and 100 energy intervals.

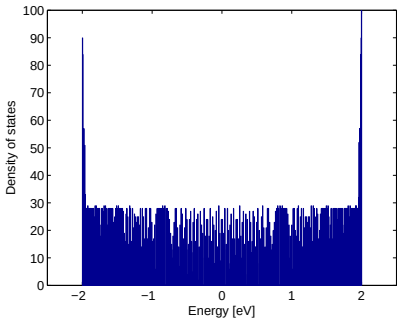

(e) Density of states for 10000 k-points and 1000 energy intervals.

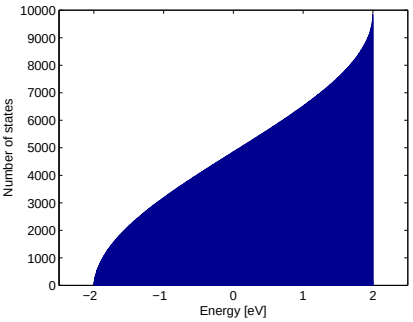

(f) Number of states for 10000 k-points and 1000 energy intervals.

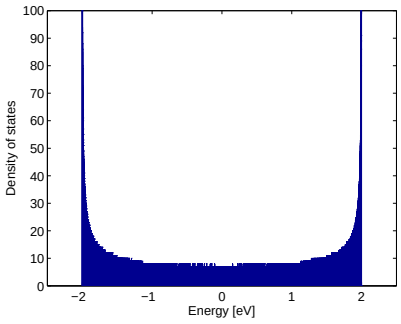

(g) Density of states for 100000 k-points and 10000 energy intervals.

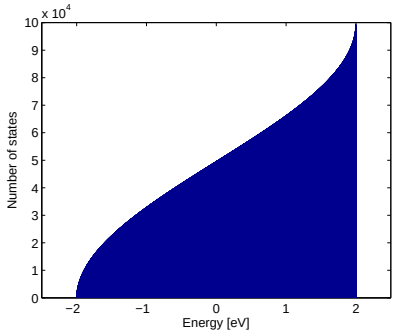

(h) Number of states for 100000 k-points and 10000 energy intervals.

Figure 22: The density of states and number of states per energy value of a one dimensional linear chain of hydrogen atoms. They were calculated using the histogram method for different numbers of k-points and energy intervals.

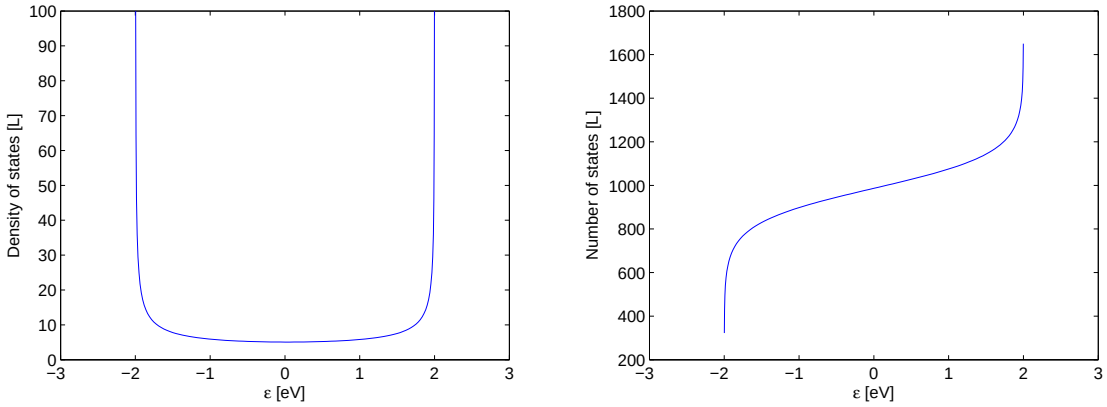

(a) Density of states.

(b) Number of states.

Figure 23: The density of states and number of states per energy value of a one dimensional linear chain of hydrogen atoms. They were calculated using a linear analytic method for 100 k-points and are given in units of L.

and from there calculate the density of states and the number of states.

The density of states and number of states are plotted for 100 k-points in figure 23. They are both plotted in units of L, with the density of states on the left and the number of states on the right.

(iv) - Comparing the different methods Three methods were used, one analytical and two numerical. One would expect the analytical result to be the most precise, since no simplifications or assumptions were used in this case.

The histogram method is an interesting approach since the density of states is defined as the number of states at a certain energy. With the histogram method, one does exactly this: count the number of states at a certain energy. The larger the number of energy intervals get, the closer the result should come to the analytical result. This is true for the shape of the graph, which resembles the graph in figure 21a for 100000 k-points and 10000 energy intervals quite nicely. However, most states are counted at $\varepsilon = \pm 2$ eV. This is expected since the density of states is actually infinity at $\varepsilon = \pm 2$ eV. The number of states resembles the analytical result quite well and in three of the four cases (the exception being figure 22b) the number of states at $\varepsilon = 2$ eV is exactly the number of k-points.

The density of states calculated with the linear analytic method also matches the shape of the analytic density of states. The differences in this case occur also because most states are counted at $\varepsilon = \pm 2$ eV, just as with the histogram method.

Looking at the analytical result and the numerical results it can be concluded that both give a nice result. One needs to keep in mind however, that the histogram method takes a lot of calculating power for a large number of k-points and energy intervals compared to the linear analytic method. On the other hand, the linear analytic method is very similar to the regular analytic method except that the derivative of the dispersion is calculated numerically instead of analytically.

Assignment 4

This section contains the solutions to assignment set 4 from the Theoretical Solid State Physics course.

3. Tight binding and phase space orbits

(a) In this case equation (30) can be used again. This time however there are different nearest neighbors, so we have:

$$\boldsymbol{k} \cdot \boldsymbol{R} = \pm a k_i (i = x, y) \tag{59}$$

and equation (30) becomes:

$$\varepsilon(\boldsymbol{k}) = \varepsilon_s - t(e^{ik_x a} + e^{-ik_x a} + e^{ik_y a} + e^{-ik_y a}) = \varepsilon_s - 2t(\cos(k_x a) + \cos(k_y a)) \tag{60}$$

(b) Starting from equation (33) the dispersion for the p-orbitals can be derived. The matrix for this equation can be written, but to make this more readable we must first determine which hopping paramters are left.

We have nine different hopping integrals, one for each matrix element. First we look at

$$\sum_{R \neq 0} \langle \phi_{p_x}(\boldsymbol{r} \,|\, \Delta U(\boldsymbol{r}) \,|\, \phi_{p_x}(\boldsymbol{r} - \boldsymbol{R}) \rangle \, e^{i\boldsymbol{k}\cdot\boldsymbol{R}} \tag{61}$$

which is drawn in figure 24a. We can see two different hopping integrals in this figure, that is -γ_1 between the wave function at the origin and the wave functions at $\pm a k_x$ and -γ_2 between the wave function at the origin and the wave function at $\pm a k_y$.

A similar situation is

$$\sum_{R \neq 0} \langle \phi_{p_y}(\boldsymbol{r} \,|\, \Delta U(\boldsymbol{r}) \,|\, \phi_{p_y}(\boldsymbol{r} - \boldsymbol{R}) \rangle \, e^{i\boldsymbol{k}\cdot\boldsymbol{R}} \tag{62}$$

as sketched in figure 24e. In this case however we have the hopping parameter -γ_2 between the wave function at the origin and the wave functions at $\pm a k_x$ and the hopping parameter -γ_1 between the wave function at the origin and the wave functions at $\pm a k_y$.

In the case of

$$\sum_{R \neq 0} \langle \phi_{p_z}(\boldsymbol{r} \,|\, \Delta U(\boldsymbol{r}) \,|\, \phi_{p_z}(\boldsymbol{r} - \boldsymbol{R}) \rangle \, e^{i\boldsymbol{k}\cdot\boldsymbol{R}} \tag{63}$$

as sketched in figure 24i we have the same hopping parameter -γ_3 between the wave function at the origin and all it's nearest neighbors.

In figure 24b the wave functions for

$$\sum_{R \neq 0} \langle \phi_{p_x}(\boldsymbol{r} \,|\, \Delta U(\boldsymbol{r}) \,|\, \phi_{p_y}(\boldsymbol{r} - \boldsymbol{R}) \rangle \, e^{i\boldsymbol{k}\cdot\boldsymbol{R}} \tag{64}$$

are plotted. The hopping between the wave function at the origin and the wave functions at $\pm a k_x$ is zero because in the xz plane the wave function at the origin is even and the wave functions at $\pm a k_x$ are odd. In the yz plane the wave function at the origin is odd while the

wave functions at $\pm ak_y$ are even zo the hopping between these wave functions is also zero. A similar argument can be made for the wave functions in figure 24d, so

$$\sum_{R\neq 0} \left\langle \phi_{p_y}(\boldsymbol{r} \,|\, \Delta U(\boldsymbol{r}) \,|\, \phi_{p_x}(\boldsymbol{r}-\boldsymbol{R}) \right\rangle e^{i\boldsymbol{k}\cdot\boldsymbol{R}} \tag{65}$$

is also zero.

Then we have the wave functions for

$$\sum_{R\neq 0} \left\langle \phi_{p_x}(\boldsymbol{r} \,|\, \Delta U(\boldsymbol{r}) \,|\, \phi_{p_z}(\boldsymbol{r}-\boldsymbol{R}) \right\rangle e^{i\boldsymbol{k}\cdot\boldsymbol{R}} \tag{66}$$

as sketched in figure 24c. In the xy plane the wave function at the origin is even while the nearest neighbor wave functions are odd. Therefore, all hopping integrals are zero. Similar arguments can be made for the hopping integrals in figures 24f to 24h, so

$$\begin{aligned}\sum_{R\neq 0} \left\langle \phi_{p_y}(\boldsymbol{r} \,|\, \Delta U(\boldsymbol{r}) \,|\, \phi_{p_z}(\boldsymbol{r}-\boldsymbol{R}) \right\rangle e^{i\boldsymbol{k}\cdot\boldsymbol{R}} = \sum_{R\neq 0} \left\langle \phi_{p_z}(\boldsymbol{r} \,|\, \Delta U(\boldsymbol{r}) \,|\, \phi_{p_x}(\boldsymbol{r}-\boldsymbol{R}) \right\rangle e^{i\boldsymbol{k}\cdot\boldsymbol{R}} = \\ \sum_{R\neq 0} \left\langle \phi_{p_z}(\boldsymbol{r} \,|\, \Delta U(\boldsymbol{r}) \,|\, \phi_{p_y}(\boldsymbol{r}-\boldsymbol{R}) \right\rangle e^{i\boldsymbol{k}\cdot\boldsymbol{R}} = 0\end{aligned} \tag{67}$$

Now we can write down the matrix equation that needs to be solved:

$$\begin{aligned}&\begin{bmatrix} \varepsilon(\boldsymbol{k}) - E_p & 0 & 0 \\ 0 & \varepsilon(\boldsymbol{k}) - E_p & 0 \\ 0 & 0 & \varepsilon(\boldsymbol{k}) - E_p \end{bmatrix} \begin{bmatrix} b_{p_x} \\ b_{p_y} \\ b_{p_z} \end{bmatrix} = \\ &\begin{bmatrix} -\gamma_1 e^{\pm iak_x} - \gamma_2 e^{\pm iak_y} & 0 & 0 \\ 0 & -\gamma_2 e^{\pm iak_x} - \gamma_1 e^{\pm iak_y} & 0 \\ 0 & 0 & -\gamma_3(e^{\pm iak_x} + e^{\pm iak_y}) \end{bmatrix} \begin{bmatrix} b_{p_x} \\ b_{p_y} \\ b_{p_z} \end{bmatrix}\end{aligned} \tag{68}$$

The solution can be found by calculating:

$$\begin{vmatrix} \varepsilon(\boldsymbol{k}) - E_p + \gamma_1 e^{\pm iak_x} + \gamma_2 e^{\pm iak_y} & 0 & 0 \\ 0 & \varepsilon(\boldsymbol{k}) - E_p + \gamma_2 e^{\pm iak_x} + \gamma_1 e^{\pm iak_y} & 0 \\ 0 & 0 & \varepsilon(\boldsymbol{k}) - E_p + \gamma_3(e^{\pm iak_x} + e^{\pm iak_y}) \end{vmatrix} = 0 \tag{69}$$

Since this is a diagonal matrix the solutions are the diagonal entries, so we have

$$\begin{aligned}\varepsilon_{p_x}(\boldsymbol{k}) &= E_p - \gamma_1 e^{\pm iak_x} - \gamma_2 e^{\pm iak_y} = E_p - 2\gamma_1 \cos(ak_x) - 2\gamma_2 \cos(ak_y) \\ \varepsilon_{p_y}(\boldsymbol{k}) &= E_p - \gamma_2 e^{\pm iak_x} - \gamma_1 e^{\pm iak_y} = E_p - 2\gamma_2 \cos(ak_x) - 2\gamma_1 \cos(ak_y) \\ \varepsilon_{p_z}(\boldsymbol{k}) &= E_p - \gamma_3(e^{\pm iak_x} + e^{\pm iak_y}) = E_p - 2\gamma_3(\cos(ak_x) + \cos(ak_y))\end{aligned} \tag{70}$$

(c) When the next nearest neighbors are considered, the wave functions in figures 24b and 24d give rise to nonzero hopping integrals between the wave function at the origin and the wave functions at the next nearest neighbor positions. For the wave functions in figures 24c and 24f to 24h the hopping integrals are still all zero however, as can be seen by looking at the integrands in the xy plane. This means the matrix is block diagonal.

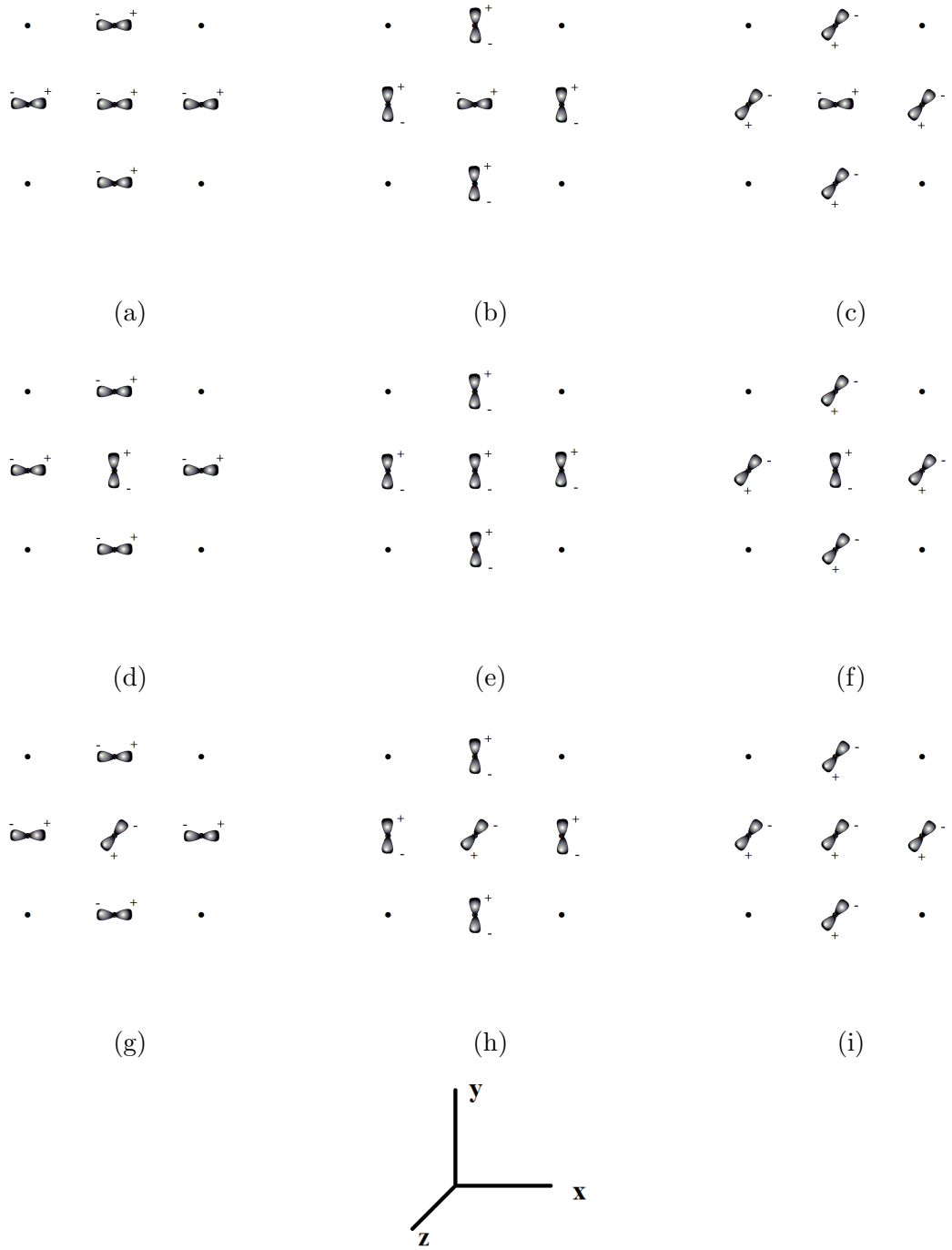

Figure 24: Wavefunctions sketched for the different hopping integrals arising from equation (33).

Assignment 5 - Tight Binding Method

Problem 1 - Tight-Binding p-Bands in Cubic Crystals

(a)

$$\beta_{xx} = \gamma_{xx}(\boldsymbol{R} = 0) = -\int d\boldsymbol{r}\psi_x^*(\boldsymbol{r})\psi_x(\boldsymbol{r})\Delta U(\boldsymbol{r}) = -\int d\boldsymbol{r}x^2|\phi(r)|^2\Delta U(\boldsymbol{r}) \tag{71}$$

[6]

with $r = |\boldsymbol{r}|$ Because of cubic symmetry, a rotation around the z-axis can be done, so that $x \to y$ and $y \to -x$. Now equation (71) becomes:

$$-\int d\boldsymbol{r}y^2|\phi(r)|^2\Delta U(\boldsymbol{r}) = -\int d\boldsymbol{r}\psi_y^*(\boldsymbol{r})\psi_y(\boldsymbol{r})\Delta U(\boldsymbol{r}) = \beta_{yy}$$

In the same way transformations around the x-axis or y-axis can be done to prove that $\beta_{xx} = \beta_{yy} = \beta_{zz} = \beta$.

$$\beta_{xy} = \gamma_{xy}(\boldsymbol{R} = 0) = -\int d\boldsymbol{r}\psi_x^*(\boldsymbol{r})\psi_y(\boldsymbol{r})\Delta U(\boldsymbol{r}) = -\int d\boldsymbol{r}xy|\phi(r)|^2\Delta U(\boldsymbol{r}) \tag{72}$$

Applying the same transformation as above ($x \to y$, $y \to -x$) to equation (72) gives:

$$\beta_{xy} = \int d\boldsymbol{r}xy|\phi(r)|^2\Delta U(\boldsymbol{r}) \tag{73}$$

Combining equations (72) and (73) gives:

$$\begin{aligned} 2\beta_{xy} &= \int d\boldsymbol{r}xy|\phi(r)|^2\Delta U(\boldsymbol{r}) - \int d\boldsymbol{r}xy|\phi(r)|^2\Delta U(\boldsymbol{r}) \\ 2\beta_{xy} &= 0 \\ \beta_{xy} &= 0 \end{aligned}$$

(b) To show that $\tilde{\gamma}_{ij}(\boldsymbol{k})$ is diagonal we first take a look at $\tilde{\gamma}_{xy}(\boldsymbol{k})$:

$$\tilde{\gamma}_{xy}(\boldsymbol{k}) = \sum_{\boldsymbol{R}} e^{i\boldsymbol{k}\cdot\boldsymbol{R}}\gamma_{xy}(\boldsymbol{R}) = \sum_{\boldsymbol{R}} -e^{i\boldsymbol{k}\cdot\boldsymbol{R}}\int d\boldsymbol{r}\psi_x^*(\boldsymbol{r})\psi_y(\boldsymbol{r}-\boldsymbol{R})\Delta U(\boldsymbol{r}) \tag{74}$$

[6]

Only nearest-neighbors $\boldsymbol{R}$ are considered, so $\boldsymbol{R} = a(\pm1, 0, 0)$, $a(0, \pm1, 0)$, $a(0, 0, \pm1)$ and $\boldsymbol{k}\cdot\boldsymbol{R} = \pm ak_i$, $i = x, y, z$.

In figure 25 the p-orbitals are drawn with $\psi_x(\boldsymbol{r})$ in the center and it's nearest neighbors $\psi_y(\boldsymbol{r} - \boldsymbol{R})$. Figure 25b shows the XY-plane, in wich $\psi_x(\boldsymbol{r})$ at the origin is even and the nearest neigbors ($\psi_y(\boldsymbol{r} - \boldsymbol{R})$) are odd. Therefore the overlap integrals between $\psi_x(\boldsymbol{r})$ and $\psi_y(\boldsymbol{r} - \boldsymbol{R})$ for $\boldsymbol{R} = a(\pm1, 0, 0)$ and $a(0, \pm1, 0)$ are zero. In figure 25a it can be seen that this is the case for $\psi_x(\boldsymbol{r})$ and all it's nearest neighbors. The same argument can be made for the other off-diagonal terms, therefore all off-diagonal terms are zero.

For the diagonal terms however, there's a different situation, as shown in figure 26. For the diagonal terms there's a $\psi_i(\boldsymbol{r})$ at the origin and a $\psi_j(\boldsymbol{r} - \boldsymbol{R})$ at it's nearest neighbors with $i = j$ (in the case of figure 26 $i = j = x$). Therefore, the product of these functions is always even and the integral is not necessarily zero.

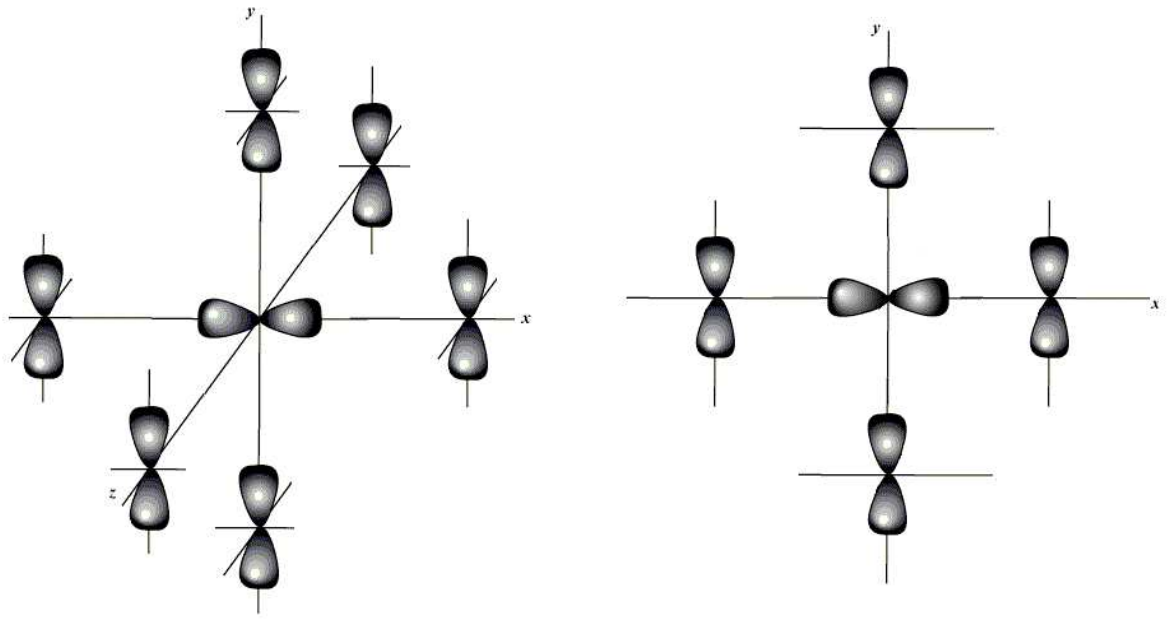

(a) 3D representation (b) XY-intersection

Figure 25: 3D representation (figure 25a) and XY-intersection (figure 25b) of the p-orbitals in a simple cubic lattice for an atom at the origin and it's nearest neighbors. The atom at the origin is a p_x state while the nearest neighbors are p_y states. Based on [16]

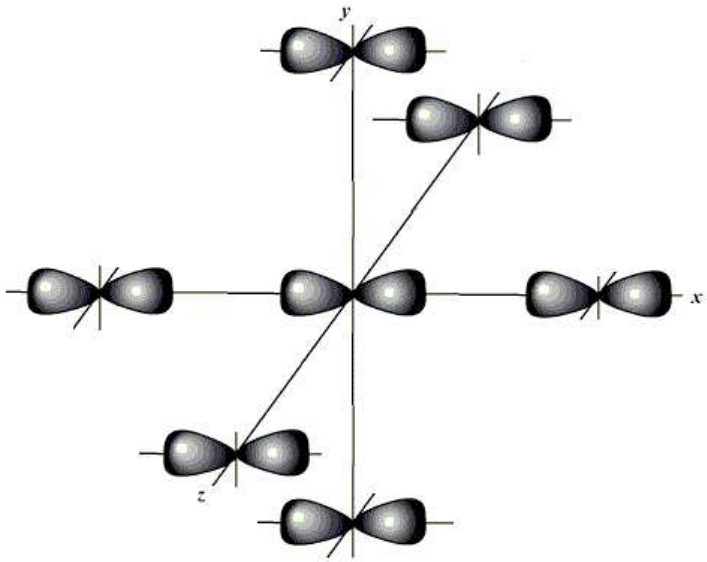

Figure 26: 3D representation of the p-orbitals of an atom at the origin of a simple cubic lattice and it's nearest neighbors. The atom at the origin and it's nearest neighbors are p_x states. Based on [16]

(c) The energies are given by:

$$|(\varepsilon(\boldsymbol{k}) - E_p)\delta_{ij} + \beta_{ij} + \tilde{\gamma}_{ij}(\boldsymbol{k})| = 0 \tag{75}$$

[6]

For the off-diagonal terms $(\varepsilon(\boldsymbol{k}) - E_p)\delta_{ij} = 0$ and $\beta_{ij} = 0$, so only $\tilde{\gamma}_{ij}$ remains.

From Ashcroft and Mermin [6] we know that $\tilde{\gamma}_{ij} = \sum_{\boldsymbol{R}} e^{i\boldsymbol{k}\cdot\boldsymbol{R}}\gamma_{ij}(\boldsymbol{R})$. The lattice is a face-centered cubic Bravais lattice and we only consider nearest neigbor atoms. Therefore $\boldsymbol{R} = \frac{a}{2}(\pm1, \pm1, 0)$, $\frac{a}{2}(\pm1, 0, \pm1)$, $\frac{a}{2}(0, \pm1, \pm1)$ and $\boldsymbol{k}\cdot\boldsymbol{R} = \frac{a}{2}(\pm k_i, \pm k_j) \qquad i, j = x, y;\ y, z;\ z, x.$

Take, for example, $\tilde{\gamma}_{xy}(\boldsymbol{k})$:

$$\tilde{\gamma}_{xy}(\boldsymbol{k}) = \sum_{\boldsymbol{R}} e^{i\boldsymbol{k}\cdot\boldsymbol{R}}\gamma_{xy}(\boldsymbol{R}) = \sum_{\boldsymbol{R}} -e^{i\boldsymbol{k}\cdot\boldsymbol{R}} \int d\boldsymbol{r}\psi_x^*(\boldsymbol{r})\psi_y(\boldsymbol{r} - \boldsymbol{R})\Delta U(\boldsymbol{r}) \tag{76}$$

[6]

In figure 27 the p-orbitals in this case are drawn. $\psi_x(\boldsymbol{r})$ can be seen at the origin with it's nearest neighbors $\psi_y(\boldsymbol{r} - \boldsymbol{R})$ around it. Three planes can be distinguished, the XY-plane, the YZ-plane and the XZ-plane.

In the XZ-plane $\psi_x(\boldsymbol{r})$ is an even function, while $\psi_y(\boldsymbol{r} - \boldsymbol{R})$ (with $\boldsymbol{R} = \frac{a}{2}(\pm1, 0, \pm1)$) are odd. Therefore the overlap integrals between the wavefunctions are zero.

In the YZ-plane $\psi_x(\boldsymbol{r})$ is an odd function, while $\psi_y(\boldsymbol{r} - \boldsymbol{R})$ (with $\boldsymbol{R} = \frac{a}{2}(0, \pm1, \pm1)$) are even. Therefore the overlap integrals between these wavefunctions is also zero.

In the XY-plane however, $\psi_x(\boldsymbol{r})$ as well as $\psi_y(\boldsymbol{r}-\boldsymbol{R})$ (with $\boldsymbol{R} = \frac{a}{2}(\pm1, \pm1, 0)$) are even functions. Therefore, these integrals are not necessarily zero.

This leaves only four terms for the summation:

$$\begin{aligned}
\tilde{\gamma}_{xy}(\boldsymbol{k}) = &-e^{i\frac{a}{2}(k_x+k_y)} \int d\boldsymbol{r}x(y - \frac{a}{2})\phi^*(r)\phi(\sqrt{(x - \frac{a}{2})^2 + (y - \frac{a}{2})^2 + z^2})\Delta U(\boldsymbol{r}) \\
&-e^{i\frac{a}{2}(k_x-k_y)} \int d\boldsymbol{r}x(y + \frac{a}{2})\phi^*(r)\phi(\sqrt{(x - \frac{a}{2})^2 + (y + \frac{a}{2})^2 + z^2})\Delta U(\boldsymbol{r}) \\
&-e^{i\frac{a}{2}(-k_x+k_y)} \int d\boldsymbol{r}x(y - \frac{a}{2})\phi^*(r)\phi(\sqrt{(x + \frac{a}{2})^2 + (y - \frac{a}{2})^2 + z^2})\Delta U(\boldsymbol{r}) \\
&-e^{i\frac{a}{2}(-k_x-k_y)} \int d\boldsymbol{r}x(y + \frac{a}{2})\phi^*(r)\phi(\sqrt{(x + \frac{a}{2})^2 + (y + \frac{a}{2})^2 + z^2})\Delta U(\boldsymbol{r})
\end{aligned} \tag{77}$$

where r is the magnitude of $\boldsymbol{r}$.

In figure 28 the XY-intersection of figure 27 is given. In this figure, one can see from rotating $\boldsymbol{R} = (-1, -1, 0)$ and $\boldsymbol{R} = (+1, -1, 0)$ for 180 ° around the x-axis that the overlap integrals of the wavefunctions at these positions with the wavefunction at the origin are the same as the overlap integrals of the wavefunctions at $\boldsymbol{R} = (-1, +1, 0)$ and $\boldsymbol{R} = (+1, +1, 0)$ respectively with the wavefunction at the origin, but with opposite signs. Also, rotating $\boldsymbol{R} = (-1, -1, 0)$ for 180 ° around the z-axis changes the sign of the overlap integral of this wavefunction with the wavefunction at the origin twice. Therefore, the overlap integral between the wavefunction at the origin and the wavefunction at $\boldsymbol{R} = (-1, -1, 0)$ is equal to the overlap integral between the wavefunction at the origin and the wavefunction at $\boldsymbol{R} = (1, 1, 0)$. It also shows that the overlap integral between the wavefunction at the origin and the wavefunction at $\boldsymbol{R} = (1, -1, 0)$

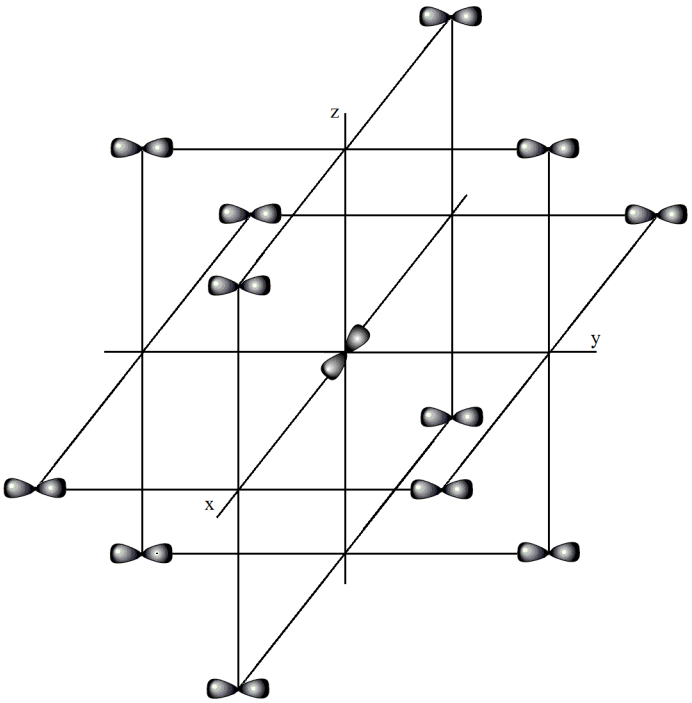

Figure 27: 3D representation of the p-orbitals of an atom at the origin of a face centered cubic lattice and it's nearest neighbors. The atom at the origin is a p_x state while the nearest neighbors are p_y states. Based on [16]

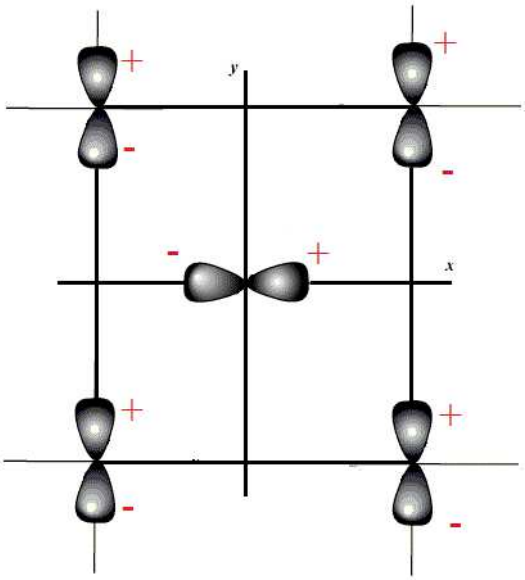

Figure 28: XY-intersection of figure 27, containing the p-orbitals of an atom at the origin of a face centered cubic lattice and it's nearest neighbors. The atom at the origin is a p_x state while the nearest neighbors are p_y states. Two directions are shown + and -. Based on [16]

is equal to the overlap integral between the wavefunction at the origin and the wavefunction at $\boldsymbol{R} = (-1, 1, 0)$.

From Ashcroft and Mermin we know that

$$-\int d\boldsymbol{r} x(y-\frac{a}{2})\phi^*(r)\phi(\sqrt{(x-\frac{a}{2})^2+(y-\frac{a}{2})^2+z^2})\Delta U(\boldsymbol{r}) = \gamma_1 \tag{78}$$

Combining equation (77) and equation (78) with the information about the overlap integrals above we get

$$\begin{aligned}
\tilde{\gamma}_{xy}(\boldsymbol{k}) &= \gamma_1(e^{i\frac{a}{2}(k_x+k_y)} - e^{i\frac{a}{2}(k_x-k_y)} - e^{i\frac{a}{2}(-k_x+k_y)} + e^{i\frac{a}{2}(-k_x-k_y)}) \\
&= \gamma_1((\cos(\frac{a}{2}k_x) + i\sin(\frac{a}{2}k_x))(\cos(\frac{a}{2}k_y) + i\sin(\frac{a}{2}k_y)) \\
&-(\cos(\frac{a}{2}k_x) + i\sin(\frac{a}{2}k_x))(\cos(-\frac{a}{2}k_y) + i\sin(-\frac{a}{2}k_y)) \\
&-(\cos(-\frac{a}{2}k_x) + i\sin(-\frac{a}{2}k_x))(\cos(\frac{a}{2}k_y) + i\sin(\frac{a}{2}k_y)) \\
&+(\cos(-\frac{a}{2}k_x) + i\sin(-\frac{a}{2}k_x))(\cos(-\frac{a}{2}k_y) + i\sin(-\frac{a}{2}k_y))) \\
&= \gamma_1(\cos(\frac{a}{2}k_x)\cos(\frac{a}{2}k_y) + i\cos(\frac{a}{2}k_x)\sin(\frac{a}{2}k_y) \\
&+i\sin(\frac{a}{2}k_x)\cos(\frac{a}{2}k_y) - \sin(\frac{a}{2}k_x)\sin(\frac{a}{2}k_y) \\
&-\cos(\frac{a}{2}k_x)\cos(-\frac{a}{2}k_y) - i\cos(\frac{a}{2}k_x)\sin(-\frac{a}{2}k_y) \\
&-i\sin(\frac{a}{2}k_x)\cos(-\frac{a}{2}k_y) + \sin(\frac{a}{2}k_x)\sin(-\frac{a}{2}k_y) \\
&-\cos(-\frac{a}{2}k_x)\cos(\frac{a}{2}k_y) - i\cos(-\frac{a}{2}k_x)\sin(\frac{a}{2}k_y) \\
&-i\sin(-\frac{a}{2}k_x)\cos(\frac{a}{2}k_y) + \sin(-\frac{a}{2}k_x)\sin(\frac{a}{2}k_y) \\
&+\cos(-\frac{a}{2}k_x)\cos(-\frac{a}{2}k_y) + i\cos(-\frac{a}{2}k_x)\sin(-\frac{a}{2}k_y) \\
&+i\sin(-\frac{a}{2}k_x)\cos(-\frac{a}{2}k_y) - \sin(-\frac{a}{2}k_x)\sin(-\frac{a}{2}k_y)) \\
&= -4\gamma_1(\sin(\frac{a}{2}k_x)\sin(\frac{a}{2}k_y))
\end{aligned} \tag{79}$$

wich matches the value given in Ashcroft and Mermin. In the same way, the othter off-diagonal terms can be derived.

Looking at the diagonal terms we have, if we take for example $i, j = x, x$:

$$\begin{aligned}
(\varepsilon(\boldsymbol{k}) - E_p)\delta_{xx} + \beta_{xx} + \tilde{\gamma}_{xx}(\boldsymbol{k}) &= \varepsilon(\boldsymbol{k}) - E_p + \beta + \sum_{\boldsymbol{R}} e^{i\boldsymbol{k}\cdot\boldsymbol{R}}\gamma_{xx}(\boldsymbol{R}) \\
&= \varepsilon(\boldsymbol{k}) - E_p + \beta + \sum_{\boldsymbol{R}} -e^{i\boldsymbol{k}\cdot\boldsymbol{R}}\int d\boldsymbol{r}\psi_x^*(\boldsymbol{r})\psi_x(\boldsymbol{r}-\boldsymbol{R})\Delta U(\boldsymbol{r})
\end{aligned} \tag{80}$$

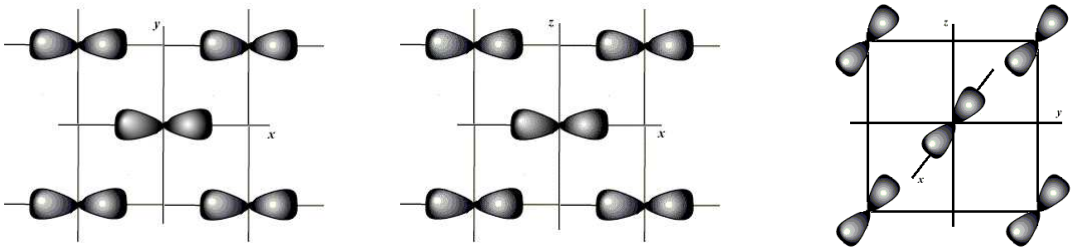

(a) XY-plane (b) XZ-plane (c) YZ-plane

Figure 29: Three planes showing an atom at the origin and it's twelve nearest neighbors in a face centered cubic lattice. All the wavefunctions are p_x-orbtials. Based on [16]

Writing this out gives us

$$\begin{aligned}
\varepsilon(\boldsymbol{k}) - E_p + \beta - e^{i\frac{a}{2}(k_x+k_y)} \int d\boldsymbol{r} x(x-\frac{a}{2})\phi^*(r)\phi(\sqrt{(x-\frac{a}{2})^2+(y-\frac{a}{2})^2+z^2})\Delta U(\boldsymbol{r}) \\
-e^{i\frac{a}{2}(k_x-k_y)} \int d\boldsymbol{r} x(x-\frac{a}{2})\phi^*(r)\phi(\sqrt{(x-\frac{a}{2})^2+(y+\frac{a}{2})^2+z^2})\Delta U(\boldsymbol{r}) \\
-e^{i\frac{a}{2}(-k_x+k_y)} \int d\boldsymbol{r} x(x+\frac{a}{2})\phi^*(r)\phi(\sqrt{(x+\frac{a}{2})^2+(y-\frac{a}{2})^2+z^2})\Delta U(\boldsymbol{r}) \\
-e^{i\frac{a}{2}(-k_x-k_y)} \int d\boldsymbol{r} x(x+\frac{a}{2})\phi^*(r)\phi(\sqrt{(x+\frac{a}{2})^2+(y+\frac{a}{2})^2+z^2})\Delta U(\boldsymbol{r}) \\
-e^{i\frac{a}{2}(k_y+k_z)} \int d\boldsymbol{r} x^2\phi^*(r)\phi(\sqrt{x^2+(y-\frac{a}{2})^2+(z-\frac{a}{2})^2})\Delta U(\boldsymbol{r}) \\
-e^{i\frac{a}{2}(k_y-k_z)} \int d\boldsymbol{r} x^2\phi^*(r)\phi(\sqrt{x^2+(y-\frac{a}{2})^2+(z+\frac{a}{2})^2})\Delta U(\boldsymbol{r}) \\
-e^{i\frac{a}{2}(-k_y+k_z)} \int d\boldsymbol{r} x^2\phi^*(r)\phi(\sqrt{x^2+(y+\frac{a}{2})^2+(z-\frac{a}{2})^2})\Delta U(\boldsymbol{r}) \\
-e^{i\frac{a}{2}(-k_y-k_z)} \int d\boldsymbol{r} x^2\phi^*(r)\phi(\sqrt{x^2+(y+\frac{a}{2})^2+(z+\frac{a}{2})^2})\Delta U(\boldsymbol{r}) \\
-e^{i\frac{a}{2}(k_x+k_z)} \int d\boldsymbol{r} x(x-\frac{a}{2})\phi^*(r)\phi(\sqrt{(x-\frac{a}{2})^2+y^2+(z-\frac{a}{2})^2})\Delta U(\boldsymbol{r}) \\
-e^{i\frac{a}{2}(k_x-k_z)} \int d\boldsymbol{r} x(x-\frac{a}{2})\phi^*(r)\phi(\sqrt{(x-\frac{a}{2})^2+y^2+(z+\frac{a}{2})^2})\Delta U(\boldsymbol{r}) \\
-e^{i\frac{a}{2}(-k_x+k_z)} \int d\boldsymbol{r} x(x+\frac{a}{2})\phi^*(r)\phi(\sqrt{(x+\frac{a}{2})^2+y^2+(z-\frac{a}{2})^2})\Delta U(\boldsymbol{r}) \\
-e^{i\frac{a}{2}(-k_x-k_z)} \int d\boldsymbol{r} x(x+\frac{a}{2})\phi^*(r)\phi(\sqrt{(x+\frac{a}{2})^2+y^2+(z+\frac{a}{2})^2})\Delta U(\boldsymbol{r})
\end{aligned} \tag{81}$$

In figure 29 the atom at the origin and it's nearest neighbors are shown. From this figure, we can see that the overlap integrals of the atom at the origin with $\boldsymbol{R} = (\pm 1, \pm 1, 0)$ and $\boldsymbol{R} = (\pm 1, 0, \pm 1)$ are all equal. Also, the overlap integrals of the atom at the origin with $\boldsymbol{R} = (0, \pm 1, \pm 1)$ are all equal.

We know that

$$\gamma_2 = -\int d\boldsymbol{r} x(x-\frac{a}{2})\phi^*(r)\phi(\sqrt{(x-\frac{a}{2})^2+(y-\frac{a}{2})^2+z^2})\Delta U(\boldsymbol{r}) \tag{82}$$

[6]

and we define

$$\gamma_3 = -\int d\boldsymbol{r} x^2 \phi^*(r)\phi(\sqrt{x^2+(y-\frac{a}{2})^2+(z-\frac{a}{2})^2})\Delta U(\boldsymbol{r}) \tag{83}$$

We rewrite equation (81) using equations (82) and (83):

$$\begin{aligned}\varepsilon(\boldsymbol{k}) - E_p + \beta + \gamma_2(e^{i\frac{a}{2}(k_x+k_y)} + e^{i\frac{a}{2}(k_x-k_y)} + e^{i\frac{a}{2}(-k_x+k_y)} + e^{i\frac{a}{2}(-k_x-k_y)} \\ + e^{i\frac{a}{2}(k_x+k_z)} + e^{i\frac{a}{2}(k_x-k_z)} + e^{i\frac{a}{2}(-k_x+k_z)} + e^{i\frac{a}{2}(-k_x-k_z)}) \\ + \gamma_3(e^{i\frac{a}{2}(k_y+k_z)} + e^{i\frac{a}{2}(k_y-k_z)} + e^{i\frac{a}{2}(-k_y+k_z)} + e^{i\frac{a}{2}(-k_y-k_z)})\end{aligned} \tag{84}$$

Rotating γ_2 for $90\,^\circ$ around the y-axis gives so that $x \to z$ and $z \to -x$:

$$\gamma_2 = -\int d\boldsymbol{r} z(z-\frac{a}{2})\phi^*(r)\phi(\sqrt{x^2+(y-\frac{a}{2})^2+(z-\frac{a}{2})^2})\Delta U(\boldsymbol{r}) \tag{85}$$

and we know that

$$\gamma_0 = -\int d\boldsymbol{r}[x^2 - y(y-\frac{a}{2})]\phi^*(r)\phi(\sqrt{x^2+(y-\frac{a}{2})^2+(z-\frac{a}{2})^2})\Delta U(\boldsymbol{r}) \tag{86}$$

[6]

Note that

$$\begin{aligned}\gamma_0 + \gamma_2 &= -\int d\boldsymbol{r}[x^2 - y(y-\frac{a}{2})]\phi^*(r)\phi(\sqrt{x^2+(y-\frac{a}{2})^2+(z-\frac{a}{2})^2})\Delta U(\boldsymbol{r}) \\ &\quad -\int d\boldsymbol{r} z(z-\frac{a}{2})\phi^*(r)\phi(\sqrt{x^2+(y-\frac{a}{2})^2+(z-\frac{a}{2})^2})\Delta U(\boldsymbol{r}) \\ &= -\int d\boldsymbol{r} x^2\phi^*(r)\phi(\sqrt{x^2+(y-\frac{a}{2})^2+(z-\frac{a}{2})^2})\Delta U(\boldsymbol{r}) \\ &\quad +\int d\boldsymbol{r} y(y-\frac{a}{2})\phi^*(r)\phi(\sqrt{x^2+(y-\frac{a}{2})^2+(z-\frac{a}{2})^2})\Delta U(\boldsymbol{r}) \\ &\quad -\int d\boldsymbol{r} z(z-\frac{a}{2})\phi^*(r)\phi(\sqrt{x^2+(y-\frac{a}{2})^2+(z-\frac{a}{2})^2})\Delta U(\boldsymbol{r})\end{aligned} \tag{87}$$

$\int d\boldsymbol{r} y(y-\frac{a}{2})\phi^*(r)\phi(\sqrt{x^2+(y-\frac{a}{2})^2+(z-\frac{a}{2})^2})\Delta U(\boldsymbol{r})$ and
$-\int d\boldsymbol{r} z(z-\frac{a}{2})\phi^*(r)\phi(\sqrt{x^2+(y-\frac{a}{2})^2+(z-\frac{a}{2})^2})\Delta U(\boldsymbol{r})$ are the same overlap integrals with different axes. Therefore

$$\gamma_0 + \gamma_2 = -\int d\boldsymbol{r} x^2\phi^*(r)\phi(\sqrt{x^2+(y-\frac{a}{2})^2+(z-\frac{a}{2})^2})\Delta U(\boldsymbol{r}) = \gamma_3 \tag{88}$$

Combining equations (84) and (88) gives us:

$$
\begin{aligned}
&\varepsilon(\boldsymbol{k}) - E_p + \beta + \gamma_2(e^{i\frac{a}{2}(k_x+k_y)} + e^{i\frac{a}{2}(k_x-k_y)} + e^{i\frac{a}{2}(-k_x+k_y)} + e^{i\frac{a}{2}(-k_x-k_y)} \\
&\quad + e^{i\frac{a}{2}(k_x+k_z)} + e^{i\frac{a}{2}(k_x-k_z)} + e^{i\frac{a}{2}(-k_x+k_z)} + e^{i\frac{a}{2}(-k_x-k_z)}) \\
&\quad + (\gamma_2+\gamma_0)(e^{i\frac{a}{2}(k_y+k_z)} + e^{i\frac{a}{2}(k_y-k_z)} + e^{i\frac{a}{2}(-k_y+k_z)} + e^{i\frac{a}{2}(-k_y-k_z)}) \\
&= \varepsilon(\boldsymbol{k}) - E_p + \beta + \gamma_2((\cos(\frac{a}{2}k_x) + i\sin(\frac{a}{2}k_x))(\cos(\frac{a}{2}k_y) + i\sin(\frac{a}{2}k_y)) \\
&\quad + (\cos(\frac{a}{2}k_x) + i\sin(\frac{a}{2}k_x))(\cos(-\frac{a}{2}k_y) + i\sin(-\frac{a}{2}k_y)) \\
&\quad + (\cos(-\frac{a}{2}k_x) + i\sin(-\frac{a}{2}k_x))(\cos(+\frac{a}{2}k_y) + i\sin(+\frac{a}{2}k_y)) \\
&\quad + (\cos(-\frac{a}{2}k_x) + i\sin(-\frac{a}{2}k_x))(\cos(-\frac{a}{2}k_y) + i\sin(-\frac{a}{2}k_y)) \\
&\quad + (\cos(\frac{a}{2}k_x) + i\sin(\frac{a}{2}k_x))(\cos(\frac{a}{2}k_z) + i\sin(\frac{a}{2}k_z)) \\
&\quad + (\cos(\frac{a}{2}k_x) + i\sin(\frac{a}{2}k_x))(\cos(-\frac{a}{2}k_z) + i\sin(-\frac{a}{2}k_z)) \\
&\quad + (\cos(-\frac{a}{2}k_x) + i\sin(-\frac{a}{2}k_x))(\cos(\frac{a}{2}k_z) + i\sin(\frac{a}{2}k_z)) \\
&\quad + (\cos(-\frac{a}{2}k_x) + i\sin(-\frac{a}{2}k_x))(\cos(-\frac{a}{2}k_z) + i\sin(-\frac{a}{2}k_z))) \\
&\quad + (\gamma_2+\gamma_0)((\cos(\frac{a}{2}k_y) + i\sin(\frac{a}{2}k_y))(\cos(\frac{a}{2}k_z) + i\sin(\frac{a}{2}k_z)) \\
&\quad + (\cos(\frac{a}{2}k_y) + i\sin(\frac{a}{2}k_y))(\cos(-\frac{a}{2}k_z) + i\sin(-\frac{a}{2}k_z)) \\
&\quad + (\cos(-\frac{a}{2}k_y) + i\sin(-\frac{a}{2}k_y))(\cos(\frac{a}{2}k_z) + i\sin(\frac{a}{2}k_z)) \\
&\quad + (\cos(-\frac{a}{2}k_y) + i\sin(-\frac{a}{2}k_y))(\cos(-\frac{a}{2}k_z) + i\sin(-\frac{a}{2}k_z))) \\
&= \varepsilon(\boldsymbol{k}) - E_p + \beta + \gamma_2(\cos(\frac{a}{2}k_x)\cos(\frac{a}{2}k_y) + i\cos(\frac{a}{2}k_x)\sin(\frac{a}{2}k_y) \\
&\quad + i\sin(\frac{a}{2}k_x)\cos(\frac{a}{2}k_y) - \sin(\frac{a}{2}k_x)\sin(\frac{a}{2}k_y) \\
&\quad + \cos(\frac{a}{2}k_x)\cos(-\frac{a}{2}k_y) + i\cos(\frac{a}{2}k_x)\sin(-\frac{a}{2}k_y) \\
&\quad + i\sin(\frac{a}{2}k_x)\cos(-\frac{a}{2}k_y) - \sin(\frac{a}{2}k_x)\sin(-\frac{a}{2}k_y) \\
&\quad \cos(-\frac{a}{2}k_x)\cos(\frac{a}{2}k_y) + i\cos(-\frac{a}{2}k_x)\sin(\frac{a}{2}k_y) \\
&\quad + i\sin(-\frac{a}{2}k_x)\cos(\frac{a}{2}k_y) - \sin(-\frac{a}{2}k_x)\sin(\frac{a}{2}k_y) \\
&\quad \cos(-\frac{a}{2}k_x)\cos(-\frac{a}{2}k_y) + i\cos(-\frac{a}{2}k_x)\sin(-\frac{a}{2}k_y) \\
&\quad + i\sin(-\frac{a}{2}k_x)\cos(-\frac{a}{2}k_y) - \sin(-\frac{a}{2}k_x)\sin(-\frac{a}{2}k_y)
\end{aligned}
\tag{89}
$$

$$
\begin{aligned}
&+\cos(\tfrac{a}{2}k_x)\cos(\tfrac{a}{2}k_z)+i\cos(\tfrac{a}{2}k_x)\sin(\tfrac{a}{2}k_z)\\
&+i\sin(\tfrac{a}{2}k_x)\cos(\tfrac{a}{2}k_z)-\sin(\tfrac{a}{2}k_x)\sin(\tfrac{a}{2}k_z)\\
&+\cos(\tfrac{a}{2}k_x)\cos(-\tfrac{a}{2}k_z)+i\cos(\tfrac{a}{2}k_x)\sin(-\tfrac{a}{2}k_z)\\
&+i\sin(\tfrac{a}{2}k_x)\cos(-\tfrac{a}{2}k_z)-\sin(\tfrac{a}{2}k_x)\sin(-\tfrac{a}{2}k_z)\\
&+\cos(-\tfrac{a}{2}k_x)\cos(\tfrac{a}{2}k_z)+i\cos(-\tfrac{a}{2}k_x)\sin(\tfrac{a}{2}k_z)\\
&+i\sin(-\tfrac{a}{2}k_x)\cos(\tfrac{a}{2}k_z)-\sin(-\tfrac{a}{2}k_x)\sin(\tfrac{a}{2}k_z)\\
&+\cos(-\tfrac{a}{2}k_x)\cos(-\tfrac{a}{2}k_z)+i\cos(-\tfrac{a}{2}k_x)\sin(-\tfrac{a}{2}k_z)\\
&+i\sin(-\tfrac{a}{2}k_x)\cos(-\tfrac{a}{2}k_z)-\sin(-\tfrac{a}{2}k_x)\sin(-\tfrac{a}{2}k_z))\\
&+(\gamma_2+\gamma_0)(\cos(\tfrac{a}{2}k_y)\cos(\tfrac{a}{2}k_z)+i\cos(\tfrac{a}{2}k_y)\sin(\tfrac{a}{2}k_z)\\
&+i\sin(\tfrac{a}{2}k_y)\cos(\tfrac{a}{2}k_z)-\sin(\tfrac{a}{2}k_y)\sin(\tfrac{a}{2}k_z)\\
&+\cos(\tfrac{a}{2}k_y)\cos(-\tfrac{a}{2}k_z)+i\cos(\tfrac{a}{2}k_y)\sin(-\tfrac{a}{2}k_z)\\
&+i\sin(\tfrac{a}{2}k_y)\cos(-\tfrac{a}{2}k_z)-\sin(\tfrac{a}{2}k_y)\sin(-\tfrac{a}{2}k_z)\\
&+\cos(-\tfrac{a}{2}k_y)\cos(\tfrac{a}{2}k_z)+i\cos(-\tfrac{a}{2}k_y)\sin(\tfrac{a}{2}k_z)\\
&+i\sin(-\tfrac{a}{2}k_y)\cos(\tfrac{a}{2}k_z)-\sin(-\tfrac{a}{2}k_y)\sin(\tfrac{a}{2}k_z)\\
&+\cos(-\tfrac{a}{2}k_y)\cos(-\tfrac{a}{2}k_z)+i\cos(-\tfrac{a}{2}k_y)\sin(-\tfrac{a}{2}k_z)\\
&+i\sin(-\tfrac{a}{2}k_y)\cos(-\tfrac{a}{2}k_z)-\sin(-\tfrac{a}{2}k_y)\sin(-\tfrac{a}{2}k_z))\\
&=\varepsilon(\boldsymbol{k})-E_p+\beta+\gamma_2(4\cos(\tfrac{a}{2}k_x)\cos(\tfrac{a}{2}k_y)+4\cos(\tfrac{a}{2}k_x)\cos(\tfrac{a}{2}k_z))\\
&+(\gamma_2+\gamma_0)4\cos(\tfrac{a}{2}k_y)\cos(\tfrac{a}{2}k_z)=\varepsilon(\boldsymbol{k})-\varepsilon^0(\boldsymbol{k})+4\gamma_0\cos(\tfrac{a}{2}k_y)\cos(\tfrac{a}{2}k_z)
\end{aligned}
$$

with $\varepsilon^0(\boldsymbol{k})=E_p-\beta-4\gamma_2(\cos(\frac{a}{2}k_x)\cos(\frac{a}{2}k_y)+\cos(\frac{a}{2}k_x)\cos(\frac{a}{2}k_z)+\cos(\frac{a}{2}k_y)\cos(\frac{a}{2}k_z))$ [6]
In the same way the other diagonal terms can be proven.

(d) If $\boldsymbol{k}=\boldsymbol{0}$, then $\varepsilon^0(\boldsymbol{0})=E_p-\beta-12\gamma_2$ and the energy bands are given by the roots of

$$
\begin{aligned}
0&=\begin{vmatrix}\varepsilon(\boldsymbol{0})-\varepsilon^0(\boldsymbol{0})+4\gamma_0 & 0 & 0\\ 0 & \varepsilon(\boldsymbol{0})-\varepsilon^0(\boldsymbol{0})+4\gamma_0 & 0\\ 0 & 0 & \varepsilon(\boldsymbol{0})-\varepsilon^0(\boldsymbol{0})+4\gamma_0\end{vmatrix}\\
&(\varepsilon(\boldsymbol{0})-\varepsilon^0(\boldsymbol{0})+4\gamma_0)(\varepsilon(\boldsymbol{0})-\varepsilon^0(\boldsymbol{0})+4\gamma_0)(\varepsilon(\boldsymbol{0})-\varepsilon^0(\boldsymbol{0})+4\gamma_0)=0\\
&\varepsilon(\boldsymbol{0})-\varepsilon^0(\boldsymbol{0})+4\gamma_0=0\\
&\varepsilon(\boldsymbol{0})=\varepsilon^0(\boldsymbol{0})-4\gamma_0=E_p-\beta-12\gamma_2-4\gamma_0
\end{aligned}
\tag{90}
$$

with degeneracy $\mu(\varepsilon(\boldsymbol{0}))=3$, so all three bands are degenerate. The corresponding eigenvector is $\frac{1}{\sqrt{3}}\begin{pmatrix}1\\1\\1\end{pmatrix}$.

Now lets say $\boldsymbol{k}$ is directed along the y-axis (ΓX). Then $\boldsymbol{k} = \frac{2\pi}{a}\begin{pmatrix}0\\ \mu\\ 0\end{pmatrix}$ with $0 \leq \mu \leq 1$ and the energy bands are given by the roots of

$$0 = \begin{vmatrix} \varepsilon(\boldsymbol{k}) - \varepsilon^0(\boldsymbol{k}) + 4\gamma_0\cos(\pi\mu) & 0 & 0 \\ 0 & \varepsilon(\boldsymbol{k}) - \varepsilon^0(\boldsymbol{k}) + 4\gamma_0 & 0 \\ 0 & 0 & \varepsilon(\boldsymbol{k}) - \varepsilon^0(\boldsymbol{k}) + 4\gamma_0\cos(\pi\mu) \end{vmatrix} \tag{91}$$

where $\varepsilon^0(\boldsymbol{k}) = E_p - \beta - 8\gamma_2\cos(\pi\mu)$. Solving equation (91) gives us:

$$\begin{aligned} \varepsilon_1(\boldsymbol{k}) &= E_p - \beta - (4\gamma_0 + 8\gamma_2)\cos(\pi\mu) \quad \vee \\ \varepsilon_2(\boldsymbol{k}) &= E_p - \beta - 4\gamma_0 - 8\gamma_2\cos(\pi\mu) \end{aligned} \tag{92}$$

where the degeneracy of the eigenvalues is $\mu(\varepsilon_1(\boldsymbol{k})) = 2$ and $\mu(\varepsilon_2(\boldsymbol{k})) = 1$. Therefore, there is double degeneracy along the cube axis. The eigenvectors corresponding to the eigenvalues are $\frac{1}{\sqrt{2}}\begin{pmatrix}1\\0\\1\end{pmatrix}$ for $\varepsilon_1(\boldsymbol{k})$ and $\begin{pmatrix}0\\1\\0\end{pmatrix}$ for $\varepsilon_2(\boldsymbol{k})$.

Now lets look at the situation where $\boldsymbol{k}$ is directed along a cube diagonal (ΓL). In this case $\boldsymbol{k} = \frac{2\pi}{a}\begin{pmatrix}\mu\\ \mu\\ \mu\end{pmatrix}$ with $0 \leq \mu \leq \frac{1}{2}$ where the energy bands are given by the roots of

$$0 = \begin{vmatrix} \varepsilon(\boldsymbol{k}) - \varepsilon^0(\boldsymbol{k}) + 4\gamma_0\cos^2(\pi\mu) & -4\gamma_1\sin^2(\pi\mu) & -4\gamma_1\sin^2(\pi\mu) \\ -4\gamma_1\sin^2(\pi\mu) & \varepsilon(\boldsymbol{k}) - \varepsilon^0(\boldsymbol{k}) + 4\gamma_0\cos^2(\pi\mu) & -4\gamma_1\sin^2(\pi\mu) \\ -4\gamma_1\sin^2(\pi\mu) & -4\gamma_1\sin^2(\pi\mu) & \varepsilon(\boldsymbol{k}) - \varepsilon^0(\boldsymbol{k}) + 4\gamma_0\cos^2(\pi\mu) \end{vmatrix} \tag{93}$$

The matrix can be diagonalized:

$$\begin{aligned} &\begin{vmatrix} \varepsilon(\boldsymbol{k}) - \varepsilon^0(\boldsymbol{k}) + 4\gamma_0\cos^2(\pi\mu) + 4\gamma_1\sin^2(\pi\mu) & 0 & -4\gamma_1\sin^2(\pi\mu) - \varepsilon(\boldsymbol{k}) + \varepsilon^0(\boldsymbol{k}) - 4\gamma_0\cos^2(\pi\mu) \\ -4\gamma_1\sin^2(\pi\mu) & \varepsilon(\boldsymbol{k}) - \varepsilon^0(\boldsymbol{k}) + 4\gamma_0\cos^2(\pi\mu) & -4\gamma_1\sin^2(\pi\mu) \\ -4\gamma_1\sin^2(\pi\mu) & -4\gamma_1\sin^2(\pi\mu) & \varepsilon(\boldsymbol{k}) - \varepsilon^0(\boldsymbol{k}) + 4\gamma_0\cos^2(\pi\mu) \end{vmatrix} = 0 \\ &\begin{vmatrix} \varepsilon(\boldsymbol{k}) - \varepsilon^0(\boldsymbol{k}) + 4\gamma_0\cos^2(\pi\mu) + 4\gamma_1\sin^2(\pi\mu) & 0 & -4\gamma_1\sin^2(\pi\mu) - \varepsilon(\boldsymbol{k}) + \varepsilon^0(\boldsymbol{k}) - 4\gamma_0\cos^2(\pi\mu) \\ 0 & \varepsilon(\boldsymbol{k}) - \varepsilon^0(\boldsymbol{k}) + 4\gamma_0\cos^2(\pi\mu) + 4\gamma_1\sin^2(\pi\mu) & -4\gamma_1\sin^2(\pi\mu) - \varepsilon(\boldsymbol{k}) + \varepsilon^0(\boldsymbol{k}) - 4\gamma_0\cos^2(\pi\mu) \\ -4\gamma_1\sin^2(\pi\mu) & -4\gamma_1\sin^2(\pi\mu) & \varepsilon(\boldsymbol{k}) - \varepsilon^0(\boldsymbol{k}) + 4\gamma_0\cos^2(\pi\mu) \end{vmatrix} = 0 \\ &\begin{vmatrix} \varepsilon(\boldsymbol{k}) - \varepsilon^0(\boldsymbol{k}) + 4\gamma_0\cos^2(\pi\mu) + 4\gamma_1\sin^2(\pi\mu) & 0 & 0 \\ 0 & \varepsilon(\boldsymbol{k}) - \varepsilon^0(\boldsymbol{k}) + 4\gamma_0\cos^2(\pi\mu) + 4\gamma_1\sin^2(\pi\mu) & -4\gamma_1\sin^2(\pi\mu) - \varepsilon(\boldsymbol{k}) + \varepsilon^0(\boldsymbol{k}) - 4\gamma_0\cos^2(\pi\mu) \\ -4\gamma_1\sin^2(\pi\mu) & -4\gamma_1\sin^2(\pi\mu) & \varepsilon(\boldsymbol{k}) - \varepsilon^0(\boldsymbol{k}) + 4\gamma_0\cos^2(\pi\mu) - 4\gamma_1\sin^2(\pi\mu) \end{vmatrix} = 0 \\ &\begin{vmatrix} \varepsilon(\boldsymbol{k}) - \varepsilon^0(\boldsymbol{k}) + 4\gamma_0\cos^2(\pi\mu) + 4\gamma_1\sin^2(\pi\mu) & 0 & 0 \\ 0 & \varepsilon(\boldsymbol{k}) - \varepsilon^0(\boldsymbol{k}) + 4\gamma_0\cos^2(\pi\mu) + 4\gamma_1\sin^2(\pi\mu) & 0 \\ -4\gamma_1\sin^2(\pi\mu) & -4\gamma_1\sin^2(\pi\mu) & \varepsilon(\boldsymbol{k}) - \varepsilon^0(\boldsymbol{k}) + 4\gamma_0\cos^2(\pi\mu) - 8\gamma_1\sin^2(\pi\mu) \end{vmatrix} = 0 \\ &(\varepsilon(\boldsymbol{k}) - \varepsilon^0(\boldsymbol{k}) + 4\gamma_0\cos^2(\pi\mu) + 4\gamma_1\sin^2(\pi\mu))^2(\varepsilon(\boldsymbol{k}) - \varepsilon^0(\boldsymbol{k}) + 4\gamma_0\cos^2(\pi\mu) - 8\gamma_1\sin^2(\pi\mu)) = 0 \end{aligned} \tag{94}$$

where $\varepsilon^0(\boldsymbol{k}) = E_p - \beta - 12\gamma_2\cos^2(\pi\mu)$. Equation (94) can easily be solved for $\varepsilon(\boldsymbol{k})$:

$$\begin{aligned} \varepsilon_1(\boldsymbol{k}) &= E_p - \beta - 12\gamma_2\cos^2(\pi\mu) - 4\gamma_0\cos^2(\pi\mu) - 4\gamma_1\sin^2(\pi\mu) \quad \vee \\ \varepsilon_2(\boldsymbol{k}) &= E_p - \beta - 12\gamma_2\cos^2(\pi\mu) - 4\gamma_0\cos^2(\pi\mu) + 8\gamma_1\sin^2(\pi\mu) \end{aligned} \tag{95}$$

where the degeneracy of the eigenvalues is $\mu(\varepsilon_1(\boldsymbol{k})) = 2$ and $\mu(\varepsilon_2(\boldsymbol{k})) = 1$. Therefore, there is double degeneracy along the cube diagonal. The eigenvectors corresponding to the eigenvalues are $\frac{1}{\sqrt{18}}\begin{pmatrix}-4\\1\\1\end{pmatrix}$ for $\varepsilon_1(\boldsymbol{k})$ and $\begin{pmatrix}0\\0\\1\end{pmatrix}$ for $\varepsilon_2(\boldsymbol{k})$.

The energy bands in the ΓX-direction and ΓY-direction were sketched in figure 30. The figures show how the energy changes when moving along these two high-symmetry directions.

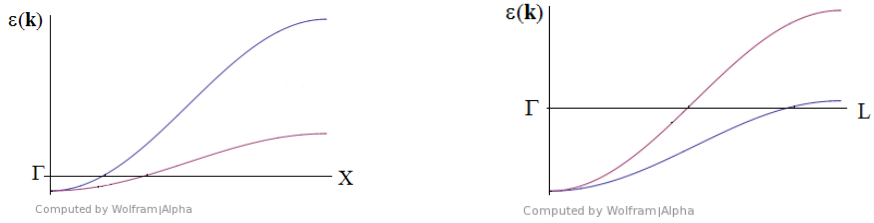

(a) ΓX-direction (b) ΓL-direction

Figure 30: Sketches of the energy of the p-bands along the ΓX direction and the ΓL direction. The band are calculated for a face centered cubic crystal using tight binding.

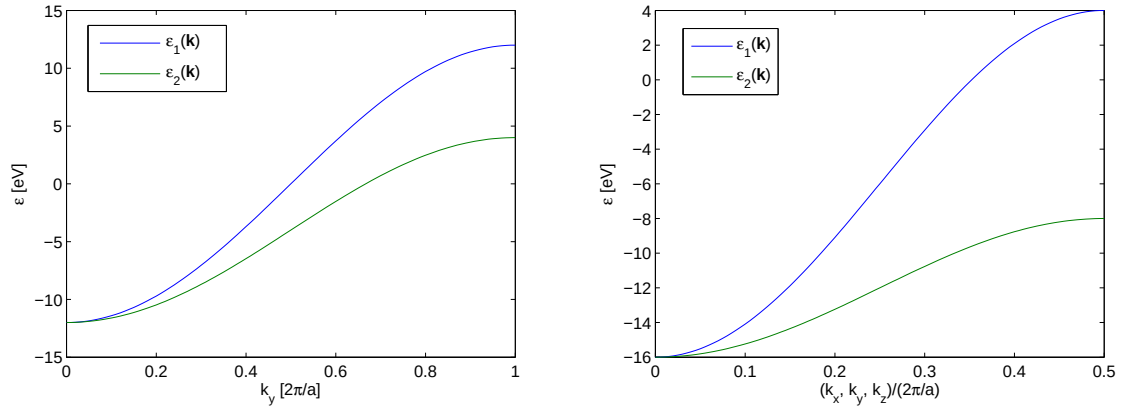

(a) ΓX-direction (b) ΓL-direction

Figure 31: Numerically solved energy bands in the ΓX-direction and the ΓL-direction. The calculations are made for a face centered cubic crystal using thight binding. They were based on equations (91) and (93).

Problem 2 - Numerical diagonalization

For this problem, the energy bands are calculated by setting up a loop over all k-points along the ΓX and ΓL-directions and solving equations (91) and (93) numerically.

In the case of equation (91) (ΓX) this can be done quite easily because the matrix is already diagonal. The energy bands that were calculated in this case are given in figure 31a. In this figure, the x-axis contains the values for k_y from 0 to $\frac{2\pi}{a}$ in units of $\frac{2\pi}{a}$, while the y-axis contains the energy $\varepsilon(\boldsymbol{k})$. The values of E_p and β were set to zero while for γ_0 and γ_2 a value of 1 eV was used. Only two energy bands are shown because $\varepsilon_1(\boldsymbol{k})$ is double degenerate.

Using a LAPACK subroutine the eigenvalues of the matrix in equation (93) (ΓL) can be determined numerically. In figure 31b the energybands in the ΓL direction are plotted. Again, the x-axis is in units of $\frac{2\pi}{a}$ and the y-axis contains the energy $\varepsilon(\boldsymbol{k})$. This time however, the bands are plotted along the line where $k_x = k_y = k_z$ from 0 to $\frac{\pi}{a}$. In this case also, E_p and β were set to zero, while for γ_0, γ_1 and γ_2 a value of 1 eV was used. Again, only two energy bands are shown because $\varepsilon_1(\boldsymbol{k})$ is double degenerate.

Comparing the numerical results to the analytical results shows that the numerical solution is a good way of solving the tight binding matrices for the dispersion.

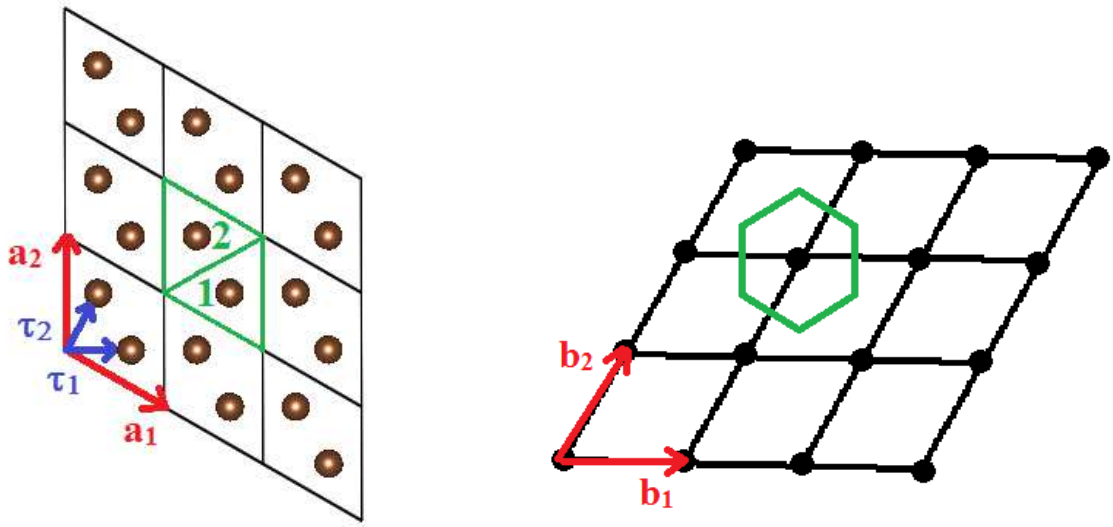

(a) Grapene lattice. The lattice vectors are indicated in red, the basis vectors are indicated in blue and the Wigner-Seitz cell is indicated in green. Based on an image made with VESTA [11].

(b) Reciprocal lattice of the graphene lattice from figure 32a. The reciprocal lattice vectors are indicated in red and the first Brillouin zone is indicated in green.

Figure 32: Lattice and reciprocal lattice of graphene.

Assignment 6

This section contains the solutions to the final assignment set from the Theoretical Solid State Physics course.

1. Graphene π bands

(a) A sketch of the lattice can be found in figure 32a. In this figure, the lattice vectors and basis vectors are indicated by $\boldsymbol{a}_1$, $\boldsymbol{a}_2$ and $\boldsymbol{\tau}_1$, $\boldsymbol{\tau}_2$ respectively. The Wigner-Seitz cell is indicated in green. Two Wigner-Seitz cells are drawn.

The reciprocal lattice vectors are:

$$\begin{aligned} \boldsymbol{b}_1 &= \frac{2\pi}{a}\left(\frac{2}{\sqrt{3}}, 0, 0\right) \\ \boldsymbol{b}_2 &= \frac{2\pi}{a}\left(\frac{1}{\sqrt{3}}, 1, 0\right) \end{aligned} \tag{96}$$

The reciprocal lattice is sketched in figure 32b. In this figure the reciprocal lattice vectors are indicated in red and the first Brillouin zone is indicated in green.

(b) In graphene the carbon atoms form covalent bonds with three other carbon atoms in their own plane. There is no covalent bonding between the planes. Since we have $(2s2p)^4$ states this means we have sp^2 hybridisation, where 1 s orbital and 2 p orbitals are involved in the bonding. Therefore we can consider the p_z orbitals separately from s, p_x and p_y orbitals.

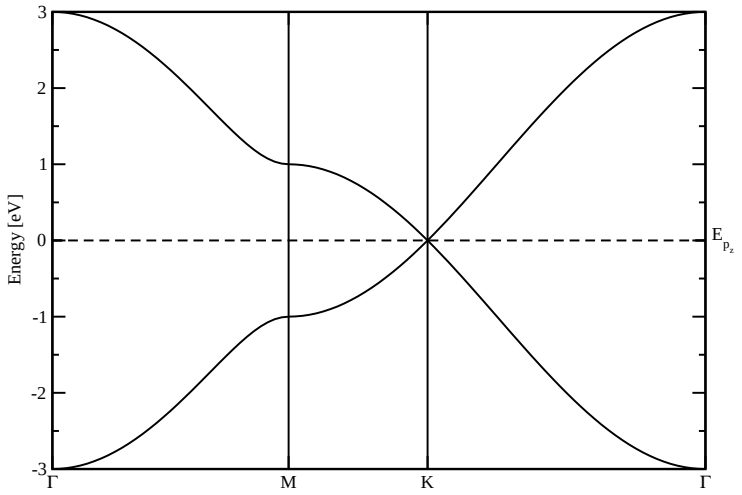

Figure 33: Graphene p_z bands plotted along the path Γ-M-K-Γ. The energy E_{p_z} was set to zero.

(c) We start from equation (33) and write down the matrix:

$$\begin{bmatrix} \varepsilon(\boldsymbol{k}) - E_{p_z} & 0 \\ 0 & \varepsilon(\boldsymbol{k}) - E_{p_z} \end{bmatrix} \begin{bmatrix} b_1 \\ b_2 \end{bmatrix} = \begin{bmatrix} 0 & \sum_{\boldsymbol{R}\neq 0} \left\langle \psi_1(\boldsymbol{r}) \middle| \Delta U(\boldsymbol{r}) \middle| \psi_2(\boldsymbol{r}-\boldsymbol{R}) e^{i\boldsymbol{k}\cdot\boldsymbol{R}} \right\rangle \\ \sum_{\boldsymbol{R}\neq 0} \left\langle \psi_2(\boldsymbol{r}) \middle| \Delta U(\boldsymbol{r}) \middle| \psi_1(\boldsymbol{r}-\boldsymbol{R}) e^{i\boldsymbol{k}\cdot\boldsymbol{R}} \right\rangle & 0 \end{bmatrix} \begin{bmatrix} b_1 \\ b_2 \end{bmatrix} \tag{97}$$

$$\begin{bmatrix} \varepsilon(\boldsymbol{k}) - E_{p_z} & 0 \\ 0 & \varepsilon(\boldsymbol{k}) - E_{p_z} \end{bmatrix} \begin{bmatrix} b_1 \\ b_2 \end{bmatrix} = \begin{bmatrix} 0 & -t \sum_{\boldsymbol{R}\neq 0} e^{i\boldsymbol{k}\cdot\boldsymbol{R}} \\ -t \sum_{\boldsymbol{R}\neq 0} e^{i\boldsymbol{k}\cdot\boldsymbol{R}} & 0 \end{bmatrix} \begin{bmatrix} b_1 \\ b_2 \end{bmatrix}$$

The solution can be found by solving:

$$\begin{aligned} \begin{vmatrix} E_{p_z} - \varepsilon(\boldsymbol{k}) & -t \sum_{\boldsymbol{R}\neq 0} e^{i\boldsymbol{k}\cdot\boldsymbol{R}} \\ -t \sum_{\boldsymbol{R}\neq 0} e^{i\boldsymbol{k}\cdot\boldsymbol{R}} & E_{p_z} - \varepsilon(\boldsymbol{k}) \end{vmatrix} &= 0 \\ \begin{vmatrix} E_{p_z} - \varepsilon(\boldsymbol{k}) & -t(1 + e^{i\boldsymbol{k}\cdot\boldsymbol{a}_1} + e^{-i\boldsymbol{k}\cdot\boldsymbol{a}_2}) \\ -t(1 + e^{-i\boldsymbol{k}\cdot\boldsymbol{a}_1} + e^{i\boldsymbol{k}\cdot\boldsymbol{a}_2}) & E_{p_z} - \varepsilon(\boldsymbol{k}) \end{vmatrix} &= 0 \\ (E_{p_z} - \varepsilon(\boldsymbol{k}))^2 - t^2(1 + e^{i\boldsymbol{k}\cdot\boldsymbol{a}_1} + e^{-i\boldsymbol{k}\cdot\boldsymbol{a}_2})(1 + e^{-i\boldsymbol{k}\cdot\boldsymbol{a}_1} + e^{i\boldsymbol{k}\cdot\boldsymbol{a}_2}) &= 0 \\ (E_{p_z} - \varepsilon(\boldsymbol{k}))^2 - t^2(3 + 2\cos(\boldsymbol{k}\cdot\boldsymbol{a}_1) + 2\cos(\boldsymbol{k}\cdot\boldsymbol{a}_2) + 2\cos(\boldsymbol{k}\cdot\boldsymbol{a}_1 + \boldsymbol{k}\cdot\boldsymbol{a}_2)) &= 0 \\ \varepsilon(\boldsymbol{k}) = E_{p_z} \pm t\sqrt{3 + 2(\cos(\boldsymbol{k}\cdot\boldsymbol{a}_1) + \cos(\boldsymbol{k}\cdot\boldsymbol{a}_2) + \cos(\boldsymbol{k}\cdot\boldsymbol{a}_1 + \boldsymbol{k}\cdot\boldsymbol{a}_2))} & \end{aligned} \tag{98}$$

(d) The energy bands resulting from equation (98) were plotted in figure 33 along the path Γ-M-K-Γ. For each of these subpaths, $\boldsymbol{k}\cdot\boldsymbol{a}_1$ and $\boldsymbol{k}\cdot\boldsymbol{a}_2$ were calculated and the number of points taken to plot each subpath was determined according to the distance between the two high symmetry points.

(e) Each band can contain two electrons so the p_z bands are half filled. This means that the Fermi level is at $\varepsilon(\boldsymbol{k}) = E_{p_z}$.

Appendix 2 - VASP-calculations

To practice using VASP different band structure and density of states calculations have been done. These results were used to analyze the differences in the electronic properties of materials when one moves in different directions in the periodic table. The result of the calculations were analyzed in a vertical direction (e.g. C → Si → Ge), a horizontal direction (e.g. C → BN) and an 'inward' direction (e.g. graphite → graphene). The results can be found in this appendix.

For some of the materials calculations were done for multiple structures. Of these structures the total energies were also calculated. One has to keep in mind that the total energies of the different materials cannot be compared, since all the materials have a different potential. Only values for the same material in different structures can be compared.

Carbon

For carbon calculations were done for diamond, graphite and graphene, one layer of graphite. After the different paragraphs containing the results of these calculations the total energies of the different structures are compared.

Diamond VASP calculations were done for carbon in it's diamond structure. The resulting band structure and density of states can be found in figure 34. The plotted path was L-Γ-X-K-Γ and the density of states and the band structure plot share the same energy axis. The Fermi energy was set to zero and is marked in the figure by a dotted line. For these calculations a PBE potential was used.

The band structure along the L-Γ-X path was calculated by Glötzel *et al.* [17] for an energy range of −13 to 17 eV. The results from figure 34 can thus be compared to their results. The only differences in the results are at points where the bands cross, but it is known that VASP can give a strange result at band crossings since the software is designed to avoid these crossings.

The band gap calculated in this case was around 4.2 eV, while it should be 5.5 eV [18]. This can be explained by the fact that VASP uses density functional theory for it's calculations, which underestimates the band gap of materials.

Graphite The band structure and density of states for graphite were calculated using a PBE and a LDA potential and are plotted in figures 35 and 36 respectively. In these plots the band structure and density of states share the same energy axis which is zero at the Fermi energy (dotted line). The band structure calculations were done along the path Γ-M-K-Γ-A-L-H-A.

Kobayashi [19] calculated the band structure within LDA along the path Γ-M-K-Γ-A-L. The band structure from figure 36 can be compared to the band structure he calculated. The band

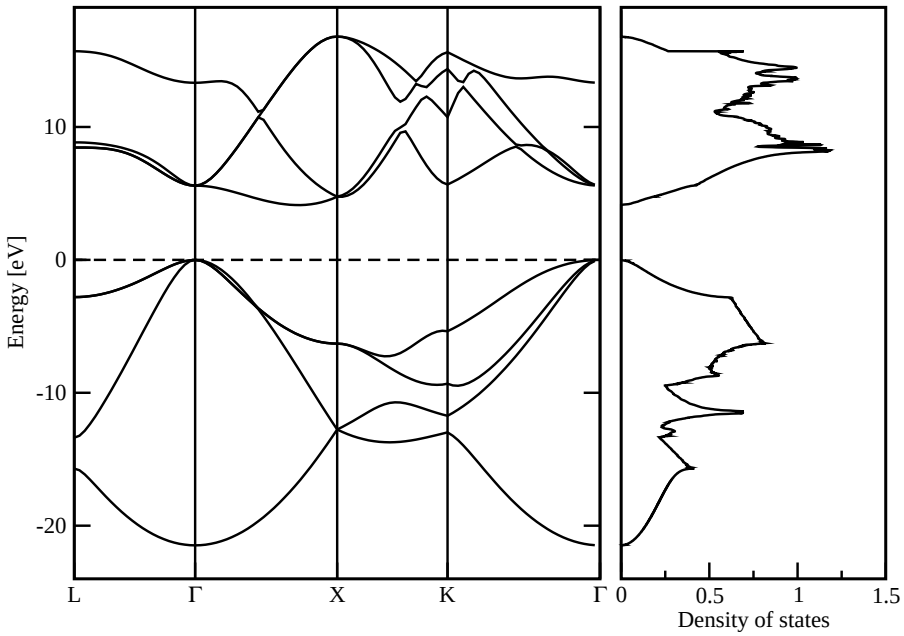

Figure 34: Band structure and density of states for diamond along the L-Γ-X-K-Γ path. The Fermi energy has been set to zero and is marked by a dotted line.

structures are the same except for the fact that Kobayashi [19] calculated more valence bands. The energy values at the high symmetry points were compared and are the same as far as one can determine by eye.

Graphite is a semi-metal [20] so the band gap should be zero. However, the band structure shows a gap of 0.02 eV in figure 36. These problems can be explained by the fact that when these calculations are done, the charge densities are calculated first for which the k-points are generated automatically. In this case, the charge densities were never calculated explicitly at the K point, the location of the band gap. Therefore, at this point the band structure was interpolated resulting in a band gap.

The difference in the band structures calculated using a PBE and a LDA potential are plotted in figure 37. The differences are mostly between two matching bands and always smaller than 0.4 eV.

Graphene The band structure and density of states have been calculated for graphene, a monolayer of graphite, using VASP with a PBE and LDA potential. These plots can be found in figure 38 for the PBE potential and figure 39 for the LDA potential. In both figures the density of states is plotted along the path Γ-M-K-Γ. The Fermi energy has been set to zero and is marked with a dotted line. The band structure shares it's energy axis with the density of states plot.

Just as graphite graphene is a semimetal and should not have a band gap. In the figures, no band gap is observable. In figure 40 the band structures calculated using a PBE and a LDA potential can be compared. The band structures are generally the same with a maximum difference between two bands of 0.3 eV.

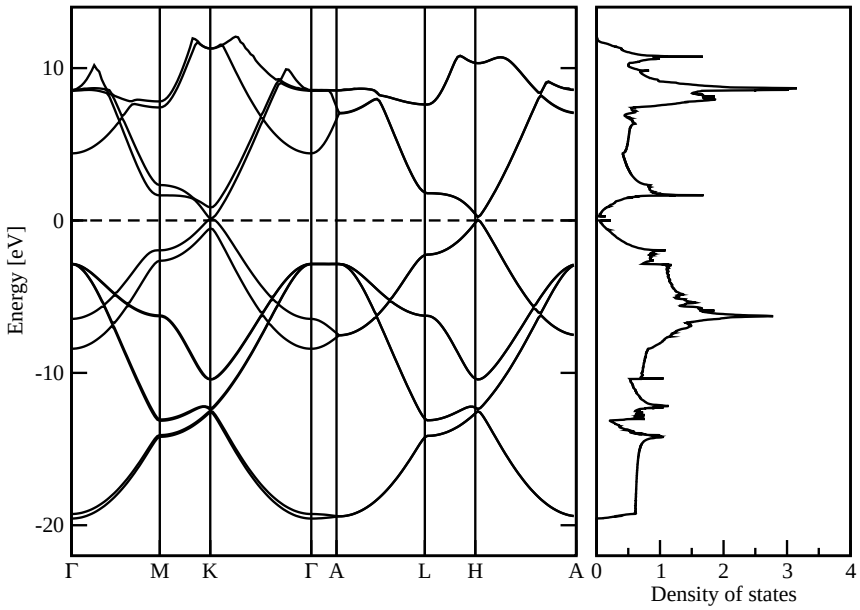

Figure 35: Band structure and density of states for carbon in a hexagonal structure, also known as graphite. The band structure is plotted along the Γ-M-K-Γ-A-L-H-A path. The Fermi energy has been set to zero and is marked by a dotted line. Calculations were done by VASP using a PBE potential.

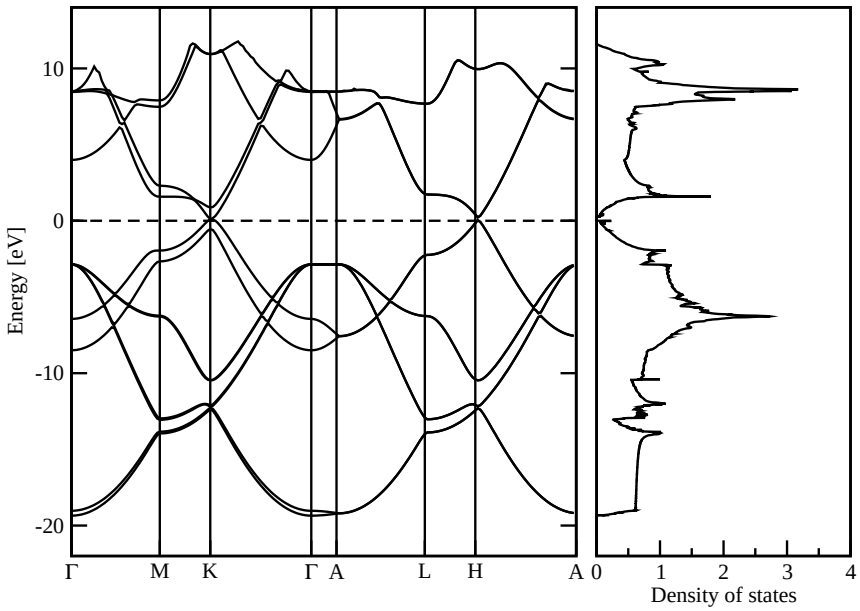

Figure 36: Band structure and density of states for graphite using a LDA potential. The band structure is plotted along the Γ-M-K-Γ-A-L-H-A path. The Fermi energy has been set to zero, marked by a dotted line.

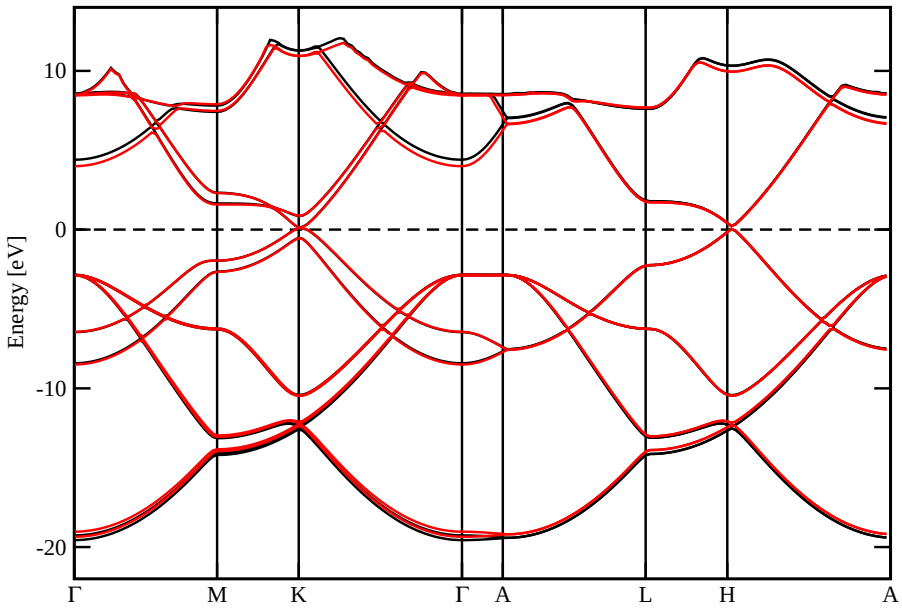

Figure 37: Band structures for graphite calculated using a PBE (black) and LDA (red) potential. They have the same x and y axis scaling to show the differences between the two calculations.

Table 2: Total energy per atom for three different carbon structures.

	Total energy per atom [eV]	
	PBE	LDA
Diamond	−9.0894745	
Graphite	−9.20588925	−10.1130285
Graphene	−9.217241	−10.09413

The total energies of the three different structures are listed in table 2. It contains the total energy per atom in eV for the three different structures and the two different potentials. Calculations for diamond with a LDA potential were not done.

The PBE calculations in table 2 suggest that graphene is the most stable structure of carbon. However the LDA calculations suggest that graphite is more stable than graphene. This could be explained by the fact that VASP doesn't take the van der Waals forces between the graphene sheets in graphite into account. This might explain why according to the PBE calculations graphite is less stable than graphene while in reality one would never encounter a sheet of graphene.

Diamond is the least stable structure. However one can encounter diamond as the structure of carbon since it takes a lot of energy to cross the barrier to go from diamond to graphite.

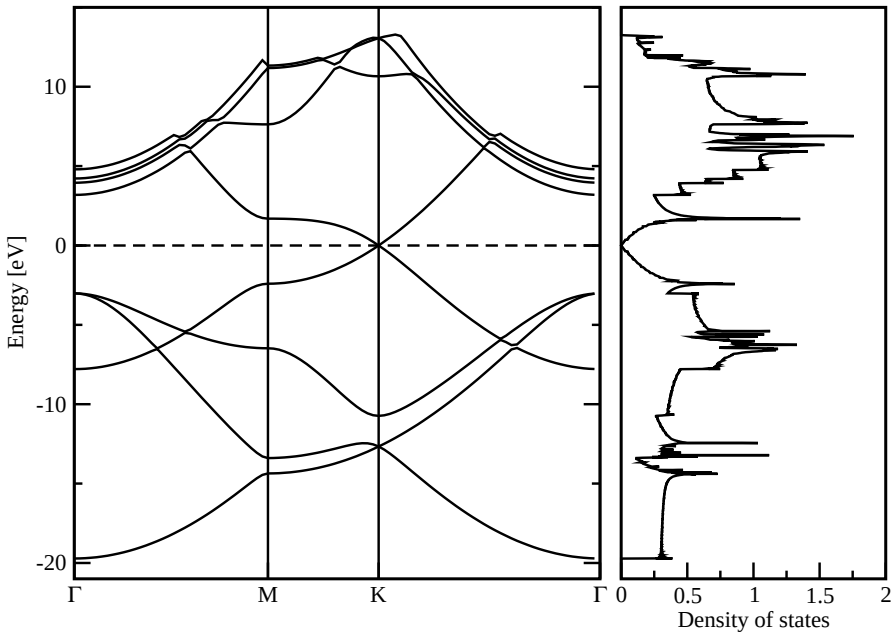

Figure 38: Band structure and density of states for one sheet of graphite, also known as graphene. The band structure is plotted along the Γ-M-K-Γ path. The Fermi energy has been set to zero, marked by the dotted line. Calculations were done by VASP using a PBE potential.

Silicon

Diamond structure After carbon VASP calculations were done for silicon, which has a diamond structure. The band structure of silicon for the path L-Γ-X-K-Γ was plotted in figure 41 along with the density of states. The density of states plot shares it's energy axis with the band structure plot. The Fermi energy has been set to zero and is marked with a dotted line. A PBE potential was used in the calculations.

The band structure for the L-Γ-X path in the energy range from −8 to 6 eV is compared to a calculation of the band structure of silicon by Glötzel *et al.* [17]. The band structures are the same except for some strange crossings as was the case with diamond.

The band gap for silicon is 1.11 eV [21]. From figure 41 one can determine a band gap of around 0.5 eV. This is again because density functional theory calculations underestimate the band gap.

Germanium

Diamond structure VASP calculations were also done for germanium using a PBE and LDA potential. The band structures and densities of states are shown in figures 42 and 43 respectively. The plotted path is L-Γ-X-K-Γ. Again the density of states shares it's energy axis with the band structure and the Fermi energy has been set to zero (dotted line).

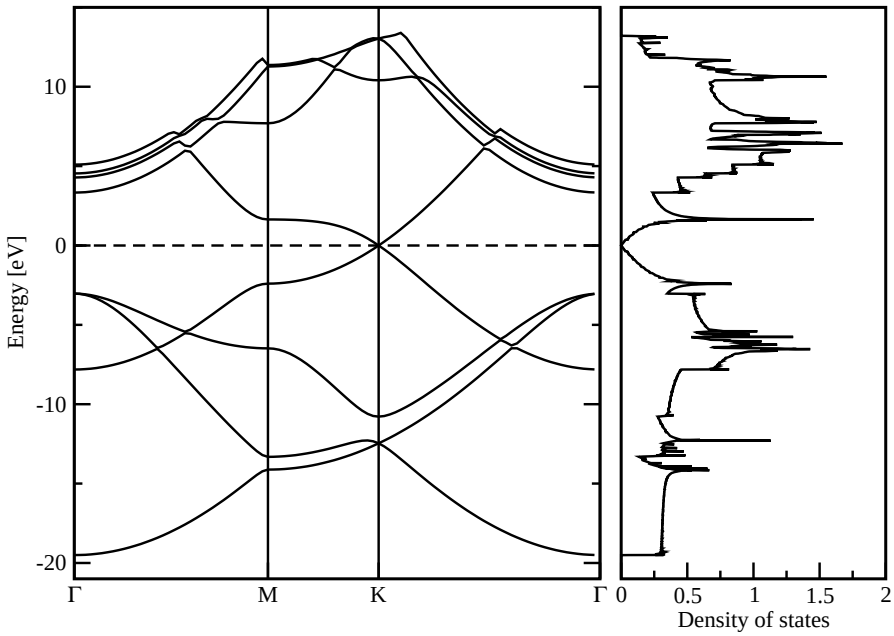

Figure 39: Band structure and density of states for graphene using a LDA potential. The band structure is plotted along the Γ-M-K-Γ path. The Fermi energy has been set to zero, marked by the dotted line.

The differences between the band structures are small as can be seen in figure 44. The biggest difference might be that the band structure shows no band gap at all for the LDA potential calculation, although the density of states shows a band gap of around 0.08 eV. Besides this the valence bands are not always exactly the same, but the differences are smaller than 0.2 eV. The band gap for germanium should be 0.66 eV [21], but the difference can again be blamed on density functional theory.

Glötzel *et al.* [17] also calculated the band structure for germanium along the L-Γ-X path in the energy range from -10 to 4 eV. Again there are some differences because of the crossings. Also, the band gap in figure 42 is smaller but Glötzel *et al.* [17] moved their lowest energy band at the gamma point up a little bit. The rest of the band structure matches.

Boron nitride

The calculations for boron nitride were done for four different structures, that is for the zinc blende, wurtzite and hexagonal structure and for a monolayer of the hexagonal structure. After the results of the different calculations the total energies of these structures are compared.

Zinc blende structure Results for boron nitride in a zinc blende structure can be found in figure 45. A PBE potential was used in the calculations, which were done by VASP. In the figure the band structure and density of states are plotted scaled to the same y axis. The Fermi level is set zero and marked by a dotted line. The band structure is plotted along the path

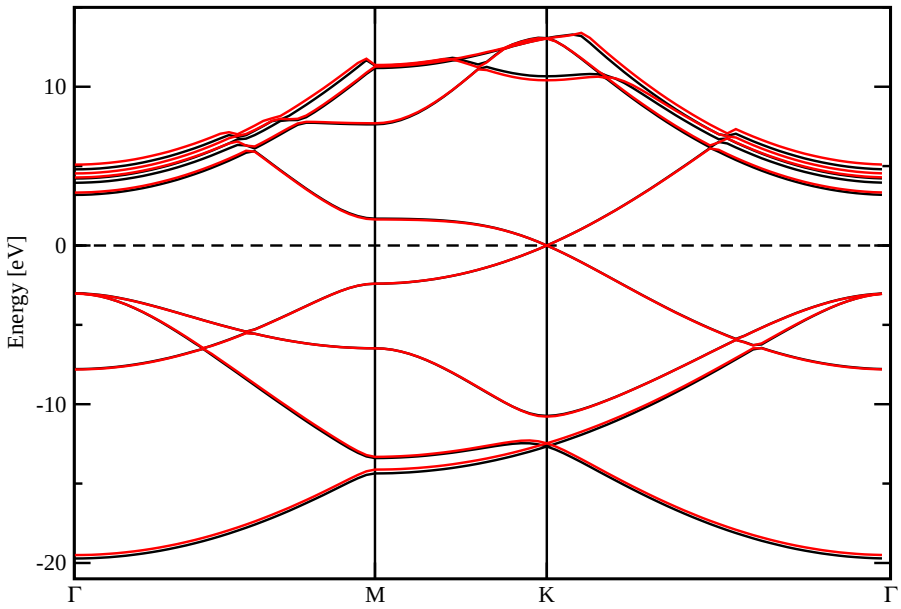

Figure 40: Band structures for graphene calculated using a PBE (black) and LDA (red) potential. They have the same x and y axis scaling to show the differences between the two calculations.

L-Γ-X-K-Γ.

The band structure can be compared to calculations done by Abdulkareem and Elias [22]. They plotted the band structure along the path L-Γ-X-Γ. The band structure they found matches the band structure in figure 45. The calculated band gap is 4.45 eV in this case, but is again underestimated. Chrenko [23] for example calculated a band gap of 6.4 ± 0.5 eV.

Wurtzite structure Calculations for the wurtzite structure of boron nitride were also done, with the resulting band structure and density of states plotted in figure 46. Calculations were done along the path Γ-M-K-Γ-A-L-H-A, using a PBE potential. The band structure and density of states plot share the same energy axis in the figure. The Fermi level is set to zero and marked by a dotted line.

The band structure can be compared along the path Γ-M-K-Γ-A-L to the band structure calculated by Kobayashi [24]. The band structures seem to match except for at some crossings of the valence bands. Where in figure 46 some conduction bands seem to cross, they clearly do not cross in the calculations by Kobayashi [24].

The band gap in figure 46 is 5.2 eV. Optical band gap calculations were done by Xu and Ching [25], however they calculated an indirect band gap between Γ and X point and the band gap in figure 46 is an indirect band gap between Γ and K point. Xu and Ching [25] also calculated direct band gaps and those can be compared. They found a direct band gap at K point of 11.7 eV, while figure 46 shows an (underestimated) direct band gap of 10.4 eV at K point.

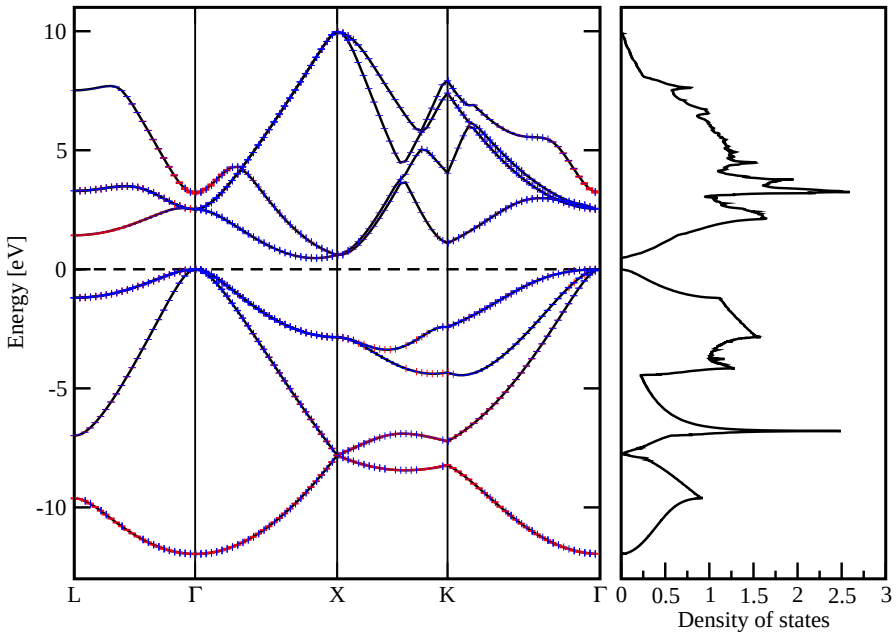

Figure 41: Band structure and density of states for silicon along the L-Γ-X-K-Γ path. The Fermi energy has been set to zero and is marked by the dotted line. The charachter of the bands is shown in this figure, with the p-charachter in blue and the s-character in red.

Hexagonal structure Also for hexagonal boron nitride calculations were done. Just as with the wurtzite structure, the calculations were done along the path Γ-M-K-Γ-A-L-H-A and a PBE potential was used. The resulting band structure and density of states can be found in figure 47. Both plots share the same energy axis. The Fermi energy was set to zero and is marked by the dotted line.

The band structure can also be compared to calculations by Kobayashi [26]. He calculated the band structure along the path Γ-M-K-Γ-A-L. The band structures are the same except that figure 47 contains one more conduction band along Γ-M-K-Γ.

The band gap has been calculated by Blase *et al.* [27]. They calculated a band gap of 5.4 eV. This is bigger than the band gap that can be determined from figure 47, which is 4.25 eV, so it's again underestimated.

Monolayer Calculations were also done for a monolayer of hexagonal boron nitride, that is one sheet from the hexagonal boron nitride structure. The band structure and density of states were calculated along the Γ-M-K-Γ path using a PBE potential. The results can be found in figure 48. In this figure, the density of states and band structure plot have the same energy axis. The Fermi level was set to zero and is marked by the dotted line.

A band structure calculation was also done by Drummond *et al.* [9] along the path Γ-K-M-Γ. Comparing the result from figure 48 to their result shows a good resemblance. The band gap determined from figure 48 is 4.63 eV, again underestimated since it should be > 5.0 eV [13].

The total energies of these four different structures are listed in table 3. For each structure the

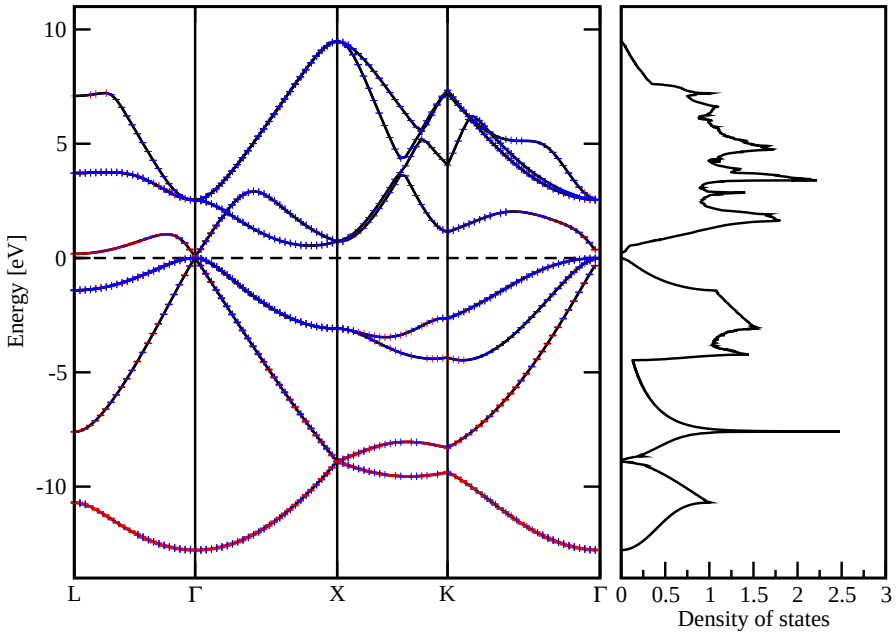

Figure 42: Band structure and density of states for germanium along the L-Γ-X-K-Γ path. The Fermi energy has been set to zero and is marked by the dotted line. Calculations were done by VASP using a PBE potential. The charachter of the bands is shown in this figure, with the p-charachter in blue and the s-character in red.

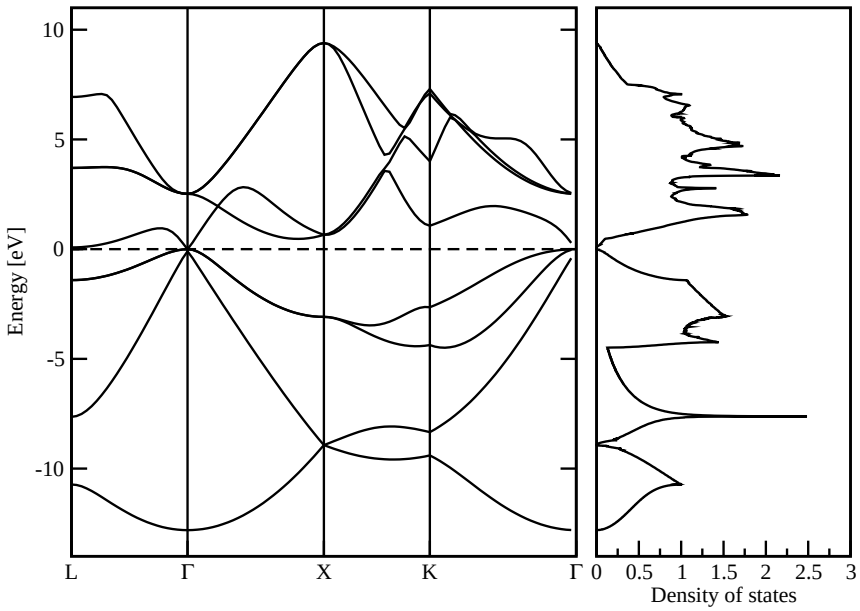

Figure 43: Band structure and density of states for germanium along the L-Γ-X-K-Γ path. The Fermi energy has been set to zero and is marked by the dotted line. Calculations were done by VASP using a LDA potential.

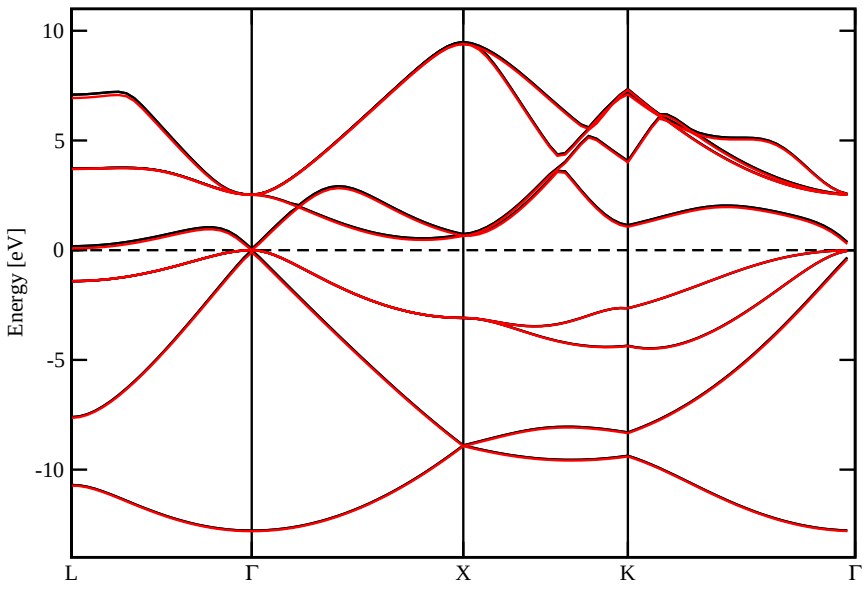

Figure 44: Band structures for germanium calculated using a PBE (black) and LDA (red) potential. They have the same x and y axis scaling to show the differences between the two calculations.

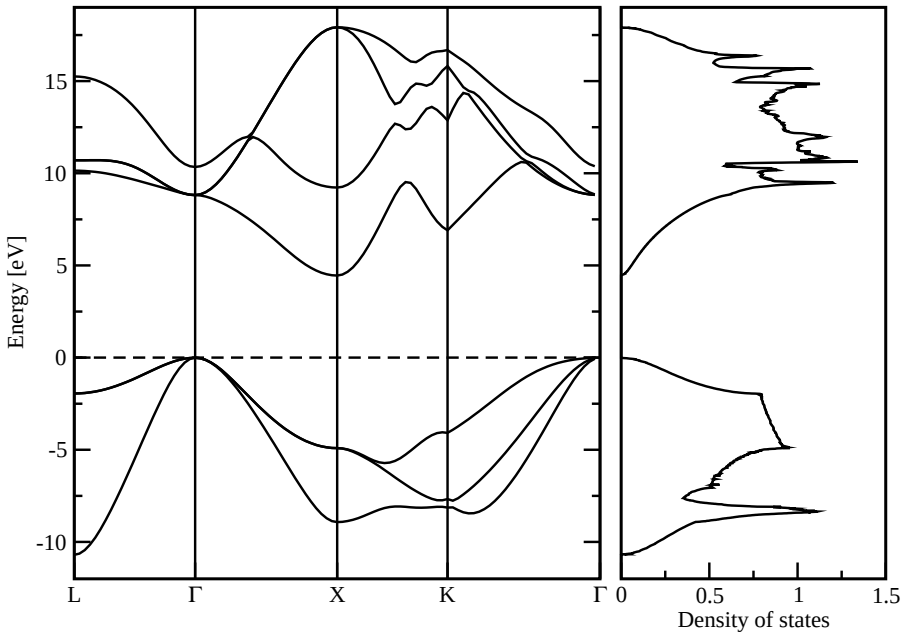

Figure 45: Band structure and density of states for boron nitride in a zinc blende structure along the L-Γ-X-K-Γ path. The Fermi energy has been set to zero and is marked by the dotted line.

Table 3: Total energy per atom for four different boron nitride structures.

Structure	Total energy per atom [eV]
Zinc blende	−8.7106
Wurtzite	−8.6900545
Hexagonal	−8.77376775
Monolayer	−8.7835655

total energy per atom in eV is given. According to these values the monolayer of the hexagonal structure is the most stable. However, just as with graphene, this is most likely wrong because the van der Waals forces are ignored in the calculations.

Therefore it can be concluded from table 3 that the hexagonal structure is the most stable structure. The zinc blende structure comes next and the wurtzite structure is the least stable structure of boron nitride.

Aluminium phosphide

Zinc blende structure The next calculation was done for aluminium phosphide which has a zinc blende structure. The band structure and density of states were calculated along the path L-Γ-X-K-Γ using a PBE potential. The plots of these calculations are shown in figure 49. The density of states and band structure have the same energy axis on which the Fermi energy was set to zero. The Fermi energy is marked in the plot by a dotted line.

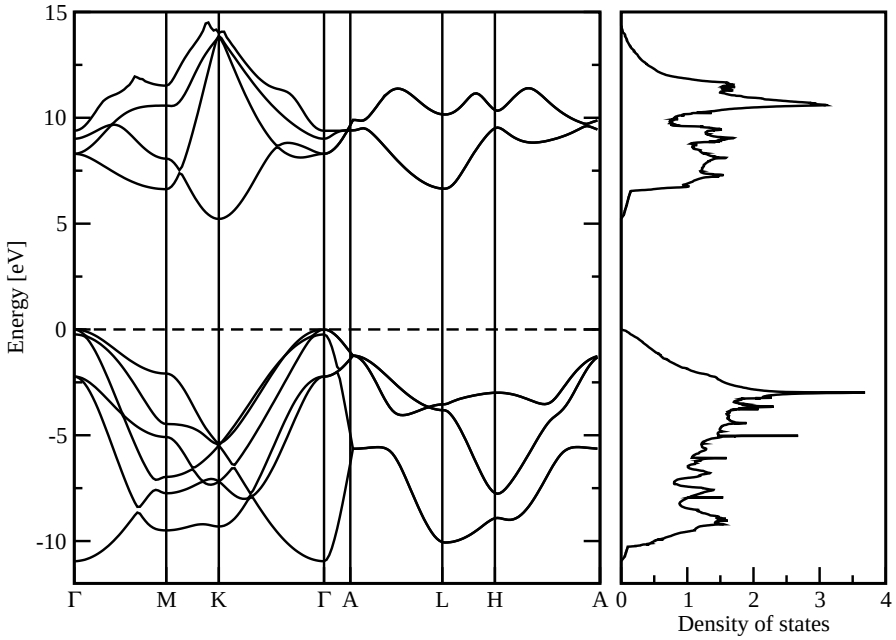

Figure 46: Band structure and density of states for boron nitride in a wurtzite structure along the Γ-M-K-Γ-A-L-H-A path. The Fermi energy has been set to zero and is marked by the dotted line.

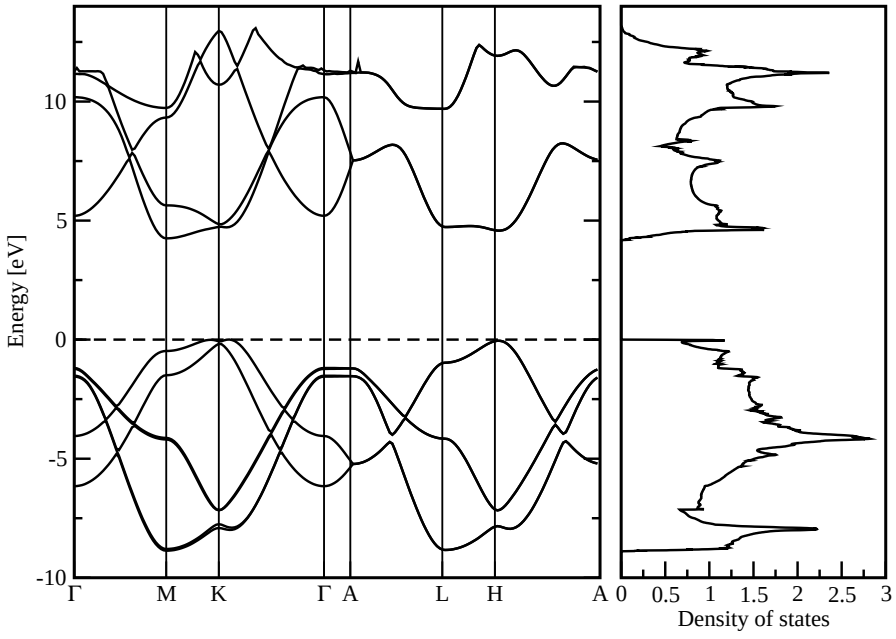

Figure 47: Band structure and density of states for hexagonal boron nitride along the Γ-M-K-Γ-A-L-H-A path. The Fermi energy has been set to zero and is marked by the dotted line.

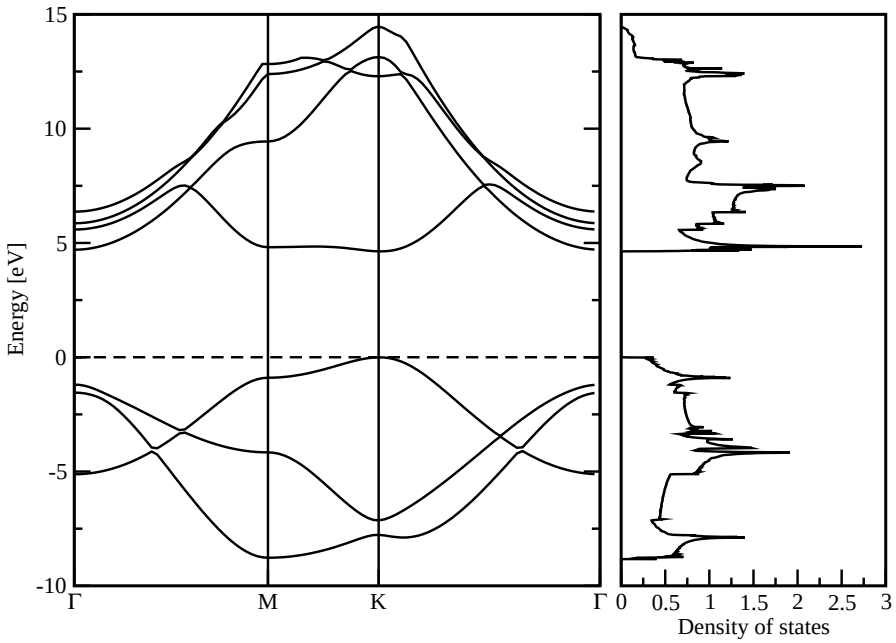

Figure 48: Band structure and density of states for a monolayer of hexagonal boron nitride along the Γ-M-K-Γ path. The Fermi energy has been set to zero and is marked by the dotted line.

The results can be compared to band structure calculations by Saliev [28]. He calculated the band structure along the same path. His results match the band structure from figure 49. The band gap determined from figure 49 is 1.5 eV but should be 2.5 eV [29], so the band gap is again underestimated.

Gallium arsenide

Zinc blende structure Next, band structure and density of states calculations were done for gallium arsenide. Just as aluminium phosphide gallium arsenide has a zinc blende structure. The results of the calculations, done using a PBE potential and along the path L-Γ-X-K-Γ, can be found in figure 50. The band structure and density of states have the same energy axis. The Fermi level is marked by the dotted line and was set to zero in the plots.

The band structure from figure 50 matches the band structure calculated by Danner [30], although he calculated the band structure for one more high symmetry point. The band gap should be 1.43 eV [21], but is 0.6 eV in figure 50, so it is again underestimated.

Zinc selenide

Final calculations were done for zinc selenide, in it's zinc blende structure and it's wurtzite structure. After the calculations the total energies are compared.

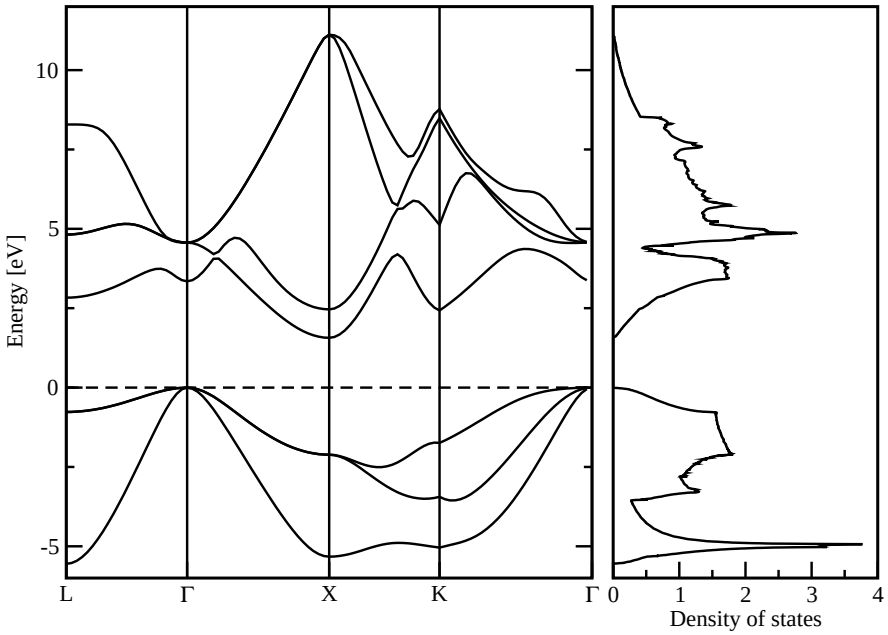

Figure 49: Band structure and density of states for aluminium phosphide along the L-Γ-X-K-Γ path. The Fermi energy has been set to zero and is marked by the dotted line.

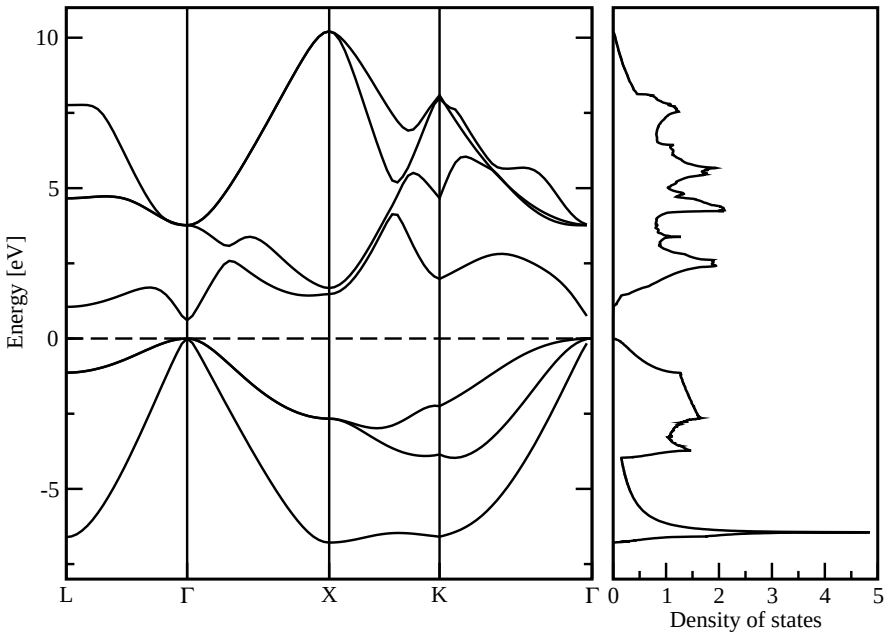

Figure 50: Band structure and density of states for gallium arsenide along the L-Γ-X-K-Γ path. The Fermi energy has been set to zero and is marked by the dotted line.

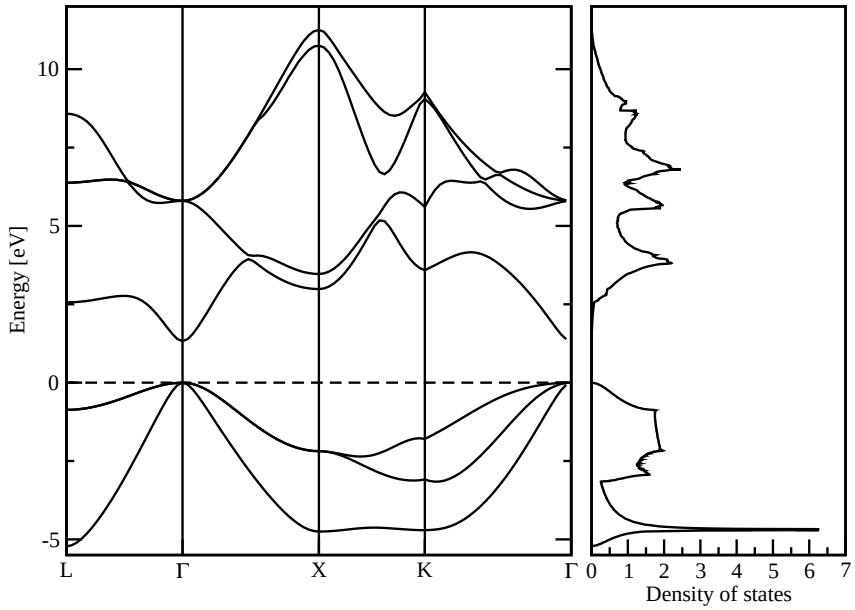

Figure 51: Band structure and density of states for zinc selenide in a zinc blende structure along the L-Γ-X-K-Γ path. The Fermi energy has been set to zero and is marked by the dotted line.

Zinc blende structure The result of these calculations can be found in figure 51. The band structure and density of states are plotted there, calculated using a PBE potential. The band structure was calculated along the path L-Γ-X-K-Γ. The energy axis is shared between the band structure and density of states and the Fermi energy was set as zero. The Fermi energy is marked by a dotted line.

The band structure is compared to the band structure calculated by Bernard and Zunger [31] and matches the band structure from figure 51. They also give a band gap of 2.8 eV. In figure 51 the band gap is 1.32 eV, again underestimated.

Wurtzite structure The last calculation is for zinc selenide in a wurtzite structure. The results of this calculation, done using a PBE potential, can be found in figure 52. In this figure the band structure and density of states are shown with the band structure plotted along the path Γ-M-K-Γ-A-L-H-A. Both these plots share the same energy axis. The Fermi level is set to zero on this axis and is marked by a dotted line.

The band structure can be compared to calculations done by Zakharov *et al.* [32]. They calculated a different path but parts of it can still be compared. The band structures generally match, but sometimes a doubly degenerate band from figure 52 isn't visible in their calculations due to poor resolution. An example of this can be seen in the valence bands between K and Γ.

The band gap determined from figure 52 is 1.44 eV. In the paper by Zakharov *et al.* [32] different values of the band gap were mentioned, for example 3.98 for a GW calculation and 3.78 and 3.85 as experimental values. Therefore we can conclude that the band gap is underestimated again.

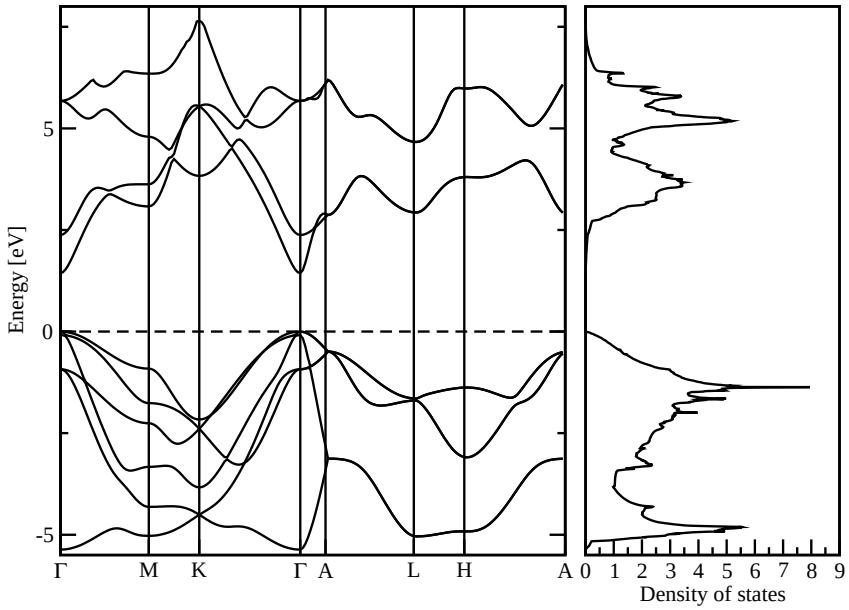

Figure 52: Band structure and density of states for zinc selenide in a wurtzite structure along the Γ-M-K-Γ-A-L-H-A path. The Fermi energy has been set to zero and is marked by the dotted line.

Table 4: Total energy per atom for two different zinc selenide structures.

Structure	Total energy per atom [eV]
Zinc blende	−3.08525795
Wurtzite	−3.07341175

The total energies of the two zinc selenide structures are listed in table 4. The total energies per atom in eV are listed for the zinc blende and the wurtzite structure. From this table it can be concluded that the zinc blende structure is more stable than the wurtzite structure.

Further analysis

Analysis that has not yet been done in the previous sections is done here. First, the dependence of the size of the band gap on the lattice constant and position in the periodic table is analyzed. After that the band structures for silicon and germanium are compared, showing the similarities and differences.

Band gap size When one moves in the periodic table from diamond to silicon to germanium the structure of the material stays the same, except for the lattice constant, which gets bigger. From the results one can notice a decline in band gap for these materials. In figure 53 the size of the band gap is plotted versus the lattice constant for the calculated value of the band gap and the value from literature. One can see that the size of the band gap is linearly dependent on the lattice constant for these materials.

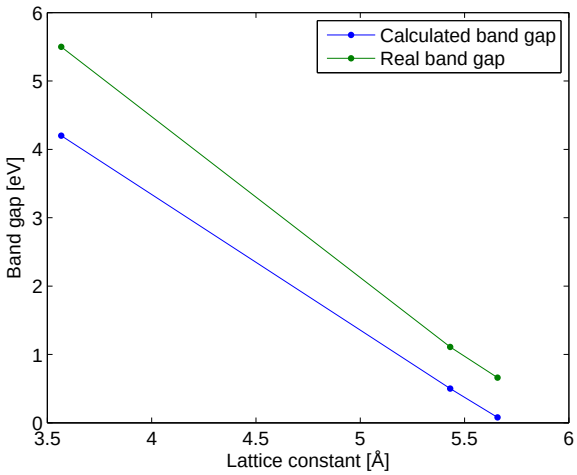

Figure 53: Size of the band gap versus the lattice constant for diamond, silicon and germanium. The calculated band gap as well as the band gap from literature are plotted.

One can also look at what happens when one moves 'outside' in the periodic table, that is from a group IV to a group III-V to a group II-VI material. Examples of this are diamond to boron nitride in it's zinc blende structure or germanium to gallium arsenide to zinc selenide in a zinc blende structure. The lattice constant stays almost the same for these materials, but the band gap increases when one moves in this direction. However, no specific relation can be seen.

Band structure In figures 41 and 42 the s- and p-character of the bands are plotted. This helps showing the similarities between the two band structures. One can see that they are the same except for one conduction band. The conduction band which has a lot of s-character at the Γ point is moved down in germanium compared to silicon. It has moved down in germanium below the bands which formed the bottom of the conduction band in silicon to almost the Fermi level. Therefore the indirect band gap in silicon becomes a direct band gap at Γ for germanium.